THE EFFECT OF FINS ON VORTEX SHEDDING

THE EFFECT OF FINS ON VORTEX SHEDDING

By

DAMON JEBODHSINGH, B. ENG. SOCIETY.

A Thesis

Submitted to the School of Graduate Studies

In Partial Fulfillment of the Requirements

For the Degree

Master of Applied Science in Engineering

McMaster University

Master of Applied Science in Engineering (2002)
(Mechanical)

McMaster University
Hamilton, Ontario

TITLE: The Effect of Fins on Vortex Shedding

AUTHOR: Damon Jebodhsingh
B. Eng. Society
McMaster University

SUPERVISORS: Dr. Samir Ziada, Professor
Department of Mechanical Engineering
McMaster University

&

Dr. David S. Weaver, Professor
Department of Mechanical Engineering
McMaster University

NUMBER OF PAGES: xiv, 122

Abstract

An experimental study in air has been performed to determine what effect fins have on the flow over circular cylinders. The tubes under investigation included one bare tube and three segmented-finned tubes of different fin densities with the same root diameter as the bare tube. The tests were performed at two Reynolds numbers (2.61×10^4 and 4.98×10^4) and two downstream distances (2.5 & 5 diameters) and involved the use of hotwire anemometry. Measurements of mean and fluctuating velocities were taken across the wake as well as two-point fluctuating velocity correlations.

It was discovered that the use of fins can result in significant differences. Fins cause larger mean velocity deficits in the wake profiles and significant shape differences in the total turbulence intensity profiles. Fins also increase the strength of vortex shedding, contrary to what would be expected, and increase the number of harmonic frequency peaks in the frequency spectra as three harmonic peaks were observed for the bare tube, while as many as ten were seen for the densest finned tube.

Correlation length measurements, and thus radiated sound intensity, proved to be inconclusive. It was discovered that correlation length changed with angular rotation suggesting that this phenomenon needs to be investigated further before making any comparisons.

Based on the differences seen with increased fin density, it is thought that there may be a critical fin density which causes fundamental changes in the cylinder wake. Also, during the course of this investigation, it was concluded that while the use of an effective diameter, D_e, proved adequate in collapsing the finned tube data, this approximation could be improved.

Acknowledgements

I would like to express my gratitude to both Dr. S. Ziada and Dr. D. S. Weaver for their invaluable guidance, encouragement, and time throughout the course of this project.

I would also like to thank the Mechanical Engineering technicians, Ron and Andrew, for their invaluable assistance in the construction of my apparatus and Joe, for his assistance with the hotwire anemometry equipment.

For his excellent instruction in the use of hotwire anemometry equipment, I am thankful to Joe Hall who, in addition to Mike Bardeleben, also helped me in Labview programming.

Finally, I would like to thank my friends and family for their support throughout the course of this program, especially during the tough times.

Table of Contents

List of Figures

List of Tables

Nomenclature

D	bare tube diameter (m)
D_e	effective tube diameter (m)
D_f	fin diameter (m)
f_s	vortex shedding frequency (Hz)
f_n	tube natural frequency (Hz)
λ_z	correlation length (m)
L	tube length (m)
Re	Reynolds number based on D
Re_{De}	Reynolds number based on D_e
$R_{uu}(z)$	correlation coefficient based on fluctuating velocity measurements
St	Strouhal number based on D
St_{De}	Strouhal number based on D_e
U	local velocity (m/s)
U_o	freestream velocity (m/s)
u'	local rms fluctuating velocity (m/s)
x	streamwise coordinate (m)
y	transverse coordinate (m)
z	axial coordinate (m)

Chapter 1

1 Introduction

Circular cylindrical structures are basic objects that have influenced every aspect of life in the world today. In terms of engineering applications, circular cylindrical structures are essential components in the design of a variety of items ranging from the simple, such as flag poles, to the more complex, such as the automobile. Of particular interest is the flow of a fluid over these cylindrical structures which is quite commonplace in engineering equipment such as marine risers, chimney stacks, and steam generators.

Any structural component placed in a flow will vibrate to some extent. This is not necessarily bad and in some cases, attempts have been made to take advantage of this vibration to enhance heat transfer in heat exchangers. When the vibrations are considered to be detrimental, they may lead to mechanical failure, and this could have devastating effects if they occur in the components of nuclear power plants such as heat exchangers and steam generators. It has become rather commonplace to shut down nuclear power plants to perform expensive repairs as well as to contain radiation exposure. Sometimes the economic loss could exceed the value of the equipment and result in significant ecologic problems. For instance, flow-induced vibration problems caused 23 power plant shut downs and power reductions in the U.S. between May 1974

and December 1975 (Polak, 1992). This lost power production also translates to significant losses in revenue.

There are several different mechanisms by which flow may generate vibrations of tube banks including turbulent buffeting, fluidelastic instability, jet switching, and periodic vortex shedding. For this study, the mechanism of vortex shedding is of particular importance as it is also the source of acoustic sound and resonant vibrations. In addition to vortices being shed from single cylinders in cross-flow, they were observed to be shed from every tube of a bank in a heat exchanger (reported by Mair et al 1975). The shedding of vortices alternately from the two sides of a cylinder generates an oscillatory transverse force. When this occurs over a long period of time, the majority of tube failures are due to fretting wear at the tube supports (*Figure 1.1* (Pettigrew *et al.*, 1978)) and to a lesser extent by fatigue, or thinning and splitting at the mid-span as a result of tube-to-tube clashing.

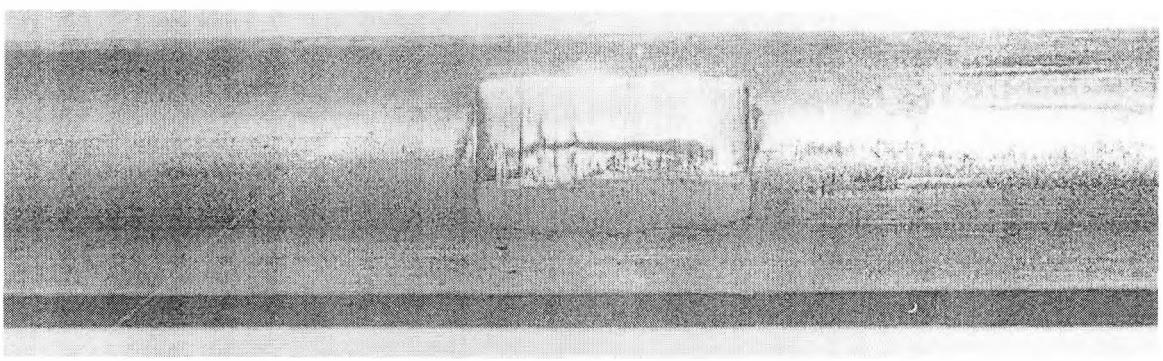

Figure 1.1: Heat exchanger tube failure due to fretting-wear at support location (Pettigrew et al., 1978).

However, when the frequency of vortex shedding approaches that of the natural frequency of the tubes, excessive vibrations can occur which could cause a sudden and catastrophic failure.

It is also known that when there is flow over a single cylinder or group of cylinders, sound is produced. These acoustic tones, or Aeolian tones, are associated with the periodic vortex shedding and it is known that their strength is related to the correlation of vortices along the span of the tube. In addition to this sound, it is also known that when the vortex shedding frequency coincides with the standing acoustic mode across the duct of the heat exchanger, intense sound can be produced. Sound levels in excess of 160dB have been experienced in tube banks which are very damaging to the ears of any personnel in the vicinity and can affect the performance of the heat exchanger. When this frequency coincides with the natural frequency of any of the components in the heat exchanger, this may also cause failure of those parts.

Given that it would be desirable to avoid these problems, much research has been performed on both single smooth tubes and banks of smooth tubes to reduce or eliminate these problems. Some solutions have been formulated such as the insertion of anti-vibration baffles into tube banks, or modifying the surface of the tube.

It has been noticed that the use of finned tubes in heat exchanger tube bundles has grown in popularity in the last few decades. It was discovered that the finning or roughening of heat exchanger tubes in cross-flow enhanced their heat transfer by basically increasing the heat transfer surface. With the increasing ease of manufacturing finned tubes over the years, and realizing that this was the most economical way of

increasing the heat transfer surface area, finned tubes have been replacing bare tubes gradually.

Intuitively, given that such modifications as helical strakes and splitter plates to the surface of the tube suppress vortex shedding, it would be expected that similar results would have occurred for finned tubes. However, like the bare tube, vortex shedding still occurs from both single finned-tubes and every tube in a bank. While the fundamentals of vortex shedding from smooth tubes are reasonably well understood, little is known for the case of finned tubes. Nonetheless, similar problems exist for finned tube banks. Fretting wear and fatigue failure also occur as well as acoustic resonance. As a result, to better design heat exchanger equipment incorporating finned tubes and to avoid vibration and acoustic problems, research needs to be performed. There has been some research undertaken on finned tubes, but it is very limited and was mostly concerned with finned tube banks. As the flow past a bank of tubes is much more complex than the flow past a single tube, it is believed that studying the flow about single cylinders will help considerably in the understanding the flow through tube banks.

This paper presents the findings of a study of air flow past single finned-tubes of different fin densities. Although there are different kinds of fins such as plain, wavy, and segmented, the experiments performed used the latter kind of fins. The experiments were performed in a wind tunnel and measurements in the wake and of the correlation of the vortices along the span of the tube were taken and compared against those taken for a bare tube. The conclusions inferred from the results are presented at the end of this study.

Chapter 2

2 Literature Review

The flow of fluid over circular cylindrical structures is well known to sometimes induce vibrations and generate sound. In this study, the focus is on tubes with fins which are used in heat exchanger tube banks found in power plants.

Previous research on this topic is limited as well as the associated literature. However, there is an abundance of literature relating to bare tubes which will be used to compare with the results of this study and with the finned tube literature.

As the flow past a bank of tubes in a heat exchanger is much more complex than that of a single tube, it is expected that satisfactory understanding of the former can not be achieved without a reasonable understanding of the latter.

2.1 Flow Induced Vibrations in Heat Exchanger Tube Banks

When a fluid flows across a tube bank, a fraction of the fluid energy is transmitted to the cylinders which manifests itself as tube vibration and/or sound generation. As mentioned previously, these flow induced vibrations could lead to severe problems with the heat exchanger components and as such, care must be taken when these components are being designed.

There are four distinct mechanisms which are thought to induce vibrations in bare tube banks:

- *Turbulent Buffeting*: In a cylinder array, there exist random noises, including turbulent pressure fluctuations and far-field flow noises with some or little coherence. These randomly varying pressures on the surface of the cylinders generally produce low-amplitude cylinder vibration (Chen, 1987).
- *Fluidelastic Instability*: At a certain flow velocity, fluid energy may feed into cylinders, resulting in larger cylinder vibrations. The dominant fluid forces are the motion-dependent fluid forces. Severe damage can result in a short period of time (Chen, 1987).
- *Jet Switching*: The vibration is produced by coupling and uncoupling of fluid jets behind a tube array (Blevins, 1986).
- *Vortex Shedding*: The periodic vortex shedding from the tubes can give rise to two types of resonance. When the vortex shedding frequency (f_s) is equal to the tube natural frequency (f_n), this could potentially damage the tubes due to large amplitude vibration, while when f_s is equal to the acoustic natural frequency of the tube shell (f_a), this could produce high noise levels which may damage the outer walls of the system as well as those working in the vicinity (Paidoussis, 1982).

It was discovered that vibrations of finned tubes operating in crossflow were induced by mechanisms similar to those operating in the case of bare tubes (Katinas *et al.*, 1991).

This review will reflect that this study is primarily concerned with the mechanism of vortex shedding in the generation of flow induced vibrations.

2.2 Vortex Shedding and Single Cylinders

2.2.1 Smooth Tubes

Vibrations of single tubes operating in crossflow are induced by turbulence-generated fluctuations of flow pressure and by the shedding of vortices from the tube surface (Katinas *et al.*, 1991). As mentioned previously, only vibrations due to vortex shedding will be examined. The separation of a uniform two-dimensional flow due to its encounter with a bluff obstacle in its path results in the formation of two shear layers across which a large velocity gradient exists. Fed by the energy in the oncoming flow, the vorticity in the shears layers keeps growing until it reaches a critical stage when the two shear layers interact and shed the vorticity in the form of a vortex that convects downstream (around Re = 40). This sequence of events, repeated periodically, results in the formation of a von Karman vortex street (Goswami *et al.*, 1993). The major regimes of vortex shedding from a circular cylinder are shown in *Figure 2.1* (Blevins, 1986).

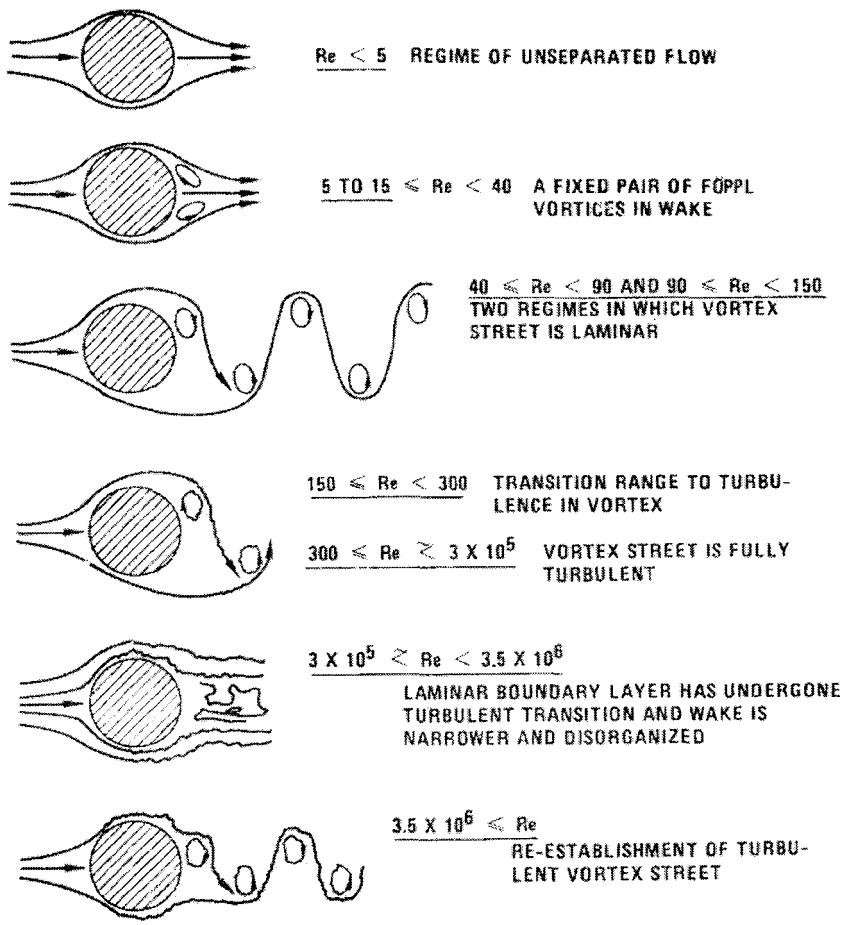

Figure 2.1: Regimes of fluid flow across circular cylinders (Blevins, 1986).

After the onset of vortex shedding, there are three main flow regimes (subcritical, critical, and post-critical). Of particular note to this study, is the subcritical flow regime ($300 < Re < 2 \times 10^5$) in which all experiments for this study were performed. However, in this flow regime, vortex shedding is highly dependent on flow confinement (blockage), surface roughness, incident freestream turbulence intensity and scale, aspect ratio, two-dimensionality of flow, and vibration amplitude (Paidoussis, 1982). How these parameters influenced this study will be discussed later.

When $40 < Re < 150$, the vortex street is laminar and then there is a transition to a turbulent street at $150 < Re < 300$. At the onset of the subcritical regime, the boundary layer over the front part of the cylinder is laminar and over the rear part, the layer separates and breaks up into a turbulent wake. The main feature of the flow field is the upstream movement of the point of transition from laminar to turbulent flow with increasing Re. At about $Re = 10^4$ this point of transition is close to the point of separation, and the major portion of the shear layer is turbulent. For $10^4 < Re < 2 \times 10^5$, there is minimal movement of the transition point and the flow field is essentially unchanged. Laminar separation on the surface of the cylinder occurs at about 80° from the stagnation point (Basu, 1985). This can be seen in *Figure 2.2* (Basu, 1985).

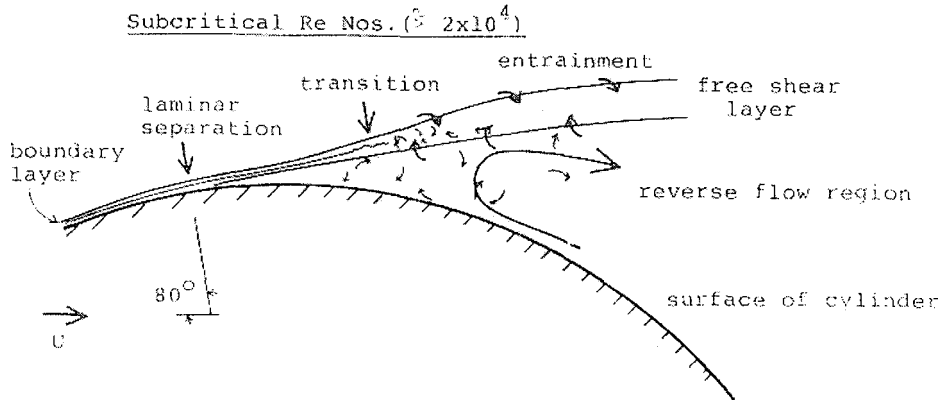

Figure 2.2: The flow field near the point of separation (Basu, 1985).

In the absence of appreciable interaction between the cylinder and its wake, these vortices are shed at a frequency directly proportional to the freestream velocity, U_0. This vortex shedding frequency, f_s, is related to the freestream velocity as well as the acrossflow dimension of the cylinder, D, through the Strouhal number, St:

$$St = \frac{f_s D}{U_0}$$

For circular cylinders in the subcritical regime, S is typically around 0.2 (*Figure 2.3*).

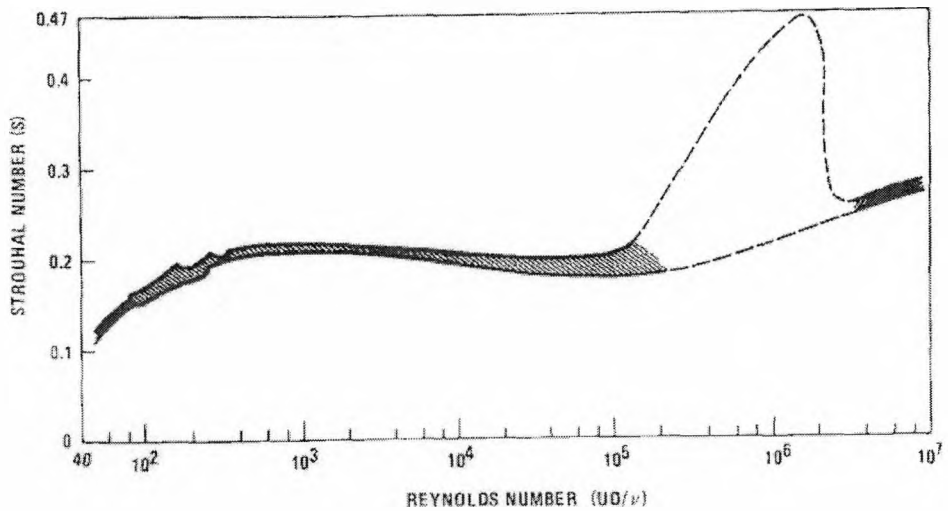

Figure 2.3: The Strouhal-Reynolds number relationship for circular cylinders (Blevins, 1986).

It is these periodically shed vortices which induce vibrations of single cylinders in crossflow. Each time a vortex is shed from the cylinder, the cylinder experiences a time-varying force in the lift direction, at the frequency of vortex shedding, and a time-varying force in the drag direction at a frequency equal to twice the shedding frequency (Chen, 1987). This occurs because as a fluid particle flows toward the leading edge of a cylinder, the pressure in the fluid particles rises from the freestream pressure to the stagnation pressure. The high fluid pressure near the leading edge impels flow about the cylinder as boundary layers develop about both sides (Blevins 1986). Alternate vortex shedding causes a periodic growth of circulation and a resulting asymmetric pressure distribution as seen in *Figure 2.4* (Blevins 1986).

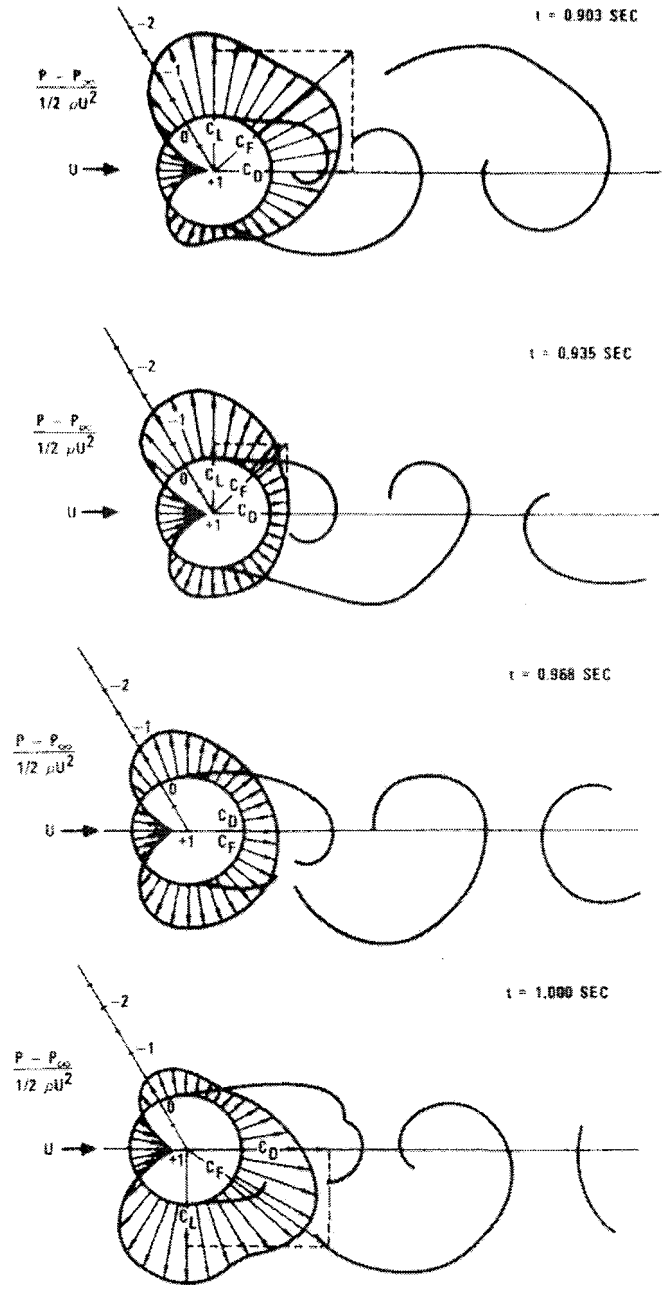

Figure 2.4: A sequence of simultaneous surface pressure fields and wake forms at Re = 1.12 x 10^5 for approximately one-third of a cycle of vortex shedding (Blevins 1986).

The overall effect is a swinging force vector with drag being the streamwise component and lift being the transverse component with changing signs. Also, the amplitudes of fluctuating drag are significantly smaller than those of fluctuating lift (Norberg, 2001). The same parameters which affect vortex shedding as mentioned above, could affect the fluctuating components of lift and drag (Paidoussis, 1982).

In addition to these fluctuating forces, there are steady forces acting on the cylinder. The steady lift force is generally zero, but there is a steady drag force due to the viscous effects of the fluid. The total forces acting on the cylinder are given by (Blevins, 1986):

$$\text{Lift Direction: } F_y = \frac{1}{2}\rho U^2 D C_L \sin(\omega t)$$

$$\text{Drag Direction: } F_x = \frac{1}{2}\rho U^2 D C_D \sin(2\omega t + \phi) + \frac{1}{2}\rho U^2 D C_d$$

where C_L is the coefficient of oscillating lift, C_D is the coefficient of oscillating drag, C_d is the coefficient of steady drag, ω is the circular vortex shedding frequency, and ϕ is a phase angle.

The fluctuating lift on a finite cylinder segment is dependent on the degree of three-dimensionality in the shedding flow close to the cylinder (Norberg, 2001). Above a critical Re, vortex shedding from nominally two-dimensional bluff bodies exhibits certain three-dimensional characteristics irrespective of how carefully the experiments are carried out (Tombazis and Bearman, 1997). Ways of quantifying the three-dimensionality include measuring the spanwise correlation length of some property related to vortex shedding such as fluctuating pressure on the cylinder surface or

fluctuating velocity in the wake. This is a very important parameter in the determination, from surface pressure measurement, of the total force experienced by the cylinder (Kacker *et al.*, 1974). It should be explained that vortices are shed in cells from stationary cylinders and the length of these cells is termed correlation length (Chen, 1987) (el Baroudi, 1960). The fluctuations are not correlated along the span of the cylinder for more than a few cylinder diameters (Zdravkovich, 1981). *Table 2.1* gives a compilation of correlation length measurements by various authors (Ribeiro, 1992).

Table 2.1: Compilation of measurements of spanwise correlation on circular cylinders (Ribeiro, 1992).

Ref.	10^{-6} Re	10^3 k/d	Regime	α'/U (%)	L_{cr}^{*}/d	L/d	d/b (%)	λ_r/d	Note
[15]	0.25–1.25	–	sub-crt	0.3	–	42.5	3.5	0.7–4.2	a
[14]	0.15–0.45	–	suber.	?		16.0	≈0.0	3.8–6.2	c
[4]	1.11	–	suber.	0.5	–	6.7	5.0	2.1	a
	2.39	–	sub-crt					1.8	a
	1.11	2.2	sub-crt					2.0	a
	2.35	2.2	superc.					3.3	a
[12]	0.42–1.0		sub-crt	≈0.5		9.0	4.2	3.2–4.5	e
[6]	0.60–3.0	–	sub-crt	0.16	–	10.0	13.1	1.3–3.2	a
[7]	0.19		suber	?	–	12.0	4.0	3.5	b
[8]	0.32		suber	1.4	–	11.0	9.1	2.5	a
[9]	0.45		suber.	0.4	–	12.9	5.6	3.3	a
[2]	3.80	1.8	ultrac.	0.5	–	6.1	11.8	3.9	a
	3.80	2.3	ultrac.					3.7	a
	3.80	2.1	ultrac.					2.9	a
[7]	0.19		suber.	11.0	1.5	12.0	4.0	2.4	b
[6]	2.3		critic	10.5	0.55	10.0	13.1	0.6	a
	2.30	–	critic.	11.0	0.19			0.4	a
[13]	0.44		suber.	2.5	9.8	38.7	3.7	3.2	a
	0.35		sub-crt	10.5	0.36			1.9	a
	0.36		suber.	10.0	4.3			2.4	a
	0.34	–	suber.	14.7	4.4			2.5	a
[8]	0.40		suber.	2.9	0.48	11.0	9.1	2.1	a
	0.27		suber.	6.4	0.79			1.8	a
	0.27		suber.	10.6	1.09			1.5	a
	0.26		sub-crt	12.8	0.79			1.1	a
[4]	1.11	–	critic.	12.9	0.50	6.7	5.0	0.6	a
	2.35	–	critic.	12.9	0.50			0.4	a
	1.11	2.2	superc.	12.9	0.50			1.6	a
	2.28	2.2	ultrac.	12.9	0.50			2.4	a
[2]	2.50	2.1	ultrac.	10.5	0.40	6.1	11.8	1.5	a

Notes:

a, b: Pressure cross-correlations measured respectively at $\theta = 90°$ and $60°$.

c, d: Velocity cross-correlations measured just outside the boundary layer respectively at $\theta = 90°$ and 2.4d downstream from the CC.

e: Batham [4] used rough CC fitted with sand grains and Ribeiro [2] used rough CC fitted with sand paper, wire screen, and ribs (tested in smooth flow) and also (tested in turbulent flow).

In this table only, d is cylinder diameter, k is roughness height, u'/U is streamwise turbulence intensity in the approaching flow, L_u^x is the streamwise turbulence length scale, L/d is the aspect ratio, d/b is the blockage ratio, and λ_z is spanwise correlation length.

Although the study is primarily focused on rigidly fixed cylinders, this is not very representative in many real problems. The oscillating forces can cause elastically mounted cylinders to vibrate and emit Aeolian tones which could be structurally and biologically detrimental. The intensity of the cross-force is greater for a cylinder vibrating at the Strouhal frequency than for a cylinder at rest (Marris, 1964). Elastically mounted cylinders create more complex problems because in addition to flow interactions leading to the vortex street, there occurs a highly complex feedback effect in the wake of the elastically supported cylinder (Goswami *et al.*, 1993). When the lift force causes transverse cylinder vibration at or near the vortex shedding frequency, this vibration has a significant influence on vortex shedding. Blevins (1990) said that the cylinder vibration could:

- Increase the strength of the vortices;
- Increase the spanwise correlation of the wake;
- Cause the vortex shedding frequency to "lock-in" to the frequency of cylinder vibration;
- Increase the mean drag on the cylinder, as it is a function of vibration amplitude;
- Alter the phase, sequence, and pattern of vortices in the wake.

As the flow velocity is changed such that the vortex shedding frequency approaches the natural frequency of the cylinder, the vortex shedding suddenly locks into the cylinder frequency such that the shedding frequency is controlled by the cylinder motion. The locked-in resonant oscillations of the near wake input energy to the cylinder so that large amplitude vibrations can be produced (*Figure 2.5*).

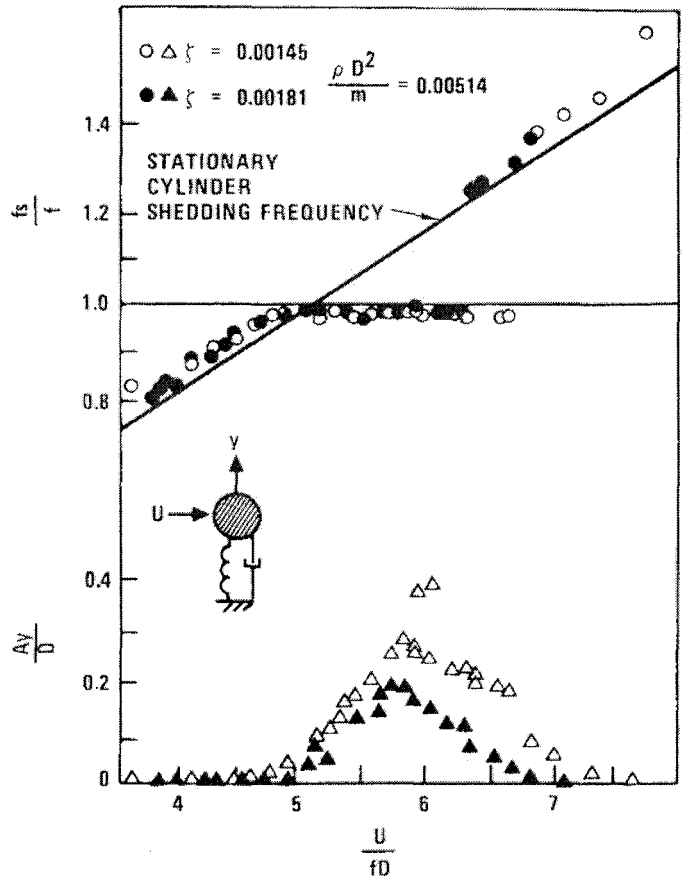

Figure 2.5: Resonance of an oscillating cylinder with vortex shedding (Blevins, 1986).

When the synchronization of the two frequencies occurs, it may persist over a 40-60% increase in velocity (Zdravkovich, 1981) depending on the damping. Within the lock-in range, experimental data shows an increase in the fluctuating lift coefficient at low

oscillation amplitudes (Chen, 1987). This is associated with the increase in strength of shed vortices over their fixed-cylinder values associated with the improved two-dimensionality of the flow and the direct effect of the cylinder movement on the flow field.

The correlation length is increased when the cylinder oscillates with an amplitude greater than a certain proportion of the cylinder diameter. This is termed the threshold amplitude (King, 1977). For crossflow oscillations, this amplitude is about 0.1D, and for in-line oscillations, it is 0.01 - 0.02D. This implies that the cylinder oscillations act to organize the vortex shedding process. Vortex formation takes place nearer to the cylinder surface, and the decrease in the Strouhal number throughout the synchronization range allows longer periods of time for vortex formation. These effects contribute to a significant increase in fluctuating lift as it has been found to increase by an order of magnitude in the upper subcritical range and almost two orders in the lower subcritical range (Zdravkovich, 1981).

If the cylinder is long compared with the correlation length, not all vortices cause forces in phase with each other, resulting in a reduction of the net oscillating force (King, 1977). Measurements of spanwise correlation showed that with increased fluctuating lift, spanwise correlation increased bringing larger portions of the flow into phase along the span (Szepessy and Bearman, 1992).

Associated with the existence of three-dimensionalities in the flow, is the sharp decay of spanwise correlation for increasing spanwise separation seen both in pressure correlation and velocity correlation measurements (Szepessy, 1994). *Figure 2.6* typifies

such observations. If the flow was perfectly two-dimensional, the hotwire signals would be fully correlated with spanwise separation.

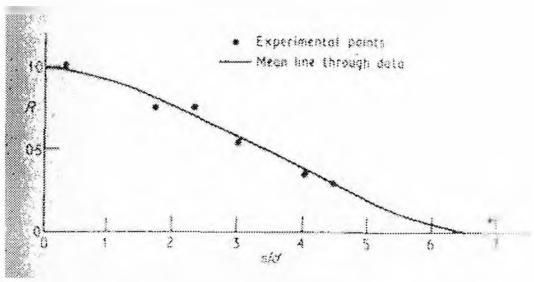

Figure 2.6: Correlation coefficient, R, as a function of separation distance, s, of the measurements on a bare tube (Kacker et al., 1974).

Since the vortex shedding frequency is constant along the span, it is expected that the decay of the correlation to be due to instantaneous differences in pressure level, small-scale turbulence and fluctuating differences in the vortex shedding phase along the span (Szepessy, 1994). However, the influence of the other factors is negligible when compared to the effect of phase drift on the main vortex shedding frequency.

Blockage ratios over a critical value have been found to affect vortex shedding. It was noted that for blockage ratios of 6%, the effects on Strouhal number were negligible (Norberg and Sunden, 1987). Ribeiro (1992) concluded that blockage ratios less than 10% did not exert an important effect on C_L. Blockage ratios larger than 10%, as far as they contribute to improve the vortex shedding organization, should exert an effect gradually greater on C_L. He suggested that experiments performed with blockage ratios larger than 15% should be accepted with reservation. It has been suggested that reliable experiments would have blockage ratios less than 10% (Weaver, 2001). Norberg and Sunden (1987) also reported that the reduction in aspect ratio had similar results to

increased blockage. With low aspect ratios, Zdravkovich (1981) stated that there was a decrease in vortex shedding frequency and an increase in the spanwise correlations of fluctuations. In Szepessy's experiments (1994), in order to minimize introducing artificial three-dimensionality to the flow, an aspect ratio of 10 was used.

When cylinders are in crossflow in wind tunnels, the boundary layers on the walls of the tunnel may have important effects. By using suitably designed end plates added to the cylinder, the effects of the wall boundary layer could be removed and cause two-dimensional flow (Stansby, 1974). In effect, it is hoped to simulate an infinitely long cylinder. With the exception of possibly high aspect ratios, end plates could cause a substantial reduction of base pressure and hence an increase in drag. Szepessy (1994) found in his experiments, that while using Stansby's end plate design recommendations, the results were not seriously affected by effects from the end plates.

The intensity and scale of the freestream turbulence promotes the transition of the separated shear layers in the subcritical regime and the transition of the boundary layers in the critical regime. The result is the shift of all three regimes towards lower Re (Zdravkovich, 1981). This could possibly explain why various authors obtained different Re for the onset of regular period shedding. The surface roughness of the cylinder produces similar effects on the transition to turbulence (Zdravkovich, 1981). Kacker and Pennington (1974) reported that freestream turbulence intensity has a significant influence on correlation length, and hence the total force experienced by the cylinder. Increased turbulence causes the point of boundary layer separation to move downstream which improves the flow over the cylinder and reduces the forces exerted on it by the

flow (Katinas *et al.*, 1991). It was seen that correlation length decreased with increasing turbulence intensity. Quantitatively, Ribeiro (1992) observed a correlation length of 3D – 4D in the subcritical regime of a smooth flow while it was reduced to 1.5D – 2.5D in a turbulent flow.

The wake behind a cylinder shedding alternate vortices is also of interest. Measurements taken by traversing probes in the wake of mean velocity and of fluctuating velocity at the fundamental frequency have been performed by many researchers. *Figure 2.7* and *Figure 2.8* shows such results (Bloor and Gerrard, 1966).

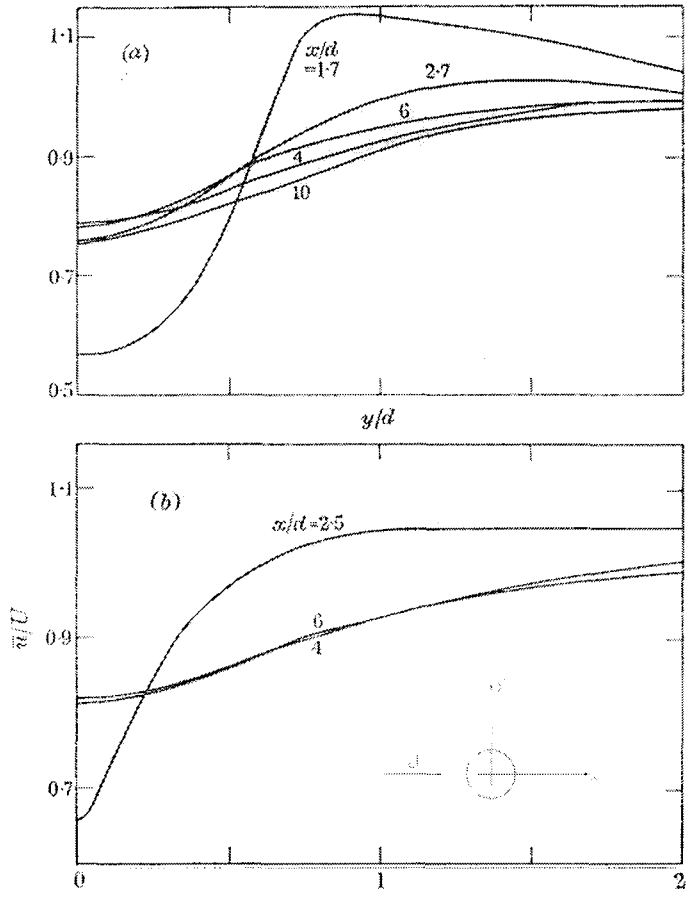

Figure 2.7: Distribution of mean velocity traverse to the wake: a) Re = 1.6 x 10^4; b) Re = 2 x 10^3(Bloor and Gerrard, 1966).

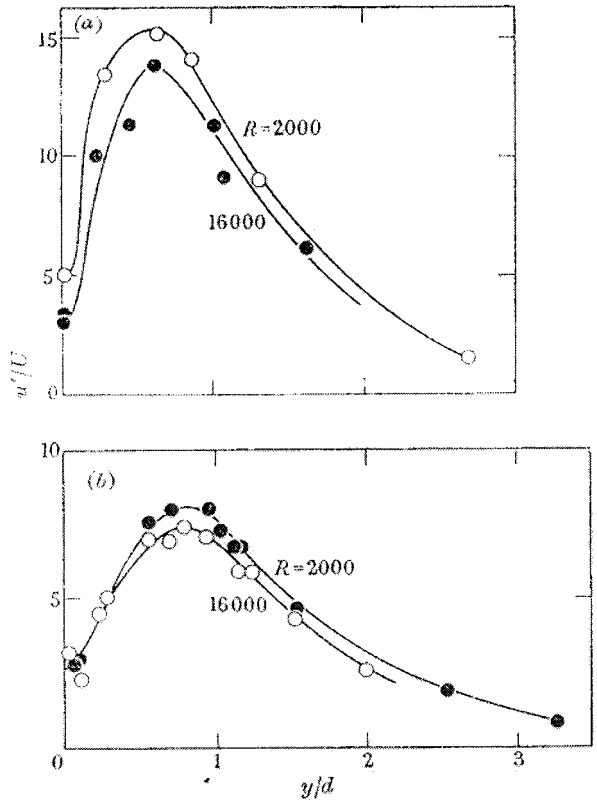

Figure 2.8: Distributions of fundamental frequency u'/U with distance perpendicular to the wake: a) x/d = 6; b) x/d = 10 (Bloor and Gerrard, 1966).

For *Figure 2.7* and *Figure 2.8*, u' was the fluctuating velocity, $\bar{u}$ was the mean velocity, U was the freestream velocity, and d was the tube diameter.

From the velocity fluctuation profiles, it can be seen that the profile flattens downstream and the peak becomes less prominent. In addition, the location of the maximum peak moves away from the centre of the cylinder as measurements were taken downstream indicating the growth of the wake. Also, the profiles were quite similar for different Re. The flattening of the profiles downstream could also be seen for mean velocity as the cylinder becomes less influential.

To reduce or eliminate vortex induced vibrations of single cylinders in crossflow, various methods have been attempted.

Avoiding resonance and lock-in is an effective strategy. This is accomplished by altering the cylinder natural frequency and keeping it ±40% away from the vortex shedding frequency (Paidoussis, 1982). If the mass or internal damping of the cylinder could be increased, resonant vibrations would diminish (Blevins, 1986). Increased damping could be achieved by permitting friction between structural elements, using composite materials, or using external dampers or bumpers. It would be preferable to always keep f_n larger than f_s so that resonance never occurs. Another possibility is to suppress vortex shedding or reduce its strength by changing the cross-section of the cylinder by such means as splitter plates, helical strakes, or perforated shrouds. Zdravkovich (1981) provides a review of the effectiveness of a number of such means. *Figure 2.9* shows the various means which were investigated.

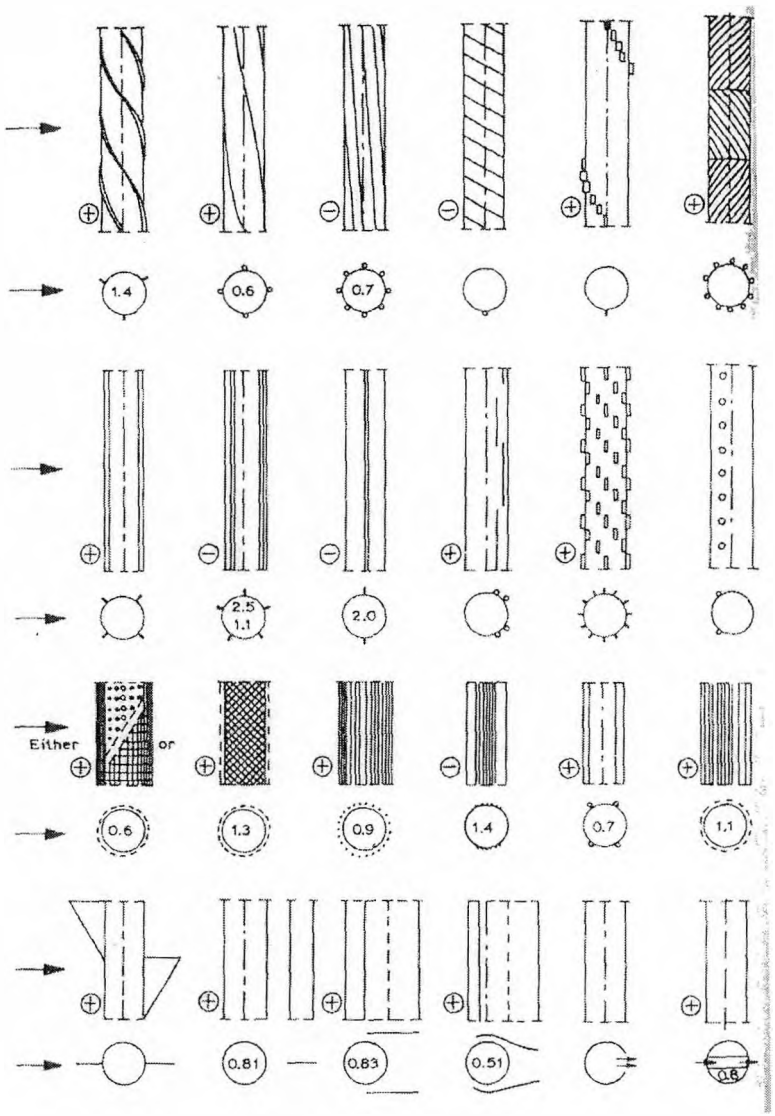

Figure 2.9: Aerodynamic and hydrodynamic means for interfering with vortex shedding (+ effective, - ineffective) (Zdravkovich, 1981).

All means were not successful. The effectiveness depended on Re, structural damping, regime of flow, the geometry of the means, and the displacement of the cylinder itself (Zdravkovich, 1981). One very interesting discovery made was that even the best means could not inhibit vortex shedding completely, but would postpone it to occur far

downstream. Measurements at 9D downstream behind a bare cylinder and a cylinder with helical strakes separately, gave better correlation for the cylinder with helical strakes (Zdravkovich, 1981). This indicated that the recovery of the vortex formation process took place farther downstream for the latter and this could be indicative of cylinders with fins.

Aeolian tones are the sounds produced by vortex shedding (Blevins, 1986). It was found that sound could exist without cylinder vibration, but its intensity was greatly increased when the shedding frequency coincided with the natural frequency of the flexible cylinder (Blevins, 1984) causing resonant vibrations. It was also discovered that if the cylinder was not resonantly excited, i.e. nearly rigid, the oscillatory sectional lift coefficient increased by two orders of magnitude over the Reynolds number range 4×10^3 to 7×10^4 and it was concluded that this effect alone was sufficient to explain the increase in radiated sound (Leehey and Hanson, 1971).

Blevins (1990) reviewed the theory of radiated sound from a circular cylinder in crossflow. Considering *Figure 2.10* (Blevins 1986), the sound pressure radiated by a vibrating cylinder could be derived.

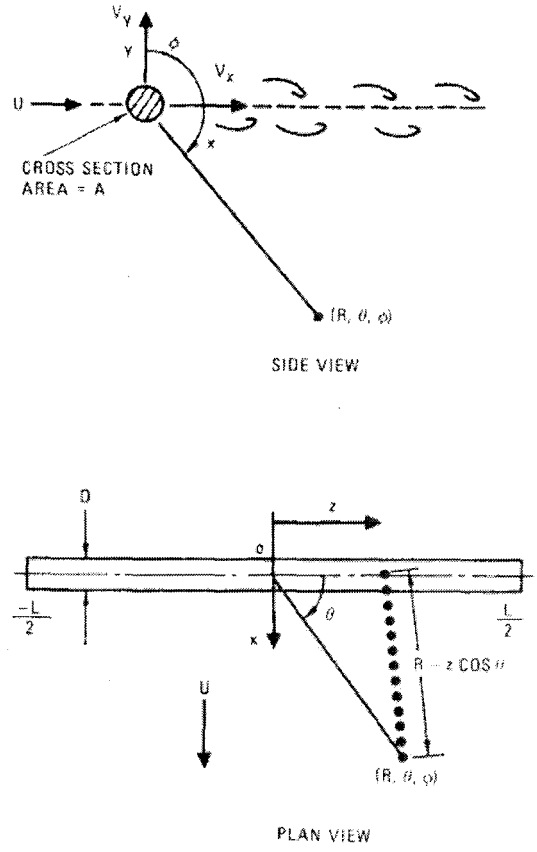

Figure 2.10: Cylinder and coordinate system (Blevins 1986).

The length and diameter of the cylinder are L and D while the flow velocity is U. A cylindrical coordinate system is employed which extends a line of length R from the axis of the cylinder to the observer of radiated sound. Vortex-induced fluid forces act on the cylinder in the lift (y) and drag (x) directions. The wavelength of the radiated sound is λ and A_y is the amplitude of cylinder vibration. Far-field assumptions were used ($\lambda >> D$, $\lambda >> A_y$, $R >> \lambda$) and the resulting expression for far-field sound pressure radiated by a vibrating cylinder is (Blevins, 1990):

$$p = \frac{\sin\theta\cos\phi}{4\pi Rc}\int_{-L/2}^{L/2}[\rho A\frac{\partial^2 V_y}{\partial t^2} - \frac{\partial F_y}{\partial t}]dz$$
$$+\frac{\sin\theta\sin\phi}{4\pi Rc}\int_{-L/2}^{L/2}[\rho A\frac{\partial^2 V_x}{\partial t^2} - \frac{\partial F_x}{\partial t}]dz$$

The total sound pressure is the sum of the sound due to the fluctuating fluid force and cylinder vibration normal to the freestream (first term), plus sound due to the fluid force and cylinder vibration parallel to the flow (second term).

For the case of a stationary cylinder with correlated vortex shedding, $V_x = V_y = 0$, the radiated sound is produced only by the fluctuating fluid forces. The far field sound pressure is then

$$p = \frac{-\sin\theta\cos\phi}{4Rc}(\frac{\sin\eta}{\eta})\rho U^3 LC_L S\cos[\omega(t-\frac{R}{c})]$$
$$-\frac{\sin\theta\sin\phi}{4Rc}(\frac{\sin 2\eta}{2\eta})\rho U^3 LC_D S\cos[2\omega(t-\frac{R}{c})+\phi]$$

where

$$\eta = \frac{kL}{2}\cos\theta = \frac{\pi L}{\lambda}\cos\theta$$

and the wave number k is

$$k = \frac{\omega}{c} = \frac{2\pi}{\lambda}$$

The sound is radiated directionally, but for this study, the cylinder length was much less than the wavelength of sound and the cylinder radiated sound like a point dipole source (*Figure 2.11*).

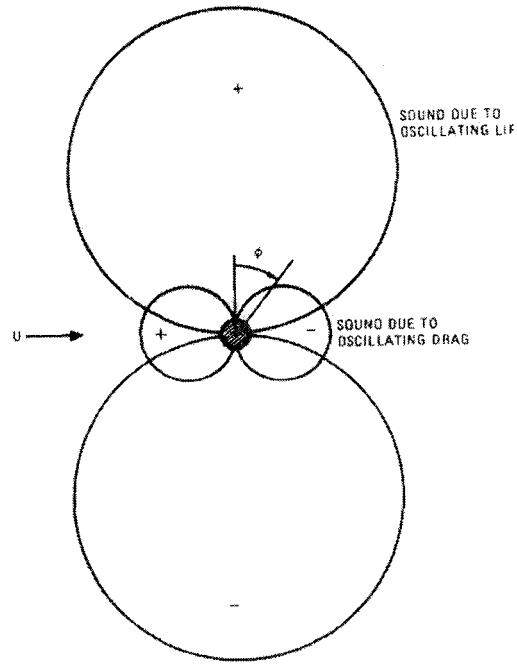

Figure 2.11: Lines of equal sound intensity for sound radiated from a cylinder (Blevins, 1986).

As mentioned before, the response amplitude in the lift direction is significantly larger than in the drag direction and as such, the sound produced by oscillating drag is negligible compared to oscillating lift.

As noted before, the spanwise correlation has a great significance for vortex-induced sound generation. At any instant, the shedding vortex sheet will not extend the full length of the cylinder. It appears that segments of much smaller length tear off. It is the average coherent length of the shedding vortex sheets that figures in the calculated strength of the Aeolian tones (el Baroudi, 1960). This average can be obtained with a procedure involving two-point correlation measurements of surface pressure or fluctuating velocity along the cylinder. The correlation coefficient is defined as follows:

$$R_{uu}(z) = \frac{\overline{u'_1 u'_2}}{\sqrt{\overline{u'^2_1}}\sqrt{\overline{u'^2_2}}} \text{ or } R_{pp}(z) = \frac{\overline{p'_1 p'_2}}{\sqrt{\overline{p'^2_1}}\sqrt{\overline{p'^2_2}}}$$

where $\overline{u}'$ and $\overline{p}'$ are the time averaged fluctuating velocity and fluctuating surface pressure respectively and the subscripts differentiates the source of the signals. The integration of this coefficient as a function of distance along the cylinder, gives a value for correlation length, λ_z:

$$\lambda_z = \int_0^\infty R(z)dy$$

Many researchers have recorded these measurements, but there is disagreement on the positioning of the probes. As the pressure measurements are taken on the surface of the cylinder, the angular position (θ) of the probes relative to the front stagnation point needs to be determined. Ribeiro (1992) noted that for the subcritical regime, for the range $60° < \theta < 120°$, R_{pp} did not change considerably and that generally, 90° was chosen. For the case of measuring fluctuating velocities, while there is much disagreement of the downstream positioning of the probes, it was generally agreed that the probes should at least be positioned outside of the boundary layer. This was located when a clear sinusoidal signal was obtained from real-time measurements. El Baroudi (1960) conducted his measurements just above the cylinder; Kacker et al. (1974) performed their measurements at 2.9D downstream, while Ribeiro (1992) reported other measurements at 2.4D downstream. *Figure 2.12* (Ribeiro, 1992) shows the locations of some of these measurements.

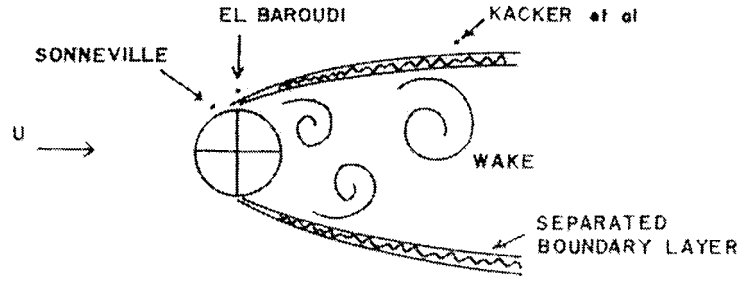

Figure 2.12: Hotwire position for measurements of spanwise cross-correlations (Ribeiro, 1992).

Szepessy and Bearman (1992) performed interesting tests by measuring the correlation between a fluctuating pressure and fluctuating velocity. Both the pressure tap and hotwire probe were positioned at 90°, with the hotwire located ⅓D above the top of the span. Conflicting results of the influence of Re on correlation length were obtained. Some results showed correlation length increasing with Re (el Baroudi, 1960) and(Predergast, 1958) while others showed the opposite trend (Kacker *et al.*, 1974).

2.2.2 Finned Tubes

To intensify the heat exchange process, finned or roughened tubes are used. The use of fins increases the heat transfer by essentially extending the bare tube surface which is more economical than increasing the number of tubes (Reid and Taborek, 1994). Initially, plain fins were generally used but with improved manufacturing techniques, segmented fins have grown in popularity. *Figure 2.13* (Reid and Taborek, 1994) shows these two types of fins.

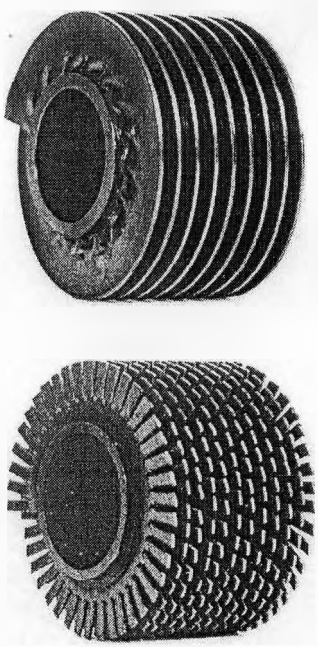

Figure 2.13: Plain fin and segmented finned tubes (Reid and Taborek, 1994).

Segmented finned tubes have several important advantages (Reid and Taborek, 1994):

- Easier to manufacture;
- The heat transfer coefficient is high because of increased turbulence and improved gas penetration to the fin root area, thus equalizing the flow velocity over the fin height. This results in a higher heat transfer coefficient (by as much as 20%);
- Higher fins are possible and fin efficiency is also improved;
- The above reasons result in a heat exchanger which is lighter and the cost is reduced.

In spite of this, the plain fin is still the most popular fin pattern used in air-cooled heat exchangers because of its superior reliability under long-term operation and its lower friction characteristics (Wang *et al.*, 2000).

The flow over finned tubes is a flow over a system of elements with a complex form determined by the configurations of the tube and fins (Sviadosch *et al.*). However, the amount of research on finned tubes pales in comparison to that on bare tubes. The following summarizes the research on tubes with segmented fins. As with bare tubes, it was discovered that an increase in upstream turbulence intensity modified the flow pattern around the tubes and resulted in a reduction of the vibrational amplitudes (Sviadosch *et al.*). Mair et al. (1975) found that for bare tubes, there was some random variation of the shedding frequency along the span of the tube, but when fins were added, there was a marked reduction in this variation and the peak in the power spectrum became correspondingly sharper. It was suggested that the presence of the fins increased the two-dimensionality of the flow.

Recalling the vortex suppression techniques reviewed by Zdravkovich (1981), it would be expected that the presence of fins would tend to disrupt the vortex shedding process. However, it was surprising that this is not the case. Experiments on tubes comparing plain fins with segmented fins twisted by a small angle were performed (Hamakawa *et al.*, 2001). They confirmed vortex shedding occurred for both cases, with the vortex shedding frequency being higher for the plain finned tube with the same root diameter and fins/inch along the span, and both frequencies were lower when compared to a bare tube with the same root diameter. Also, the vortex shedding frequency

decreased with increasing fins/inch which is equivalent to increasing the tube diameter. They also confirmed that the vortex shedding frequency was constant along the span of the tube. Correlation coefficient measurements were also taken and they showed that the spanwise correlation was larger for a finned tube when compared to a bare tube with the same root diameter. The spanwise correlation seemed to increase with the increasing number of fins/inch along the span and it was seen that for the more densely packed tubes, the correlation was greater even for a bare tube with the fin diameter. Some sample results are shown in *Figure 2.14* (Hamakawa *et al.*, 2001). This would suggest that more noise would be produced from a finned tube and also with increased fin density.

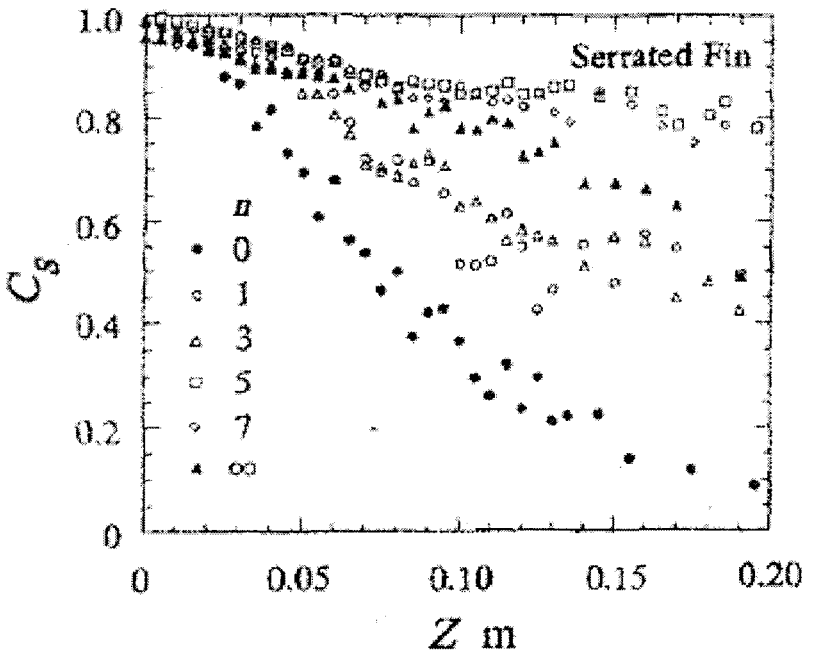

Figure 2.14: Correlation coefficient as a function of separation distance of the measurements on a finned tube (Hamakawa et al., 2001).

2.3 Vortex Shedding and Tube Banks

2.3.1 Vortex Shedding Excitation in Tube Banks

Depending on tube spacings, as well as other system parameters such as upstream turbulence, vortex shedding may or may not exist in the tube bank. When this periodic excitation mechanism did exist, as the flow velocity was increased, so did the vortex shedding frequency, f_s, and as it approached the natural frequency of the tubes, f_n, excessive vibrations occurred in this resonance situation. In the case of bare (Zukauskas and Katinas, 1979) and finned-tube banks (Mair *et al.*, 1975), vortex shedding frequency is a function of pitch ratio and flow velocity and it was observed that vortex shedding frequency was much higher for finned tubes than bare tubes (Katinas *et al.*, 1991). If the flow velocity was increased further, f_s would remain equal to f_n and would be said to be locked-in such that the tube natural frequency controlled the vortex shedding frequency. Eventually vortex shedding excitation reappears when the velocity is increased sufficiently. This can be seen in *Figure 2.15* (Weaver and Fitzpatrick, 1988).

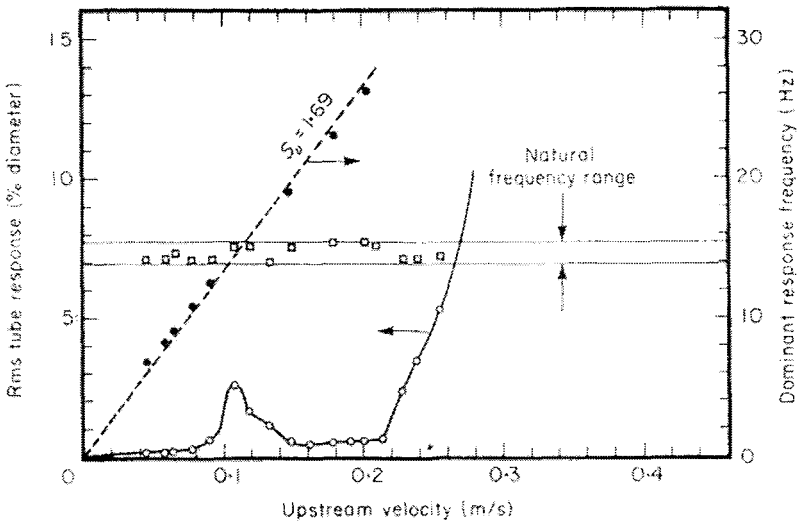

Figure 2.15: Tube amplitude and frequency response, normal triangular array in water, pitch ratio 1.5 (Weaver and Fitzpatrick, 1988).

Besides excessive vibrations at resonance, other observations have been made by a number of researchers. According to Paidoussis (1982), vortex shedding in the interstitial flow within the first few rows of bare-tube arrays did commonly occur, unless the upstream turbulence level was sufficiently high to suppress it. However, deep within the array, vortex shedding may or may not survive, depending on Reynolds number, cylinder layout geometry, and cylinder vibration amplitude. He also reported that the spanwise correlation drastically increased with cylinder motion. Zukauskas and Katinas (1979) observed that the highest amplitude occurred in the leading rows of both in-line and staggered bare-tube banks while Katinas et al. (1991) discovered similar findings for finned-tube banks. In the paper by Mair et al. (1975), it was noted that the frequency of audible vibrations produced by finned-tube banks increased continuously with flow velocity, in contrast to the behaviour found with bare tubes.

Over the years, attempts have been made to neutralize these resonant vibrations. Approaches used have included suppressing vortex shedding by increasing the upstream turbulence in the flow. Weaver and Fitzpatrick (1988) have reported that the use of turbulence grids could suppress vortex shedding although some grids have been known to be ineffective. Their effectiveness was attributed to their ability to break up the correlation of the fluid forces on the cylinders (Paidoussis, 1982). Paidoussis (1982) also reported that turbulators be used at least for tightly spaced arrays so that vortex shedding resonances could be suppressed altogether. He believed that the same effect would be unlikely for more widely spaced arrays. It would be expected that the use of turbulators for finned-tube banks would achieve the same results since Katinas et al. (1991) observed that the amplitudes of vibrations decreased with increased upstream turbulence.

Weaver and Fitzpatrick (1988) and Paidoussis (1982) have both suggested structural changes such as changing natural frequency of the tubes so that it does not coincide with the vortex shedding frequency. Paidoussis (1982) said that if the Strouhal number was known fairly accurately, $\frac{U_0}{f_n D}$ should be ±40 or ±50% away from S^{-1}.

2.3.2 Acoustic Resonance in Tube Banks

Acoustic resonance has been observed in heat exchanger tube banks with tubes in-line and staggered, in tube rows, in helically coiled heat exchangers, in boilers, in power plants, in rectangular shell heat exchangers, and in cylindrical shell heat exchangers (Blevins and Bressler, 1987).

When the vortex shedding frequency approaches the acoustic natural frequency of a transverse bound acoustic mode, a resonance can occur. The acoustic mode is primarily associated with acoustic fluid velocity perpendicular to both the tube axis and the flow and decays outside of the tube bank (Blevins and Bressler, 1987). This results in intense sound amplification and large fluctuating pressure levels on the containing walls. The deafening sound levels that could result from this kind of resonance could cause ear damage and can also be structurally harmful if these frequencies coincide with the natural frequencies of any of the structural components such as the tubes or walls. A standing wave can also affect the performance characteristics of the heat exchanger by increasing pressure drop through the resonant section. *Figure 2.16* (Blevins and Bressler, 1987) shows the turbulence spectra of an array before and during resonance where it could be seen that resonance strengthens the vortex shedding peak.

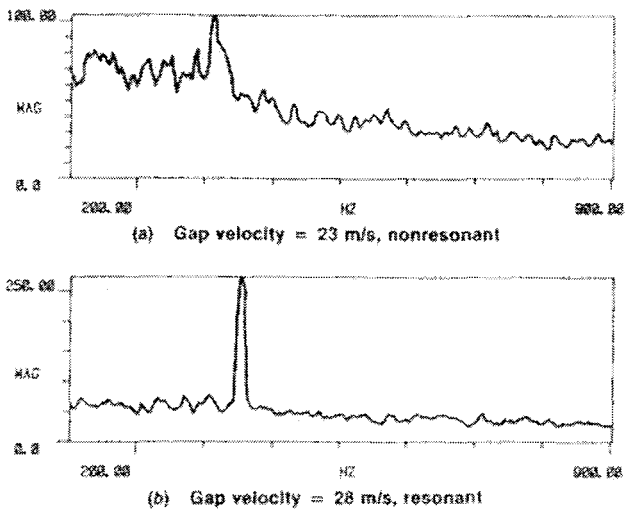

Figure 2.16: Spectra of hotwire anemometer signals within bundle in 196-tube triangular array (Blevins and Bressler, 1987).

Blevins and Bressler (1987) also made the observation that tightly spaced tube bundles were generally quieter than more widely spaced arrays. In addition, they realized that during resonance the vortex shedding from all tubes in the bank became highly correlated with the generated sound and that the tubes shed vortices in unison. Similar results were obtained for fin-tube banks (Kouba, 1986). Weaver and Fitzpatrick (1988) further confirmed the bare-tube results noting that sound levels of 162 dB could correlate vortex shedding along the length of the cylinder resulting in a 6.5 increase in the force exerted on the cylinder. Also, if resonance with an acoustic mode was established, then periodicity was strong and omnipresent (Paidoussis, 1982). Sound levels as high as 173 dB have been reported in the literature for bare tube banks (Blevins and Bressler, 1987) while levels as high as 160 dB were measured for twisted-finned tube banks (Fan, 2002). This suggested that the fins had little effect on disrupting vortex shedding and thus avoiding acoustic resonance.

Other experiments comparing bare-tube banks and finned-tube banks under acoustic resonant conditions have been performed (Nemoto and Yamada, 1992; Nemoto and Yamada, 1994). They concluded that no special airflow generated sounds due to fins were produced in the horizontal direction normal to tube axes. In both types of banks, some resonances consisted of both a transverse and lengthwise mode. Also, acoustic resonance in finned-tube banks showed no special phenomena due to the fins. In some cases, while acoustic resonance occurred in bare-tube banks, no such resonance occurred in finned-tube banks. They believed this to be attributed to lower sound to noise ratios for finned-tube banks (noise levels were about 5 dB higher)

Given the possible damage resulting from acoustic resonance, efforts have been made to avoid or at least reduce the problem. As in the case for vortex induced vibrations, similar vortex shedding suppression techniques have been employed. In the cases where acoustic resonances can not be avoided, the most successful solution is the use of antivibration baffles. The baffles would be placed parallel with the flow and perpendicular to the direction of the standing waves (Eisinger, 1980). These baffles were located so as to increase the transverse acoustic natural frequencies well above any excitation frequency (Weaver and Fitzpatrick, 1988). Nemoto and Yamada (1992, 1994) showed that this method was effective for finned-tube banks as well. One problem with using baffles is that no cooling is provided and this limits the lifespan of the baffle. So it was suggested that fin barriers could be used. The fins would be welded longitudinally to the tube and the tubes would be arranged to form a fin "wall" parallel to the direction of the flow (Eisinger, 1980). Other remedial actions to detune the excitation include using unequal longitudinal pitches in successive rows and removing some tubes in the array (Paidoussis, 1982).

2.4 Research Objectives

Given that flow induced vibrations can give rise to serious structural and biological problems in many industrial applications, it is only prudent to gain a fundamental understanding of the source of these problems in order to facilitate sensible designs. As with bare tubes, vibration problems have been observed in heat exchangers incorporating

finned tubes, and with the scarcity of research on this topic, it was decided that there was a need to expand the knowledge base of the flow characteristics of finned tubes in crossflow.

Therefore, there is a need to understand the effect of fins on vortex shedding for the simplest case, which is an isolated cylinder in crossflow. As there is an abundance of literature for a single bare tube in crossflow, and as a finned tube can be simply described as a bare tube with fins, the proposed research will be compared to the bare tube to discover what effect, if any, that the fins have on the velocity fluctuations and correlation length. It is believed that without improving our understanding of this simple case, there is little chance that the mechanisms of vortex shedding and acoustic resonance in finned tube banks can be understood.

Chapter 3

3 Experimental Setup

In order to investigate the flow over single tubes, it was decided that the experiments would be performed in an open-circuit, subsonic wind-tunnel equipped with a variable speed controller. Four tubes were selected for testing which involved exposing the tubes to different flow speeds and taking hotwire measurements at various spatial locations with the aid of a computer controlled traversing mechanism. These measurements were used to investigate the wake characteristics and potentially yield information about the noise which could be generated by the tubes.

3.1 The Tubes

Of the four tubes selected for testing, three were segmented-finned tubes of different fin densities and the other was a bare tube which was considered to be a baseline against which the finned tubes could be compared (*Figure 3.1*). The finned tubes had the same tube diameter as the baseline bare tube.

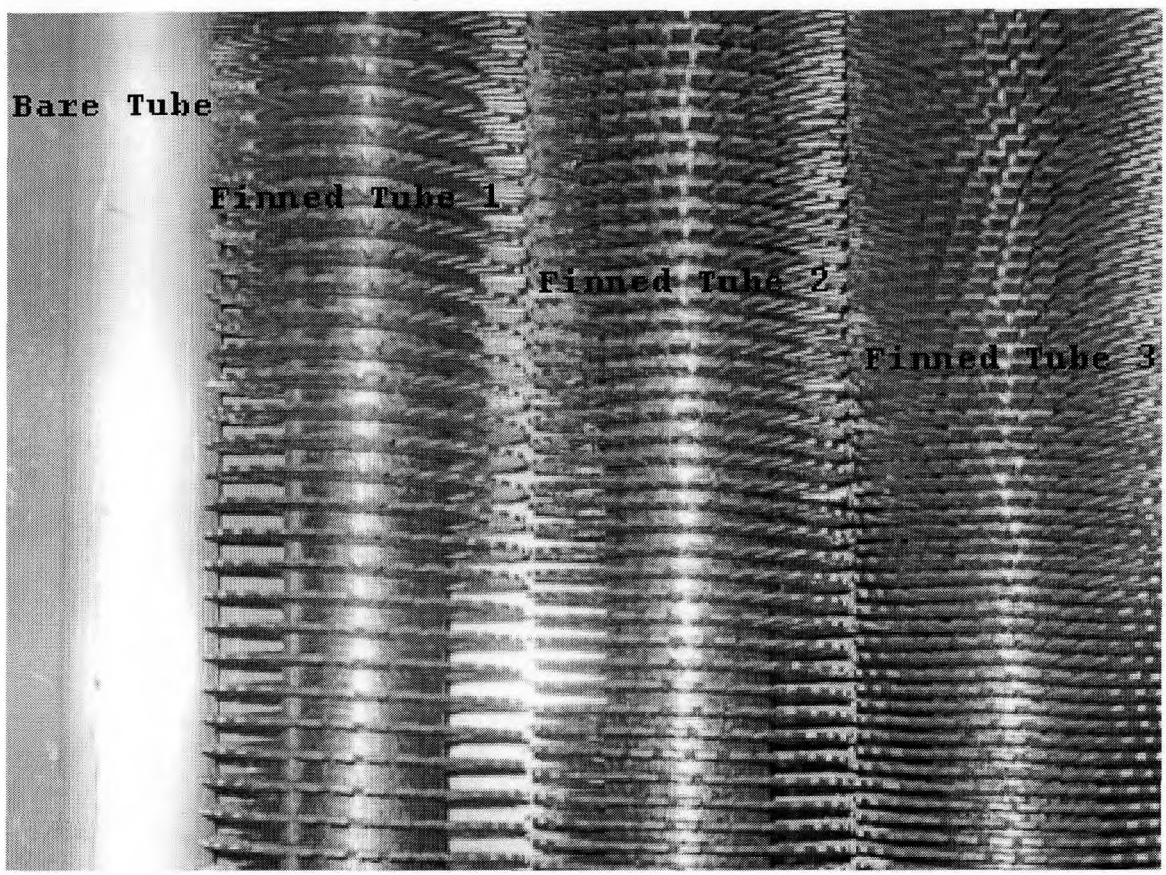

Figure 3.1: The four tubes used for the investigation.

The finned tubes were provided by Foster Wheeler Corporation which were actual full-sized tubes used in Heat Recovery Steam Generators (HRSG). The tubes were made of steel, with the segmented fins being helically wound along the axis of the tube. The specifications of these tubes can be found in *Table 3.1* and *Figure 3.2*.

Table 3.1: Physical specifications of the test tubes.

	Bare Tube	Finned Tube 1	Finned Tube 2	Finned Tube 3
Length, L (inch)	21.5	21.5	21.5	21.5
Bare Tube Diameter, D (inch)	1.5	1.5	1.5	1.5
Fin Thickness, t (inch)	-	0.05	0.05	0.05
Fins/inch	-	3.5	5	7
Fin Height	-	0.75	0.75	0.75
Fin Spacing, s (inch)	-	0.286	0.200	0.143
D_f (inch)	-	3	3	3
D_e (inch)	1.5	1.7625	1.875	2.025
Blockage Ratio (%)	6.76	7.94	8.45	9.12

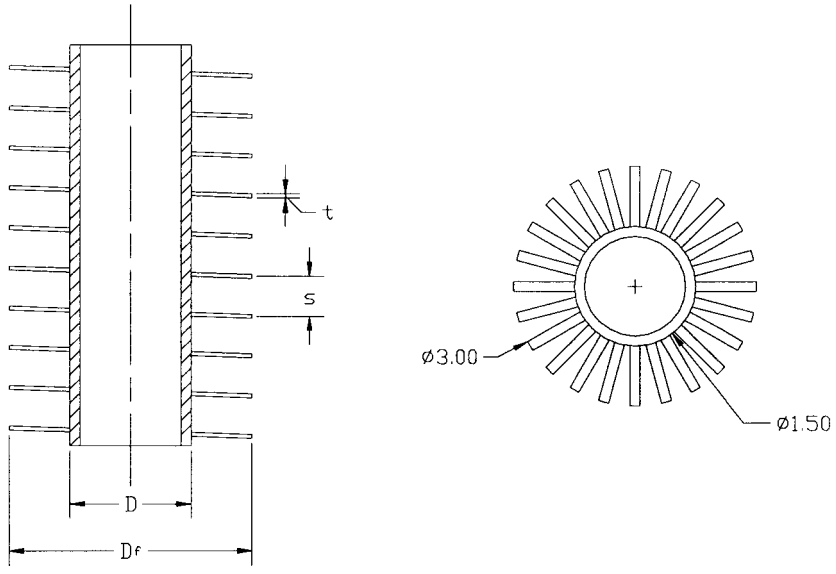

Figure 3.2: Longitudinal and transverse cross-sections of a finned tube (all dimensions in inches).

As seen, a finned tube has two characteristic diameters (D and D_f) and neither is quite correct to use as the characteristic length. As fins are added to a bare tube, this has the effect of increasing the cross-sectional area of the tube above that of a bare tube with diameter D, but less than that of a bare tube with diameter D_f. The equation proposed by Mair et al. (1975) takes this into consideration to formulate a characteristic length known as the effective diameter (D_e). Referring to *Figure 3.2*:

$$D_e = (1/s)[(s-t)D + tD_f]$$

This has the effect of equating the cross-sectional area of the finned tube to the cross-sectional area of a bare tube with diameter D_e. However, this estimation does not take into consideration the helix angle of the fins or how the fins affect the flow over the tube.

The bare tube was made of aluminum with its outer diameter being the same as the base diameter of the finned tubes. There were two primary reasons for selecting the bare tube for testing. First, the present experiments for the bare tube could be compared with published results and thereby validate the used experimental procedure. The second reason was as a result of the scarcity of literature on the flow characteristics over single finned-tubes. Hence, it was decided that the results from the bare tube could be used as a baseline with which to compare the results from the finned tubes.

3.2 The Test Section

An open-circuit, subsonic wind-tunnel was used during the investigation. Air was forced through the tunnel by means of an axial fan operated by a DC motor and a speed

controller. This equipment was capable of achieving a maximum flow velocity of 30 m/s. The tests performed occurred over a Reynolds number range (based on D_e) of 2.61 x 10^4 to 4.98 x 10^4 which is clearly in the sub-critical flow regime and where the vortex shedding process can be considered turbulent.

Of particular interest is the 27 inch long test section, as it was specially designed to facilitate the investigation of the available tubes. As seen in *Figure 3.3*, the cross-section of this section was octagonal in shape with the walls made of ¾ inch thick clear acrylic. The perpendicular distance between the flats of the section was 24 inches with the tube being rigidly mounted across the middle of the section.

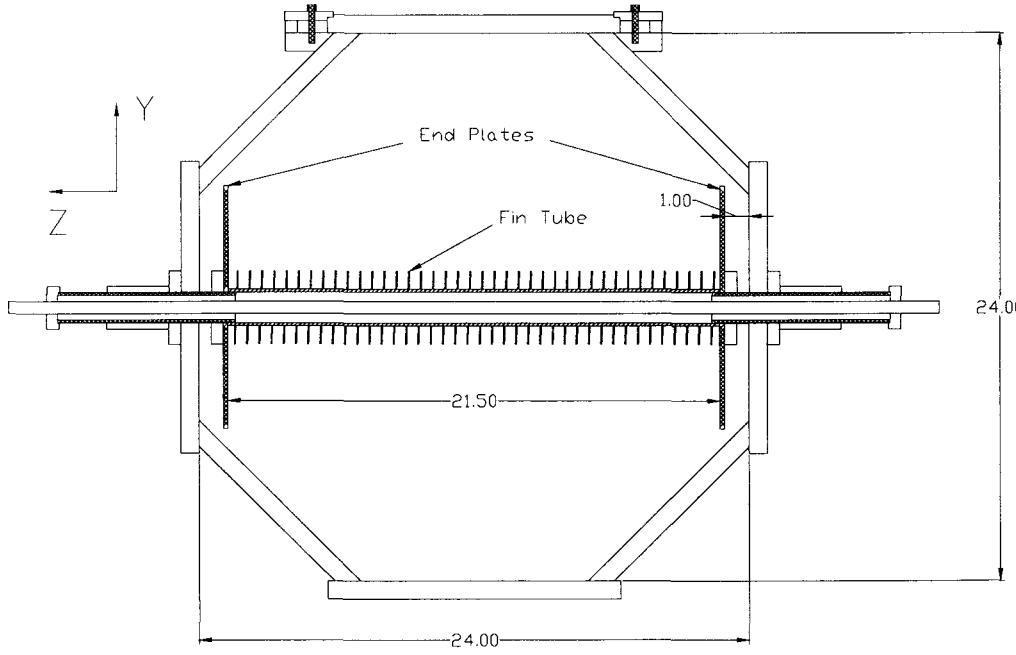

Figure 3.3: A cross-section of the test section (all dimensions in inches).

The tube was held rigidly in place by clamping between two end plates which were supported by the vertical sides of the test section. The details of the supporting system are shown in *Figure 3.4*. It should also be noted that the blockage ratios for these

experiments varied from 6.75% for the bare tube to 9.12% for the densest finned tube which were within the generally accepted blockage ratio range.

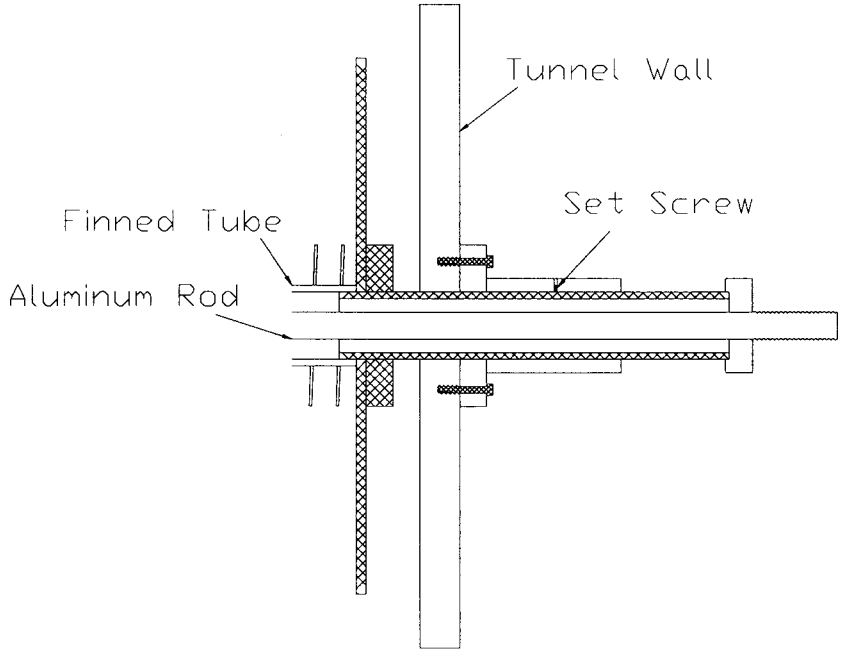

Figure 3.4: An enlargement of the supporting system for the tube.

It should be noted that end plates were mounted at both ends of the tube to reduce three-dimensional flow effects due to the boundary layer on the tunnel wall. The plates were designed following the guidelines provided by Stansby (1974) and were located at least ¾ of an inch away from the tunnel wall to ensure that they were outside of the boundary layer. As shown in *Figure 3.5*, the end plates were constructed of 3/16 inch thick clear acrylic, and depending on the tube in use, corresponded to a range of $2.96D_e$ – $4D_e$ from the leading edge of the plate to the axis of the tube and a range of $3.95D_e$ – $5.33D_e$ from the trailing edge to the tube axis.

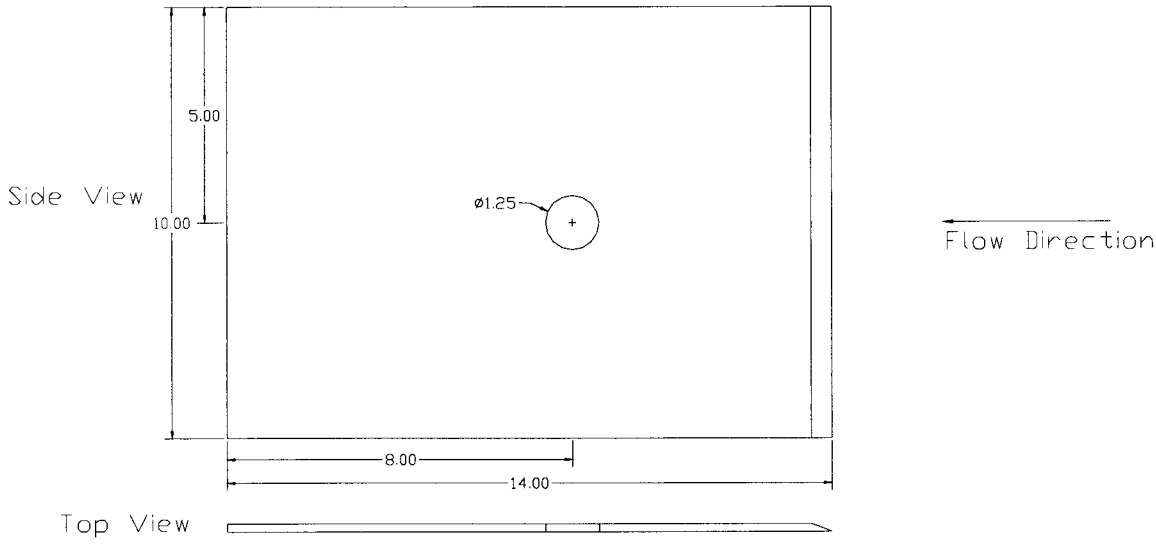

Figure 3.5: Top and side view of the end plates (all dimensions in inches).

In *Figure 3.6*, a cross-section of the side view of the test section can be seen in which the tube axis was located 3.5 inches from the front of the test section. This was done to allow for the largest possible downstream region in which the measuring equipment could be positioned.

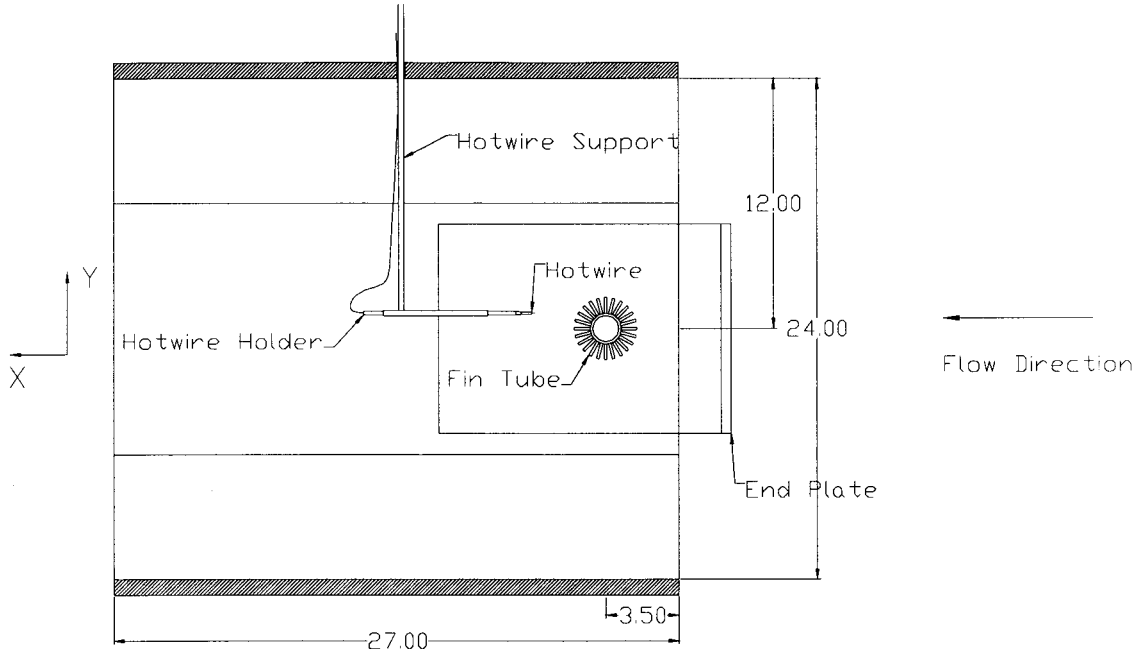

Figure 3.6: Cross-section of the side view of the test section (all dimensions in inches).

As it was required to take measurements in the wake of the tubes at various downstream distances, this posed a problem in that the hotwire support protruded through the top of the section making it difficult to traverse the support in both the downstream and axial directions while keeping the section airtight. It was decided that the top plate should be divided into a number of smaller plates as shown in *Figure 3.7*.

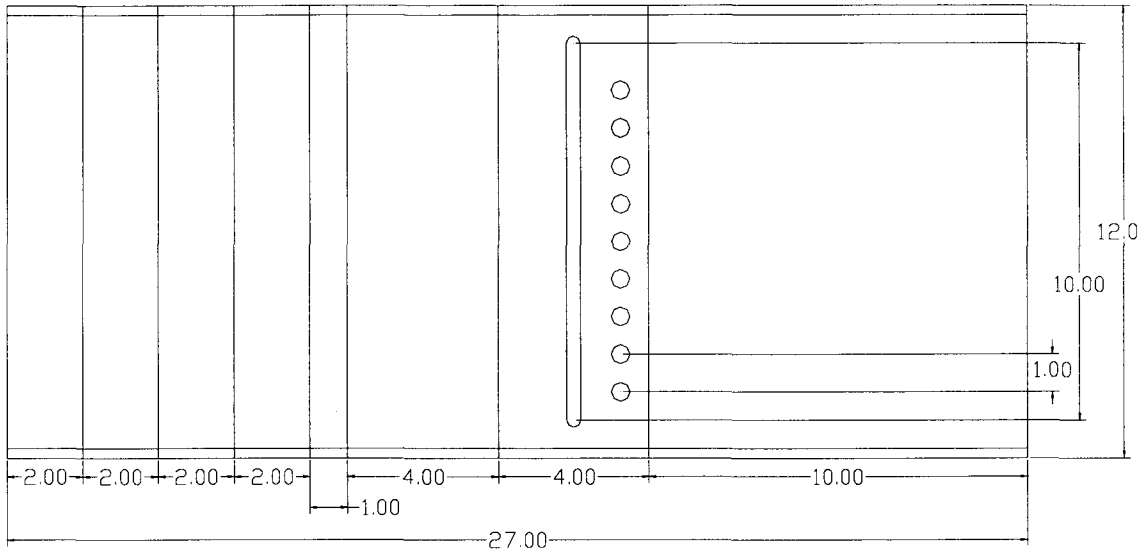

Figure 3.7: A view of the top section of the test section (all dimensions in inches).

A slot was machined in the axial (i.e. the spanwise) direction of one of the 4 inch plates to allow for the hotwire support to be moved. In order to maintain a seal, the mouth of a plastic bag was taped around the slot and the hotwire support passed through a small hole at the other end which was also taped. The lengths of the smaller plates allowed for the hotwire support to be moved in the downstream direction in 1 inch increments. If smaller adjustments were needed, this could be accomplished by adjusting the position of the hotwire holder within the hotwire support. When the appropriate adjustments were made, the plates were then clamped into place.

3.3 The Traversing Mechanism

As all of the measurements required involved positioning the instrumentation at various spatial points, a three-axis traversing mechanism was employed (*Figure 3.8*) and was positioned above the test section.

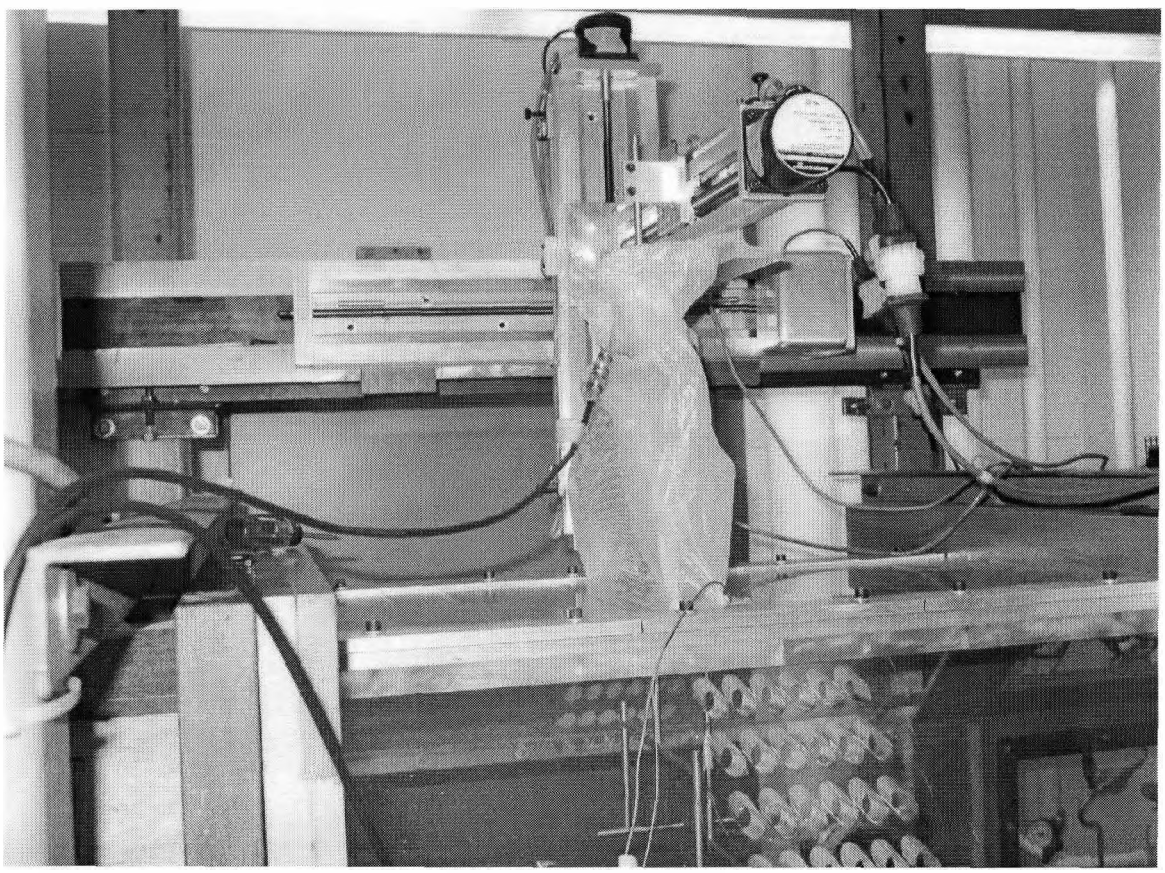

Figure 3.8: Traversing mechanism position above the test section.

This UNISLIDE device (Model # MB4018Q2J-S4) was driven by three stepper motors which were controlled by a programmable stepping motor controller (NF90 Series made by Velmex Inc.). The controller could be programmed using National Instruments Labview software which could be used to facilitate simple unidirectional movements or

complex multidirectional paths and has a resolution of 0.005mm (0.0002 inches). During testing, the traverse was moved from point to point manually to be able to scrutinize the results as they were collected to ensure that there were no obvious problems with the equipment and therefore avoid re-testing.

Hotwire supports were affixed to the traverse via a specially machined connector. Four supports of different geometries were made as was required by the various tests performed (*Figure 3.9*).

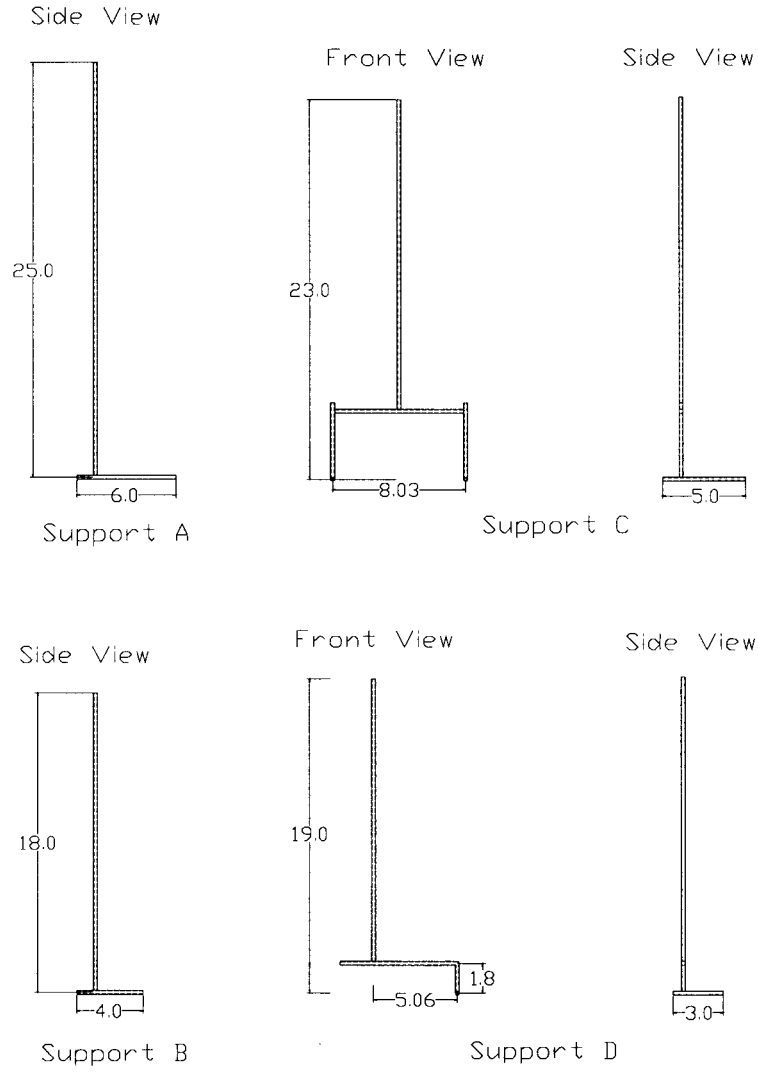

Figure 3.9: Hotwire supports used during the investigation (all dimensions in inches).

Supports A and B were simple L-shaped supports while supports C and D were more complex. All supports were constructed from ¼ inch stainless steel tubing with the inside diameter being larger than that of the hotwire holders so that they could be fixed with set screws.

3.4 Hotwire Anemometry

All measurements taken throughout this investigation were hotwire velocity measurements. Two Dantec 55P11 hotwire probes were used which were each connected to one-channel Dantec 55M10 CTA Standard Bridges employing an overheat ratio of 0.7. The signals from the hotwire probes were digitized using a National Instruments PCI-6024E, 8 channel, 12 bit, simultaneous sampling data acquisition system. This hardware is shown in *Figure 3.10.*

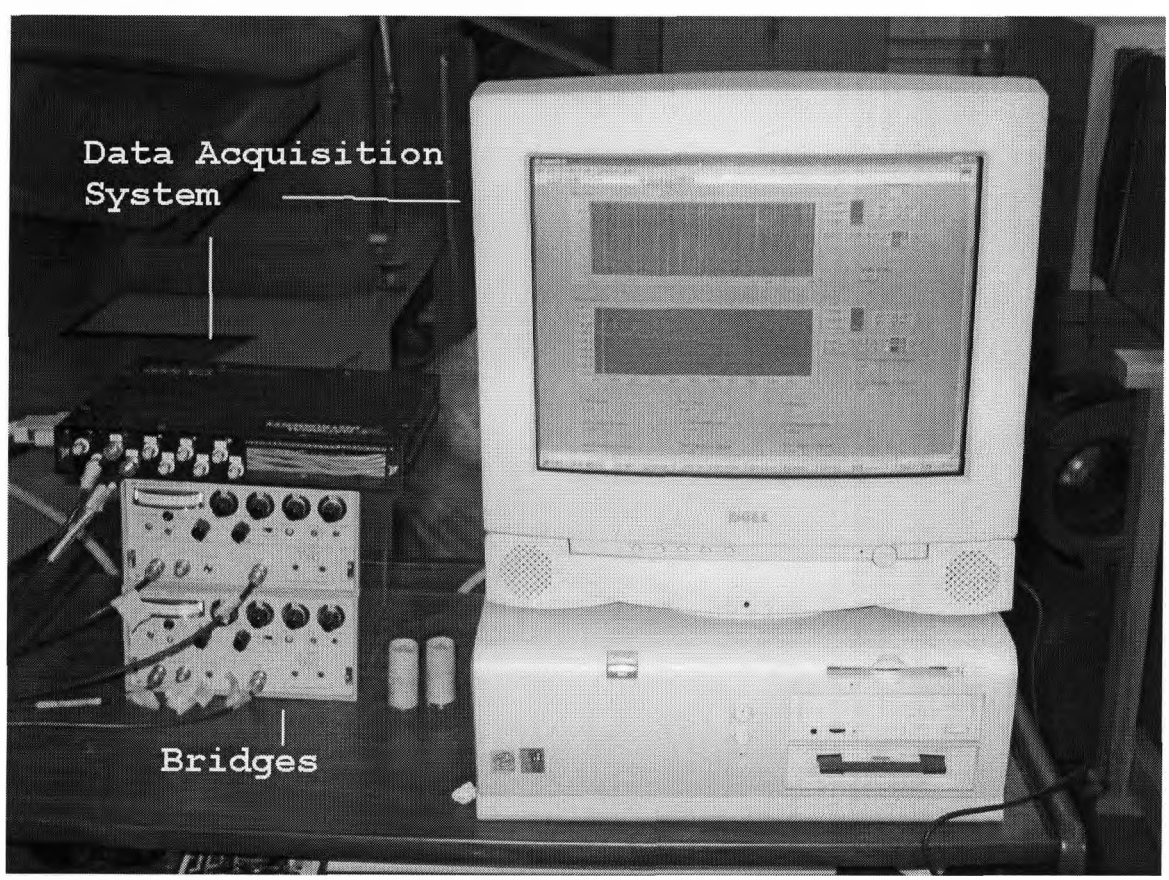

Figure 3.10: Hotwire anemometry equipment.

The data was collected using a real-time Labview program which was able to display and record time-signals, power spectrum, and fluctuating velocities for each channel, as well

as the correlation coefficient between the two signals. The signals were sampled at 1024 Hz with the data being collected in 0.5 second blocks resulting in a spectral resolution of 2 Hz. A copy of the Labview program which was designed and employed can be found in Appendix B.

The signals detected by the hotwire probes were measured in volts. These measurements were not very useful unless they were linearized. This was accomplished by first calibrating the hotwires and inputting this data into Labview so that the time signals were in velocity rather than volts.

The hotwire calibration was performed in the wind tunnel. Firstly, the tube and end plates were removed. Two hotwire holders and probes were then used with hotwire support C (*Figure 3.9*) and were positioned in the centre of the cross-section close to a pitot tube. The speed of the motor was increased while recording of both hotwire voltage and pitot pressure which was later converted to velocity. As hotwire probes are quite sensitive instruments, it is well know that calibrations stray with changes in temperature and also with the buildup of dust and other particles on the wire. As a result, throughout the course of this investigation, many calibrations were recorded and used to compensate for any temperature changes.

3.5 Flow Tests

Two kinds of flow tests were performed from which mean velocity wake profiles, total turbulence intensity wake profiles, vortex shedding intensity wake profiles, and

correlation length were determined. Mean velocity was obtained from the mean signal of the hotwire, turbulence intensity was based on the total RMS amplitude of the signal, while the vortex shedding turbulence intensity was the RMS amplitude at the vortex shedding frequency. The correlation coefficient was determined by comparing the fluctuating signals from two hotwires. As it was desirable to know how the results would change with Reynolds number and downstream distance, two Reynolds numbers and originally two downstream distances were chosen. Both the low Reynolds number (approximately 2.61×10^4) and high Reynolds number (approximately 4.69×10^4) were chosen to both be in the subcritical regime where the vortex street is fully turbulent. The downstream distance of $2.5D_e$ was chosen because as mentioned earlier, a number of researchers performed correlation length measurements on bare tubes in the x = 2.4D – 2.9D region and it was desirable to have results which could be compared to available literature (such as Ribeiro (1992)). The distance of $x = 5D_e$ was chosen simply because it was farther downstream and the wake would be more developed.

3.5.1 Wake Profiles

Obtaining wake profiles involved using just one hotwire probe and hotwire support A with the setup being similar to *Figure 3.6.* When the hotwire was in the appropriate position downstream and $2.53D_e$ – $3.41D_e$ from the tube axis in the transverse direction, and the velocity was set using the pitot probe, the hotwire was traversed in the transverse direction by 1cm (0.39 inches) increments initially becoming smaller as the hotwire approached the tube axis. With this procedure, the entire wake at that

downstream distance was mapped and was repeated for all Reynolds numbers, distances, and tubes. Data at each point was recorded while taking 100 averages and was plotted to give wake profiles.

After these results were obtained and analyzed, it was realized that further wake profiles were required for finned 3 to observe the development of the wake. Profiles were also taken at x = $1.5D_e$, $3D_e$, and $4D_e$. In addition, wake profiles at x = $1D_e$ were taken for all four tubes in order to investigate if the local effects of the fins could be detected.

3.5.2 Correlation Length

To measure correlation length required both hotwire probes and the use of two hotwire supports. Correlation length is generally measured by placing the two hotwires as close as physically possible together at a particular downstream point, and then moving one hotwire (called the roving wire) away from the stationary wire in the axial (z) direction (*Figure 3.11*).

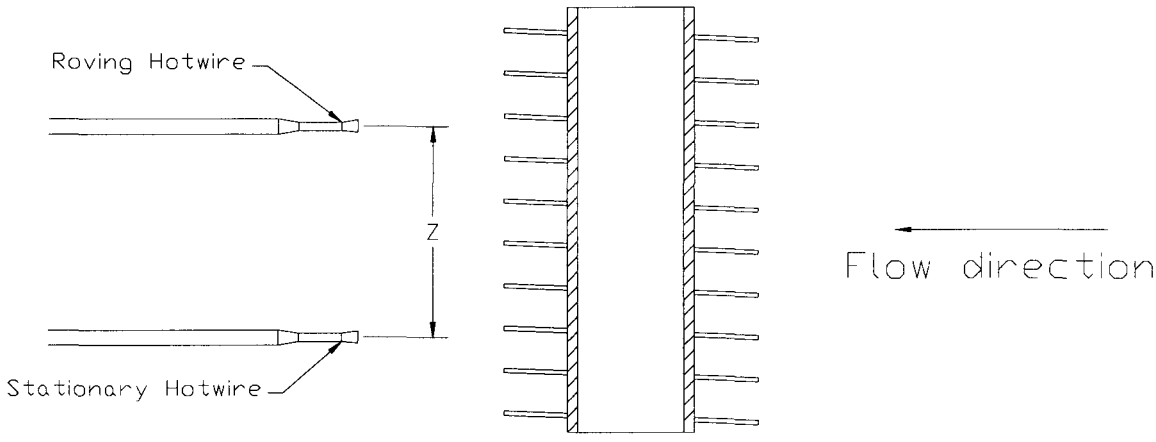

Figure 3.11: The method of measuring correlation coefficient.

At various points during this process, the correlation coefficient was recorded and then plotted against a non-dimensionalized separation distance with the area under the graph giving correlation length.

However, as mentioned in the literature survey, there is a lack of consistency and also a lack of detail as to where the hotwires were positioned in previous research. The only consistent parameter was that the hotwires were positioned outside of the wake.

For this investigation, it was decided that it would be helpful to know how the correlation coefficient varied as the hotwires were positioned at various transverse positions. This was done at three separation distances between the wires and for the bare tube and one finned tube. The results were similar for both cases with the bare tube results shown in *Figure 3.12* and the finned tube in *Figure A.20.* y/D = 0 corresponded

to the tube axis and the values increased as the hotwire was traversed in the transverse direction.

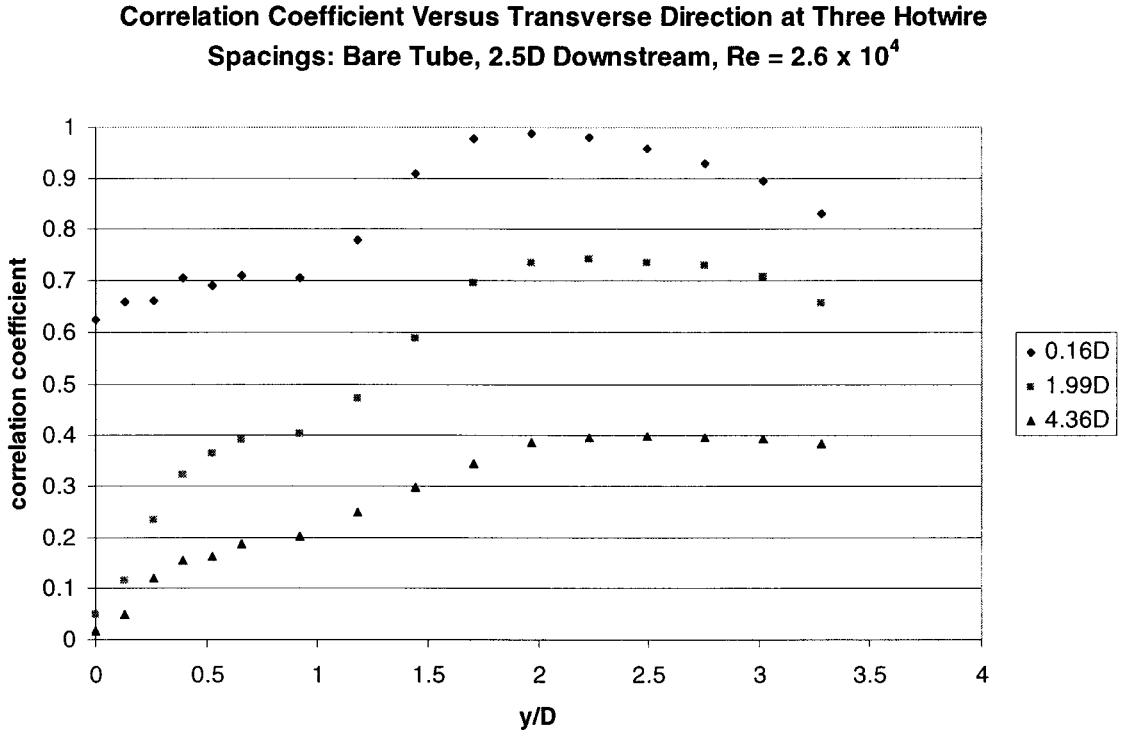

Figure 3.12: How correlation coefficient varies in the transverse direction.

It can be seen that the correlation coefficient peaks at approximately the same transverse distance for the three separation distances between the wires. It was thus decided that in order to be consistent, all correlation length measurements would be taken at this maximum point which in all cases was barely outside of the shear layer. In this particular case, the measurements were taken at $y/D \approx 2$. It should be noted that this distance varied from test to test depending on the tube, Reynolds number, and streamwise location.

It should be noted that in this investigation, all correlation coefficients were calculated using Labview and the following equation (Bendat and Piersol, 1980):

$$R_{xy}(0) = \frac{C_{xy}(0)}{\sqrt{C_{xx}(0)C_{yy}(0)}}$$

where x(t) and y(t) represent the two time varying signals and C_{xy} is the cross-correlation function and C_{xx} and C_{yy} are the auto-correlation functions. τ is the time delay and μ_x is the mean value of x.

$$C_{xx}(\tau) = \underbrace{\lim}_{T\to\infty} \frac{1}{T} \int_0^T \{x(t) - \mu_x\}\{x(t+\tau) - \mu_x\} dt$$

In addition, it should be noted that the hotwire support for the stationary probe was fixed to the 4 inch plate with the machined slot so that whenever the plates at the top of the section were moved, both hotwires would be moved the same distance. There were nine possible positions for the stationary probe as there were nine holes spaced 1 inch apart, which were parallel to the slot and these could be used to fix the hotwire support.

When correlation coefficients were being measured, either supports A and B were used together, or supports C and D (see *Figure 3.9*). Due to the geometry of the cross-section of the test section, the use of supports C and D could allow for a larger distance traversed in the axial direction and thus larger separation distances. Support D allows for the stationary probe to be placed closer to the end plate while support C could enable a similar situation with the other end plate.

To verify that the chosen position for the stationary hotwire was not influenced by end effects, correlation measurements were performed on the bare tube at x = 2.5D and at low Reynolds number while changing the axial position of the stationary probe. Moving the stationary probe from 1.75D away from the end plates to 4.42D resulted in a 4%

change in the correlation length. It was found that changes in axial position had little effect on the results. So during the tests when support D was in use, the stationary probe was located $1.3D_e - 1.75D_e$ away from the end plate.

As with the wake profiles experiments, correlation length measurements were performed for all tubes at both Reynolds numbers and downstream distances.

Chapter 4

4 Results & Discussion

In this chapter, the results obtained from experimentation will be presented and discussed. As noted earlier, the results from the bare tube will be used as a basis of comparison for the finned tubes and as such, the bare tube results will be presented first.

The majority of measurements were performed at two downstream distances ($2.5D_e$ and $5D_e$) and two Reynolds numbers (approximately 2.61×10^4 and 4.69×10^4) which will be referred to as the *low Re* and *high Re* respectively. Measurements of mean velocity, fluctuating velocity, and correlation coefficient were taken using hotwire anemometry. From these measurements, wake profiles of mean velocity, total turbulence intensity, turbulence intensity due both to the fundamental vortex shedding frequency and the first harmonic, and correlation length were derived. From these results it was hoped that a better understanding of flow phenomena over a finned tube could be obtained.

4.1 The Bare Tube

In order to validate the experimental procedure as well as to provide a basis of comparison, tests were performed on a tube with a smooth surface. As mentioned previously, the diameter of the bare tube was the same as the root diameter of the finned

tubes so that it was hoped to observe the progression of results as more fins were added to the bare tube. It should be noted that due to physical constraints related to the traversing mechanism and the test section, fewer measurements on the positive y/D side of the tube were taken.

4.1.1 Mean Velocity Profiles

Measurements of the mean velocity across the wake were taken and the results are shown in *Figure 4.1*.

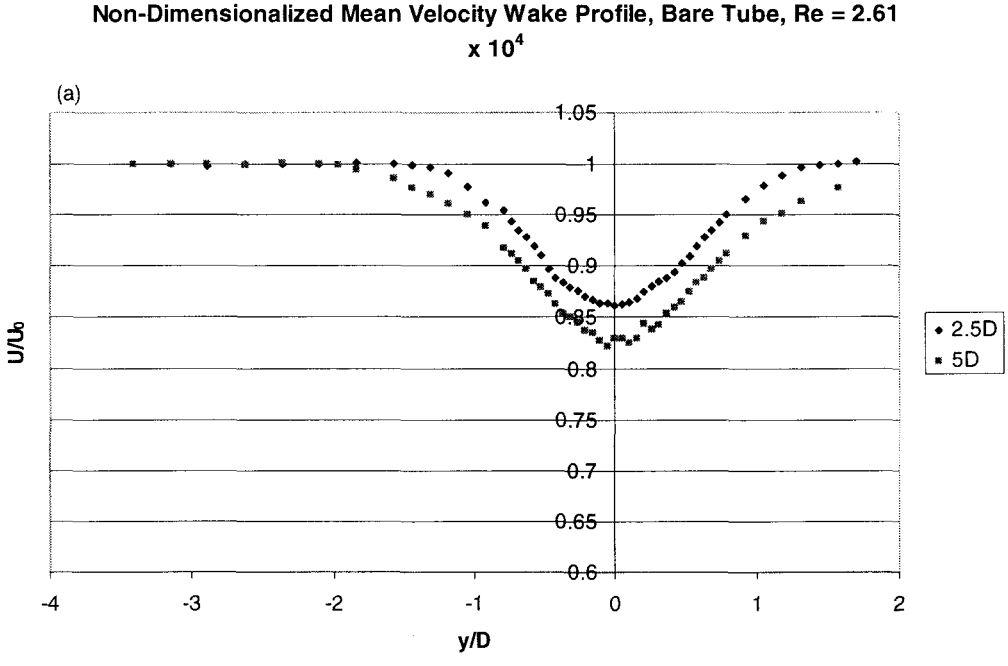

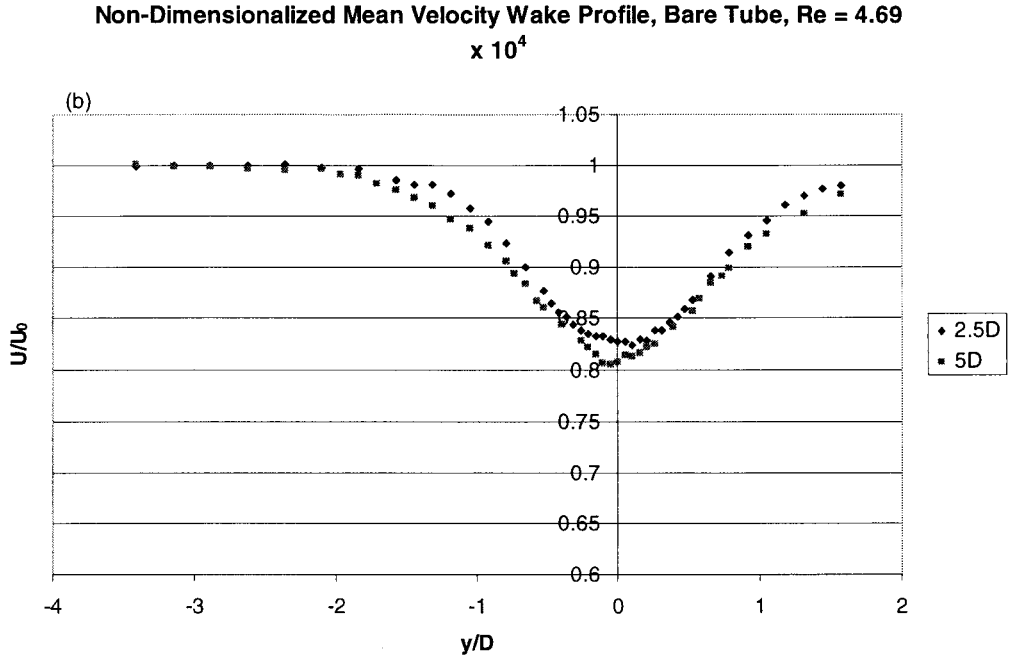

Figure 4.1: Distribution of non-dimensionalized mean velocity across the wake of a bare tube: a) low Re; b) high Re.

From these figures, it is seen that these results comparable to those of Bloor and Gerrard (1966). The general shape of the profiles is quite similar. In addition, the wake is seen to become wider with distance downstream and there is a gentler return of the velocity to the freestream value. The hump seen in *Figure 2.7a* for x/d = 1.7 is also seen in the present experiments for x/D = 1 (*Figure A.14*). Also of interest is the larger velocity deficit seen for higher Reynolds numbers and downstream distance. It is also seen that there is less of a difference between velocity deficits for the high Re case.

4.1.2 Fluctuating Velocity Profiles

Comparing the turbulence intensity due to the fundamental frequency component profiles (*Figure 4.2*) to those of Bloor and Gerrard (1966) (*Figure 2.8*) once again reveal comparable results.

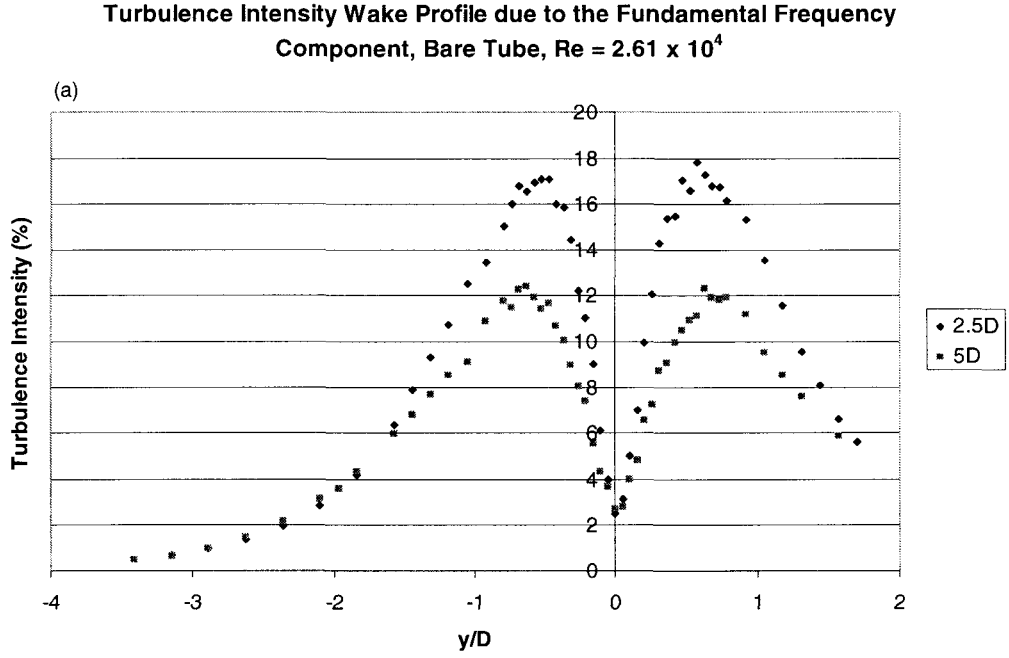

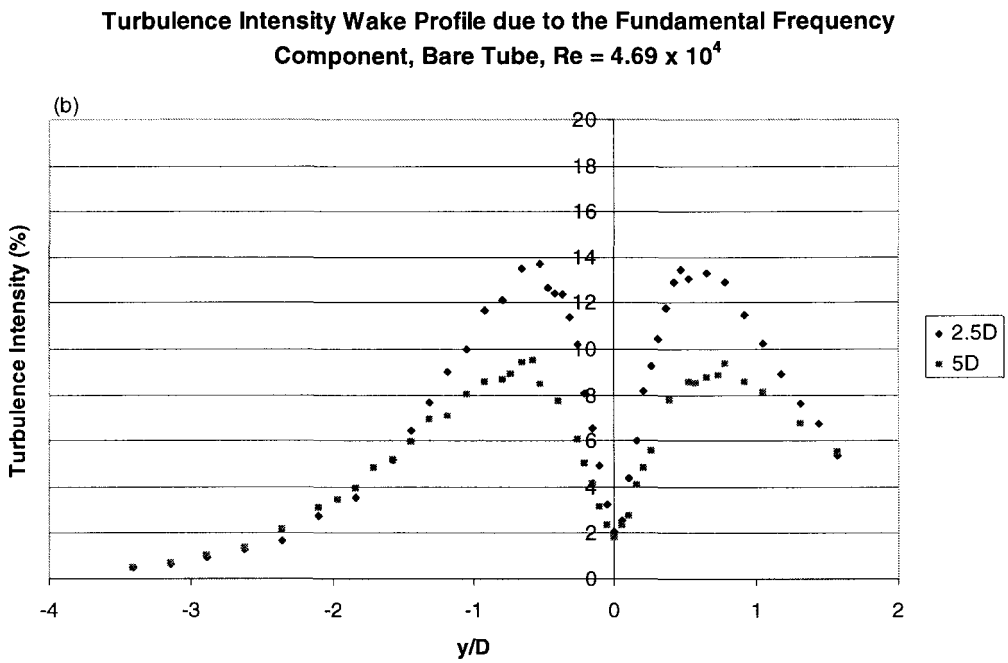

Figure 4.2: Distribution of turbulence intensity due to the fundamental frequency component across the wake of a bare tube: a) low Re; b) high Re.

The main features observed are that these profiles also show the widening of the wake with downstream distance as well as a decrease in magnitude with increased Reynolds number and downstream distance. With downstream distance the strength of the vortices decreases as a result of the influence of entrainment by vortices on the other side of the street (opposite circulation) as well as the turbulent characteristics of the freestream. Also of interest is that the intensity at the tube axis is close to zero (around 2%) regardless of the magnitude of the peak (and therefore turbulence intensity deficit) suggesting that vortex shedding at the fundamental frequency is not strong near to the tube axis. Bloor and Gerrard (1966) suggested that it would not be expected to find a fundamental frequency signal on the axis of a regular vortex street but these small values could be the result of fluctuations in the vortex strength from one vortex to another and

fluctuation in their position. It is also noted that the level at the peak values is less precise than elsewhere and Bloor and Gerrard (1966) proposed that this is the result of large low frequency fluctuations in intensity near the peak.

When *Figure 4.2* is compared to the profile of the total turbulence intensity (*Figure 4.3*), it is seen that the fundamental frequency is responsible for a large portion of the overall turbulence except close to the axis of the tube.

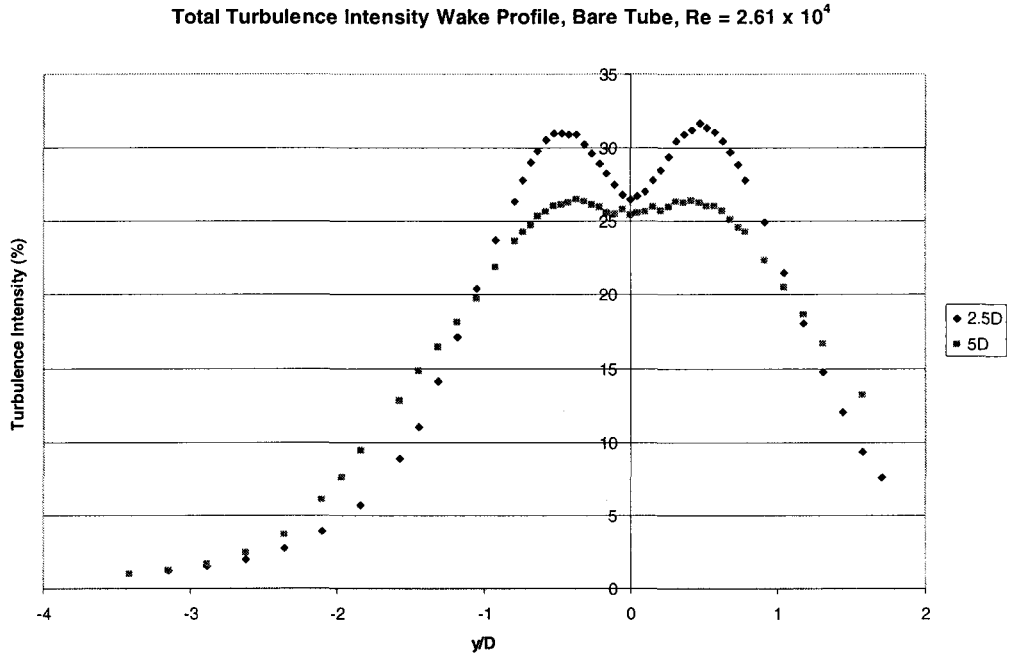

Figure 4.3: Distribution of total turbulence intensity across the wake of a bare tube at low Re.

Only the profile at low Re is shown here as it is very similar in shape and magnitude to that at high Re (*Figure A.1*). Like *Figure 4.2*, the shapes of the profiles are similar and turbulence intensity deficits are seen, although not as significant. The smaller deficits quantitatively suggest that there are other components contributing positively to the

overall turbulence levels especially close to the tube axis. Higher harmonics are such components as seen in *Figure 4.4*. Also from *Figure 4.3*, it is seen that the turbulence intensity deficit is much less at x = 5D suggesting that the influence of the fundamental frequency of vortex shedding has decreased and/or the influence of other components have increased. From a fluid mechanics point of view, this is not surprising as it would be expected that further downstream the influence of the tube on the flow would be reduced as the measurements are taken farther away from the stagnation region behind the tube producing flatter profiles.

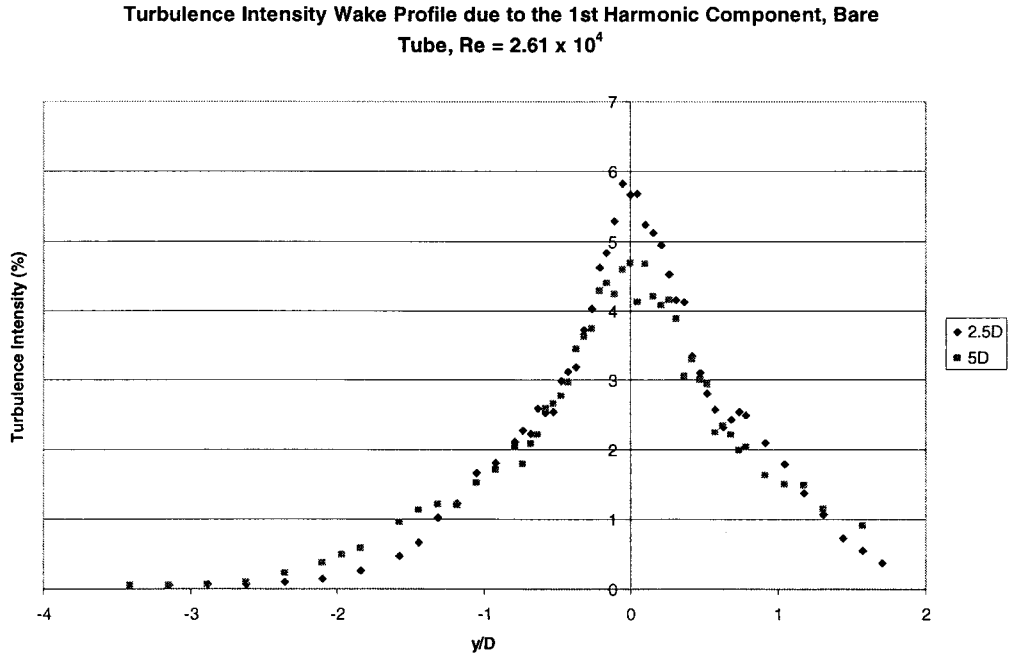

Figure 4.4: Distribution of turbulence intensity due to the first harmonic component across the wake of a bare tube at low Re.

From this figure, it can be seen that as the axis of the tube is approached, as the contribution to total turbulence of the fundamental frequency decreases, the contribution

of the first harmonic increases. *Figure 4.5* confirms the trend seen for the fundamental frequency and first harmonic. It shows the frequency spectra as the hotwire was traversed across the wake.

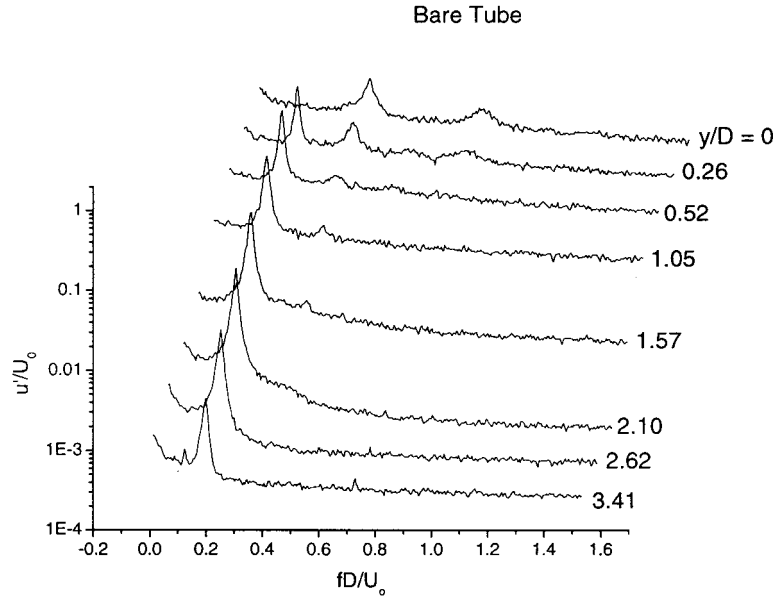

Figure 4.5: Frequency spectra waterfall plot at various transverse positions of the bare tube at high Re and x/D = 2.5.

It is clearly seen that starting far from the tube axis (y/D = 3.41) and approaching the wake centerline, y = 0, the magnitude of the fundamental frequency peak (at St = 0.2) increases to a maximum and then decreases until a peak is no longer discernable. Simultaneously, the first harmonic frequency peak (at St = 0.4) is seen to increase to a maximum at y/D = 0. In addition, the number of higher harmonics is seen to increase as

the tube axis is approached with the magnitude of the odd harmonics increasing while the even harmonics show similar trends as the fundamental frequency.

4.1.3 Correlation Length Measurements

Measurements of correlation coefficient ($R_{uu}(z)$) as a function of spanwise spacing (z) were also taken for the bare tube and typical results are plotted and shown in *Figure 4.6*. One hotwire was held stationary at a particular location (x_1, y_1, z_1) while the roving hotwire was placed close to the stationary hotwire (x_1, y_1, $z_2 \approx z_1$) and moved axially along the span of the tube (Δz).

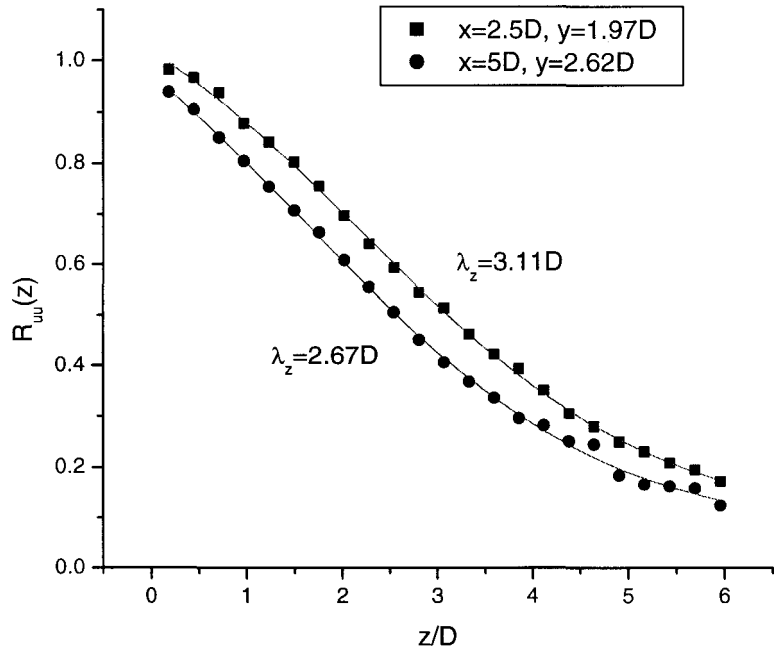

Figure 4.6: Measurements of correlation coefficient along the span of the bare tube at high Re.

This figure is quite similar to those found in the literature with $R_{uu}(z)$ starting close to 1 and then asymptoting to 0 and exhibiting an inflection point. As expected, the correlation coefficient decreases with increased spanwise separation as the signals become more out of phase and these values are lower with increased downstream distance, resulting in a smaller correlation length (λ_z). As mentioned earlier, further downstream the strength of the vortices decreases and as such, the signals that are recorded by the two hotwires become less correlated. It is also noted that as Reynolds number is increased, correlation length decreases slightly for both downstream distances (*Figure A.3*) which agrees with Kacker et al. (1974). The values of λ_z obtained in this study are quite similar to those seen in the literature (*Table 4.1*).

Table 4.1: A summary of bare tube correlation length measurements obtained from previous research.

Reynolds Number	**λ_z /D**	**Source**
$150 - 10^5$	2 – 3	King (1977)
$1.1 \times 10^4 - 4.5 \times 10^4$	3 – 6	King (1977)
$2.5 \times 10^4 - 1.25 \times 10^5$	0.7 – 4.2	Ribeiro (1992)
$1.5 \times 10^4 - 4.5 \times 10^4$	3.8 – 6.2	Ribeiro (1992)
1.9×10^4	3.5	Ribeiro (1992)
3.2×10^4	2.5	Ribeiro (1992)
4.5×10^4	3.3	Ribeiro (1992)

4.1.4 Strouhal Number

Also, as seen in the literature for single smooth cylinders, the vortex shedding frequency increases linearly with flow velocity (*Figure 4.7*) giving a Strouhal number ≈ 0.2.

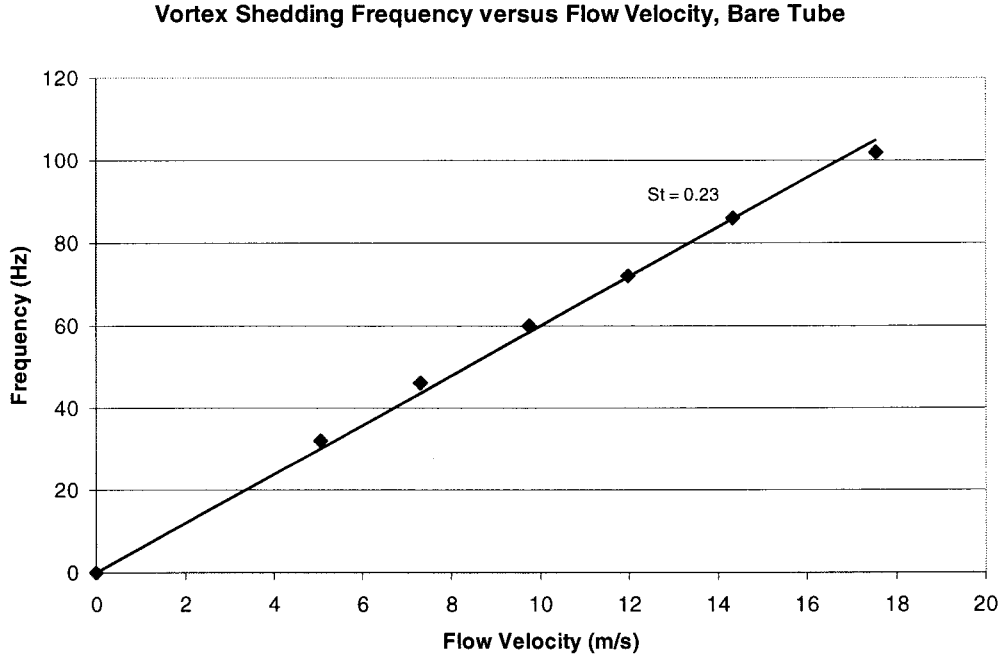

Figure 4.7: Vortex shedding frequency as a function of flow velocity.

As can been seen from the figure, the Strouhal number which is obtained is larger than what is in the literature. This difference will be explained in Section 4.2.3.

4.2 The Finned Tubes

Similar tests were performed on the finned tubes and these results are plotted on the same figures with the bare tube results for comparison purposes.

4.2.1 Mean Velocity Profiles

Figure 4.8 shows the results of the non-dimensionalized velocity wake profiles. It should be noted that for all of the results for the finned tubes, an effort was made to normalize the results by using the effective diameter, D_e, as the characteristic dimension of the finned tubes.

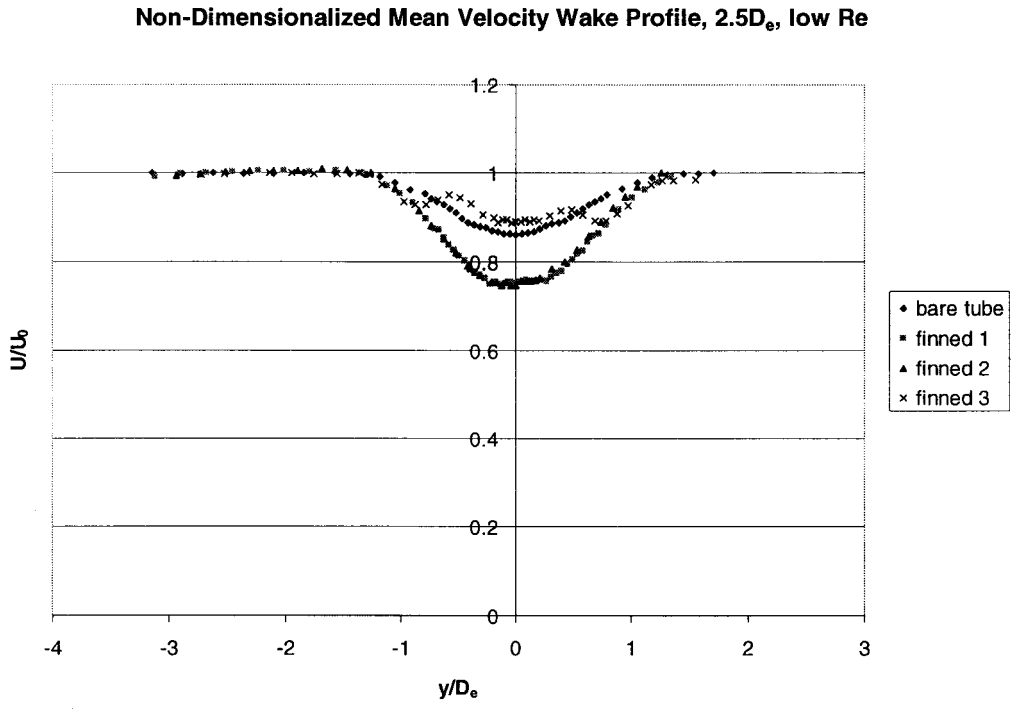

Figure 4.8: Non-dimensionalized mean velocity wake profiles of all tubes at low Re and x/D_e = 2.5.

From this figure, it is seen that the profiles for finned 1 and finned 2 are very similar in shape to that of the bare tube and each other with the exception of having a much larger velocity deficit. This suggests that even though the finned tubes have larger effective diameters due to the presence of the fins, the fins may have had an additional influence as

the increase in the effective diameter may not account for such a large difference in velocity deficit. In addition, as noted earlier, D_e was used as the characteristic dimension for the finned tubes and as such, the location of the measurements was larger for the finned tubes. Even though the measurements were taken further downstream for the finned tubes, the velocity deficits for finned 1 and 2 are still larger than that for the bare tube.

The most striking feature of this figure is the profile for finned 3. It is seen that the shape is unlike that of any of the other tubes. As the tube axis is approached, the magnitude decreases, then increases, then decreases once more until the axis of the tube is reached. This figure suggests that perhaps there may be a transition point related to the fin density which results in a significant change in the flow over the finned tube. All profiles are more or less symmetrical about the tube axis with a slight deviation seen for finned 3 where the magnitudes are a bit lower on the right side.

The anomalous nature of finned 3 is further exemplified in the velocity profiles further downstream (*Figure 4.9*).

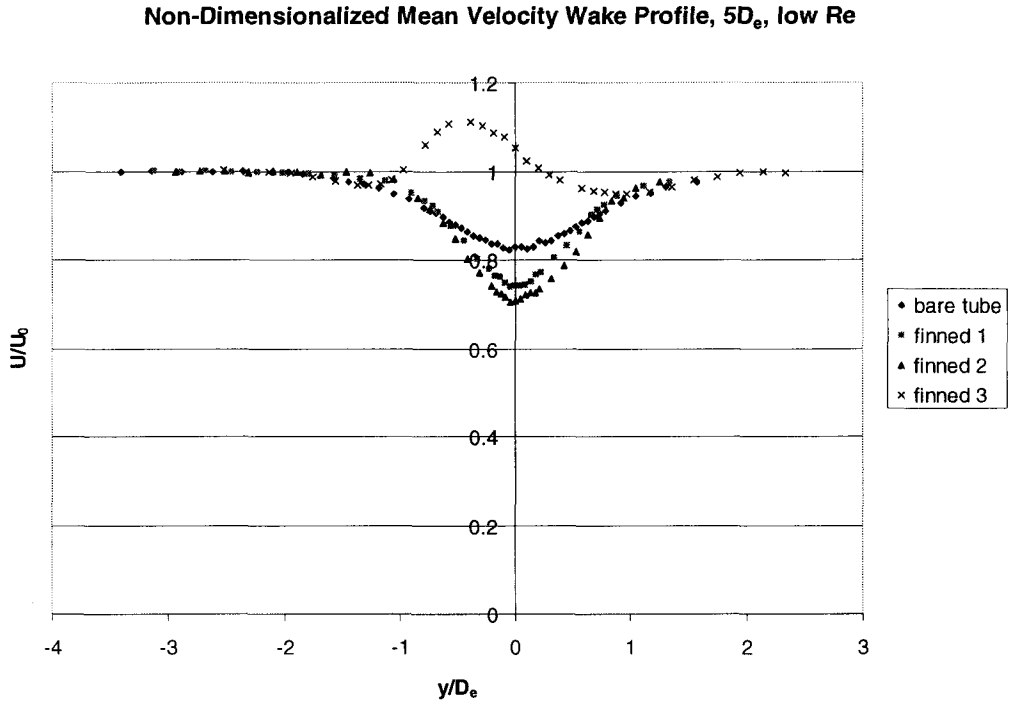

Figure 4.9: Non-dimensionalized mean velocity wake profiles of all tubes at low Re and $x/D_e = 5$.

In addition to being of a different shape, the profile is not symmetric and shows characteristics of being a velocity surplus rather than a deficit. Similar results are seen at high Re for all tubes (*Figures A.4* and *A.5*). Also of interest are the trends seen when the bare tube is compared to finned 1 and finned 2. The bare tube profile is observed to become wider with a larger velocity deficit further downstream while finned 1 and finned 2 become narrower with a larger velocity deficit. The narrowing of the profiles suggests that the wakes narrow with downstream distance. The only differences are seen for the x = $5D_e$, high Re case where the velocity deficit for finned 2 is reduced as well as the velocity surplus for finned 3.

4.2.2 Fluctuating Velocity Profiles

To illustrate the difference between using the bare tube diameter and the effective diameter to present results, the total turbulence intensity profiles are plotted for both cases (*Figure 4.10* and *Figure 4.11*).

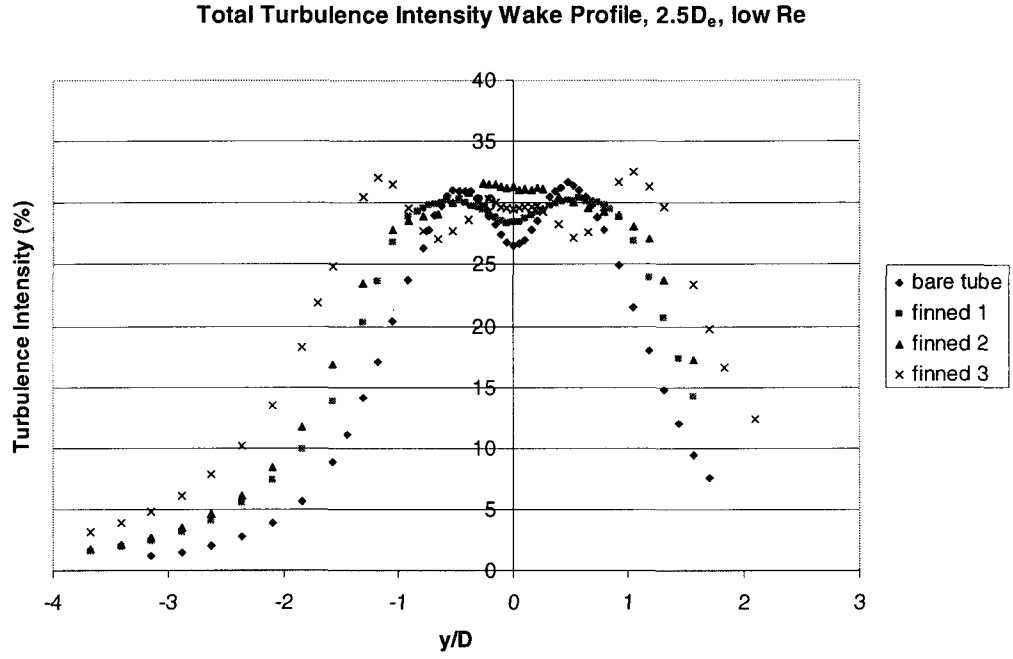

Figure 4.10: Total turbulence intensity wake profiles of all tubes at low Re and x/D_e = 2.5 based on the bare tube diameter.

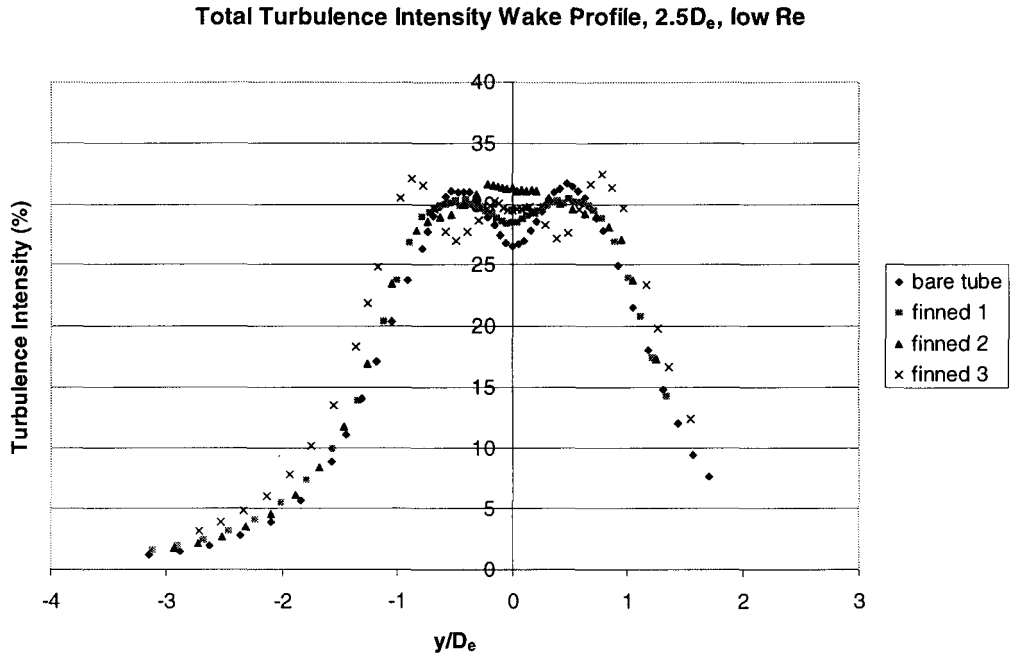

Figure 4.11: Total turbulence intensity wake profiles of all tubes at low Re and x/D_e = 2.5 based on the effective diameter.

As is clearly seen, when comparing the two figures, the wake is larger for the case using the bare tube diameter, and the wake is seen to become larger with fin density. It is also observed that when the effective diameter is utilized, the curves appear to collapse together. Finned 1 and finned 2 appear to have similar values to the bare tube outside of the wake with wake widths being similar. However, the collapse for finned 3 is not as effective as it can be seen that its values are larger and the wake is wider. This suggests that the use of D_e is only somewhat appropriate for use in the comparison of results.

By comparing the total turbulence levels in the wake of the tubes, significant differences can be seen (*Figure 4.11*). It is seen from the profiles that there seems to be a gradual transition with increased fin density from the bare tube to finned 3. The profile

of finned 1 is very similar to the bare tube with the exception of having a smaller turbulence intensity deficit. For finned 2, it is seen that there is only a very slight deficit at the wake centerline. This slight deficit is seen for finned 3, but there are two other turbulence intensity deficits observed around $y = \pm 0.45D_e$. As mentioned for the case of the bare tube, the differences in the magnitude of turbulence intensity deficit is influenced by the appearance of higher harmonics. From *Figure 4.11*, it could then be inferred that increases in fin density increase the strength and/or number of higher harmonics present thus giving more complex profile shapes near to the wake centerline. This is confirmed in the *Figure 4.12*.

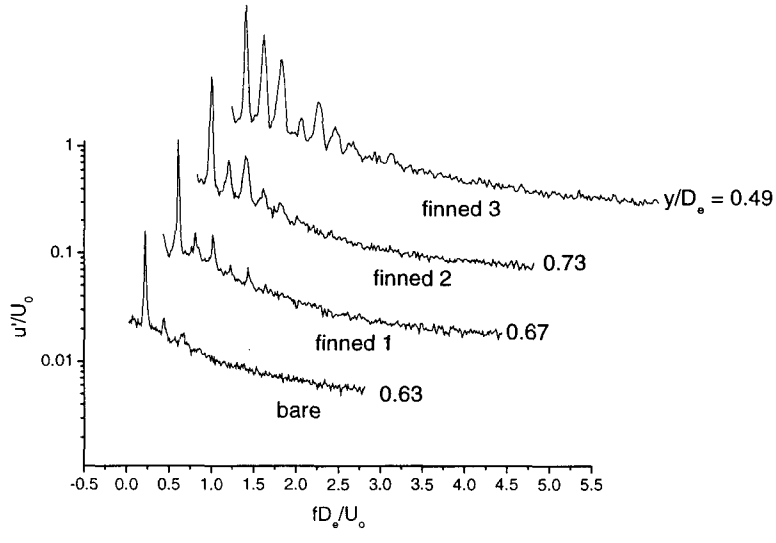

Figure 4.12: The frequency spectra of all tubes at low Re and x/D_e = 2.5. y/D_e corresponded to the halfway point of the velocity deficit (i.e. $U = U_0 - 0.5\Delta U$).

At x/D_e = 2.5 and high Re, the magnitude of the total turbulence intensity profiles are reduced and flattened for finned 1 and finned 2 while they increase for the bare tube and finned 3 (*Figure 4.13*). In addition, the shape of finned 3 changes such that there is a maximum peak at the tube axis rather than a minimum.

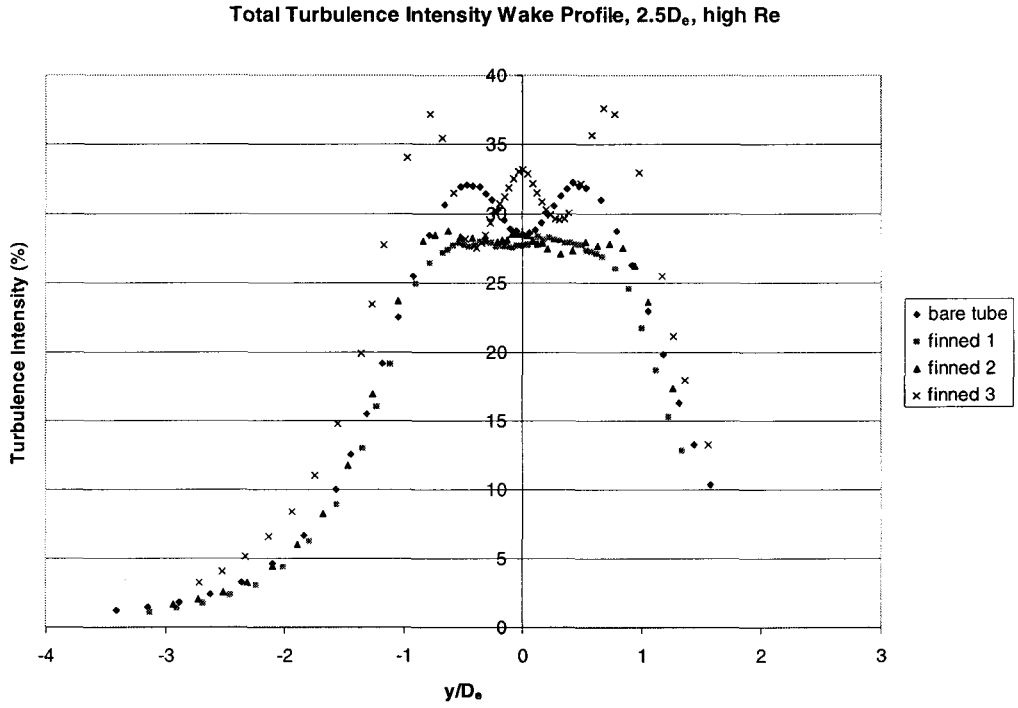

Figure 4.13: Total turbulence intensity wake profiles of all tubes at high Re and x/D_e = 2.5.

At x/D_e = 5, the profiles change once again. At low Re, the magnitudes decrease, when compared to x/D_e = 2.5, for all tubes and the profiles appear more flattened for all tubes except finned 3. The shape for finned 3 changes as well since there is no decrease followed by an increase and is not as symmetric (*Figure 4.14*).

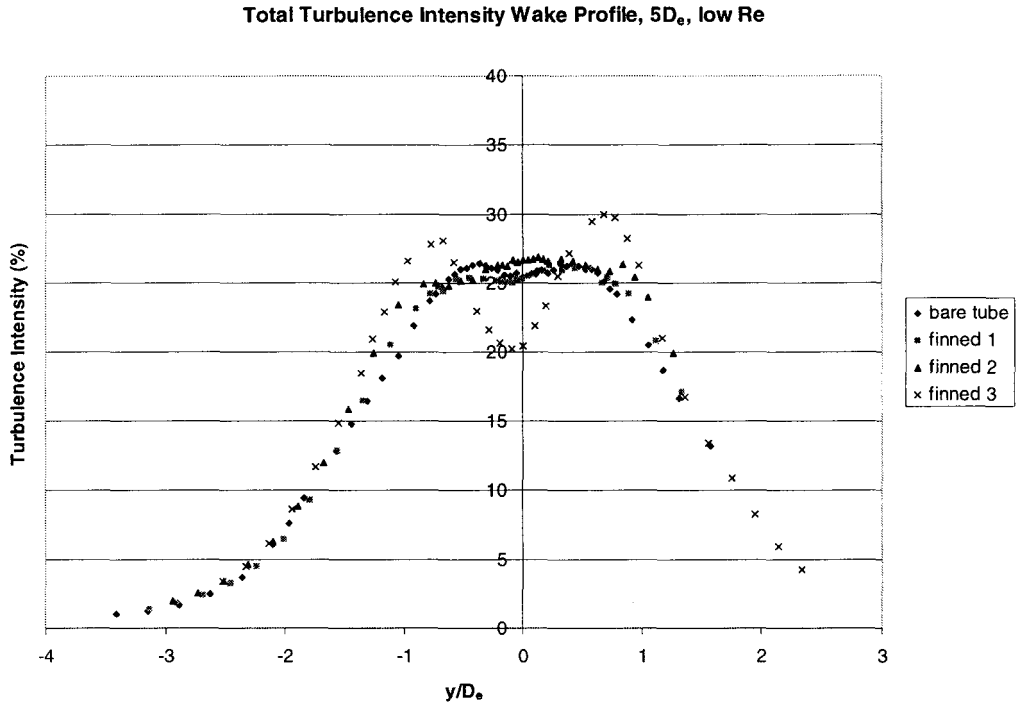

Figure 4.14: Total turbulence intensity wake profiles of all tubes at low Re and x/D_e = 5.

Comparing turbulence intensities at x/D_e = 5 at different Reynolds numbers, it is seen that the magnitudes decrease at high Re for all tubes except finned 3 which hardly changes (*Figure 4.15*). The peak values also occur at larger y/D_e values at high Re and the profiles for finned 1 and finned 2 can be distinguished from the bare tube as their magnitudes are smaller and because of the hump at the tube axis.

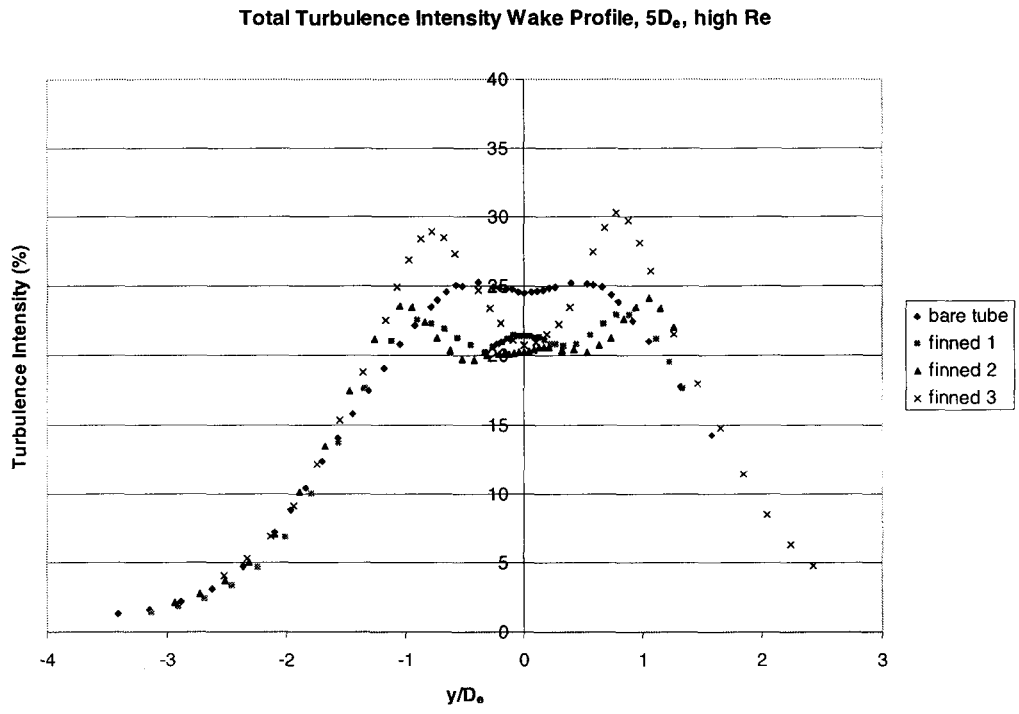

Figure 4.15: Total turbulence intensity wake profiles of all tubes at high Re and $x/D_e = 5$.

The contribution of the fundamental frequency and the first harmonic to the total turbulence intensity is presented in *Figure 4.16* and *Figure 4.17* respectively.

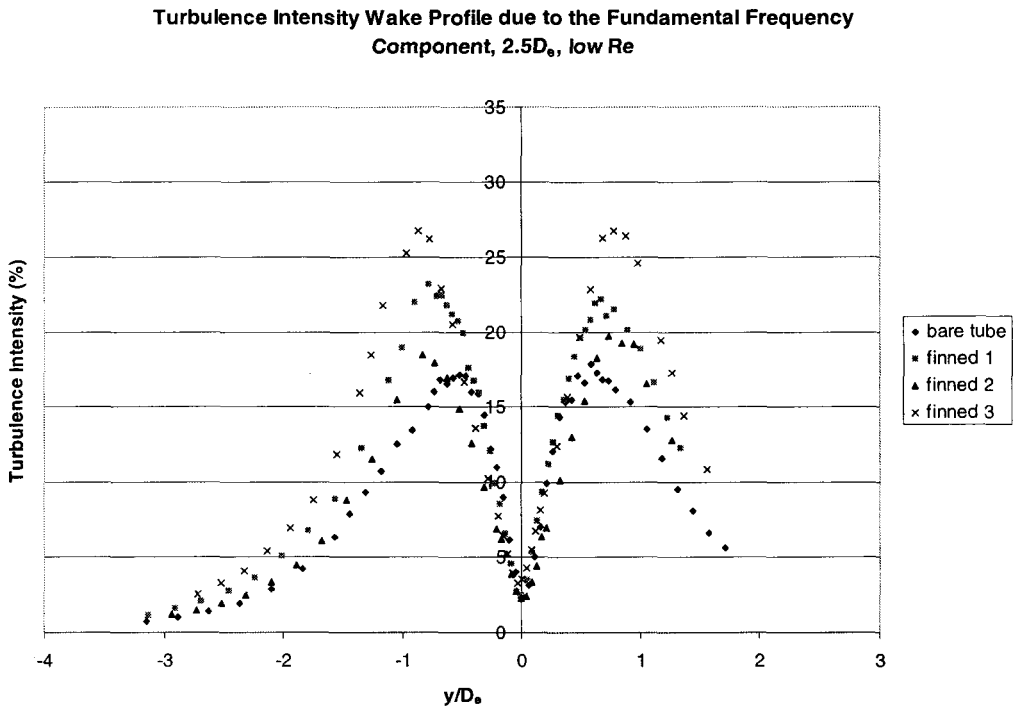

Figure 4.16: Fundamental frequency component of the total turbulence intensity wake profiles of all tubes at low Re and $x/D_e = 2.5$.

From *Figure 4.16*, it is noted that the fins have the effect of increasing the magnitude of the turbulence intensity with finned 3 showing the largest increase ($\approx$ 53%) when compared to the bare tube. For all cases, finned 3 has the largest peak values while the bare tube has the smallest. However the results do not show a progression in the magnitude of the peak values with increased fin density. Only for the case of $x = 5D_e$ and low Re (*Figure A.6*) does the trend of increased peak height with fin density occur. Also, the fundamental frequency component is seen to contribute a significantly larger portion to the overall turbulence for tubes with fins. For instance, in this particular case at the

peak value, the fundamental frequency component accounts for 82% of the total value for finned 3 but only 54% for the bare tube.

With the exception of finned 3, the other finned tubes show the same trends with increased Reynolds number and downstream distance in that the magnitudes of the peak values decrease and the profiles become flatter. On the other hand, finned 3 shows the opposite trend for all cases except at high Re and $x/D_e = 5$ (*Figure A.7*). In all other cases, the magnitude is observed to increase or not change appreciably. The most striking difference is seen at high Re and $x/D_e = 2.5$ (*Figure 4.18*). Comparing *Figure 4.16* to *4.18*, it can be seen that the peak value for finned 3 is significantly larger than those of the other tubes (almost double that of the closest profile). One other feature of note is that for all cases, with the exception of finned 3, the increase in fin density results in larger y/D_e values at which the maximum values occur.

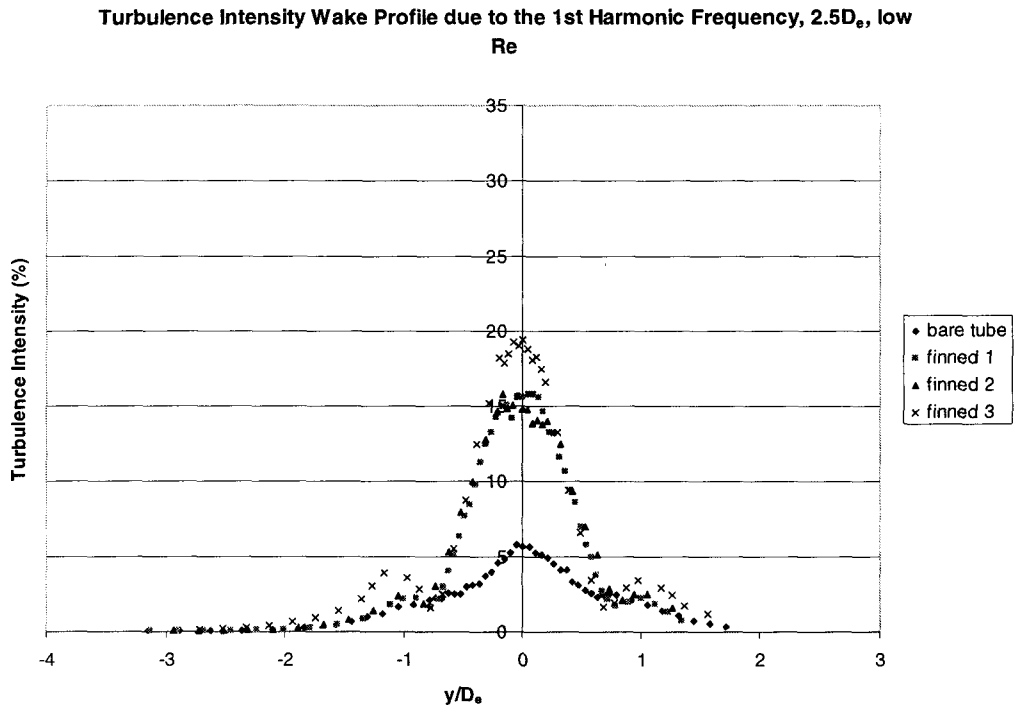

Figure 4.17: First harmonic component of turbulence intensity wake profiles of all tubes at low Re and $x/D_e = 2.5$.

Looking at *Figure 4.17*, almost identical trends can be seen for the first harmonic compared to the fundamental frequency. The fins increase the magnitude of the turbulence intensity, while it decreases with increased Reynolds number and downstream distance. Again the magnitude for finned 3 is always the largest while the magnitude for the bare tube is the smallest and the link between increased turbulence intensity with fin density is not apparent. The anomalous behaviour of finned 3 is also observed as the magnitude of the peak increases at $x/D_e = 2.5$ as Reynolds number increased. The only difference in the trends between *Figure 4.16* and *Figure 4.17* involved the general shape of the profiles. The fundamental frequency profiles are seen to increase to a maximum then decrease to a minimum at the tube axis, while the first harmonic profiles increase to

a maximum at the tube axis. Also, while the fundamental frequency profiles are seen to have similar shapes, the first harmonic profiles are seen to change with increased fin density. In addition to a peak at $y/D_e = 0$ for the finned tubes, another peak is observed at around $y/D_e = \pm 1$ becoming much more prominent with increased Reynolds number and less prominent with downstream distance. Once again, the profile for finned 3 differs. At $x/D_e = 5$ (*Figure A.9*), while all other tubes are seen to have a barely detectable second peak, finned 3 exhibits an obvious second peak, but only at $y/D_e = -1$ resulting in a profile which is not symmetric. These second peaks are barely detectable for the bare tube and occur at smaller y/D_e values.

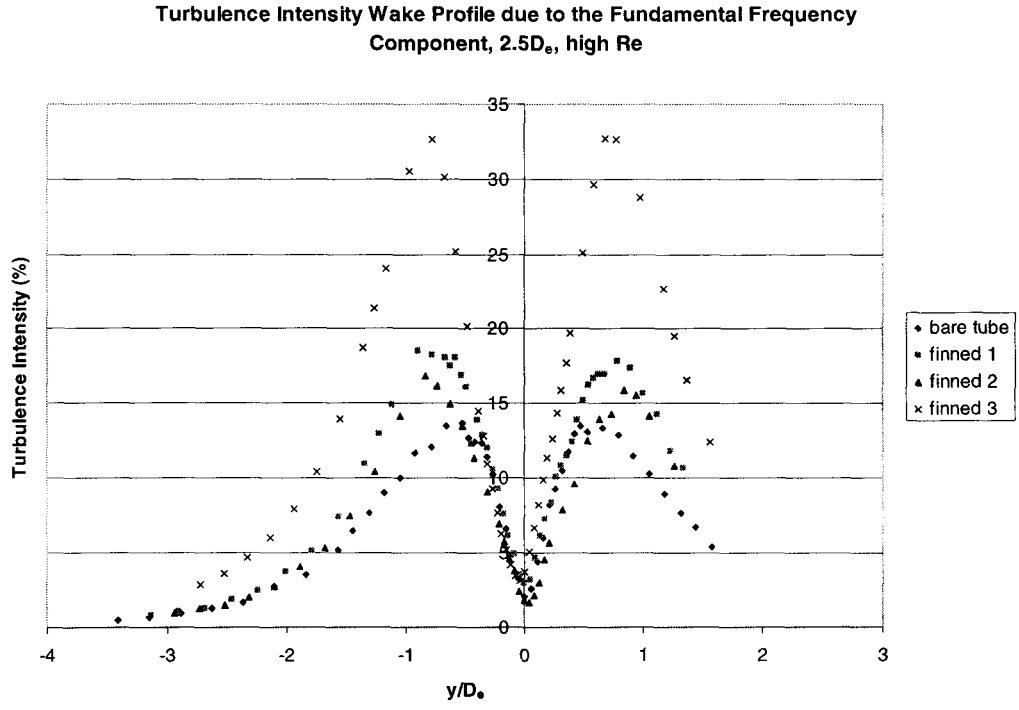

Figure 4.18: Fundamental frequency component of the total turbulence intensity wake profiles of all tubes at high Re and $x/D_e = 2.5$.

A comparison of the frequency spectra for each tube as the hotwire was traversed across the wake presents interesting differences (*Figure 4.19*).

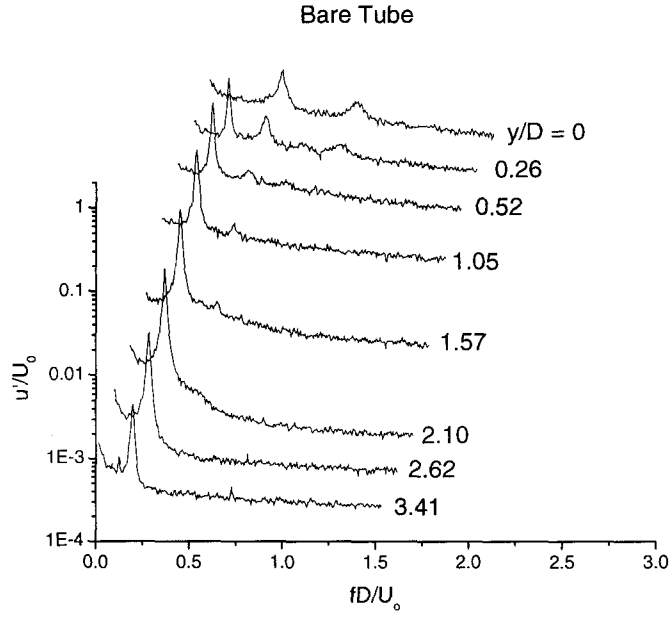

Finned 1

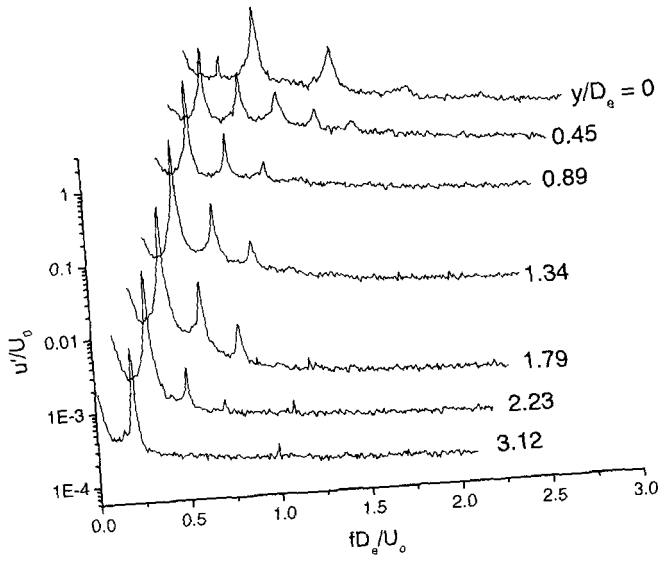

Finned 2

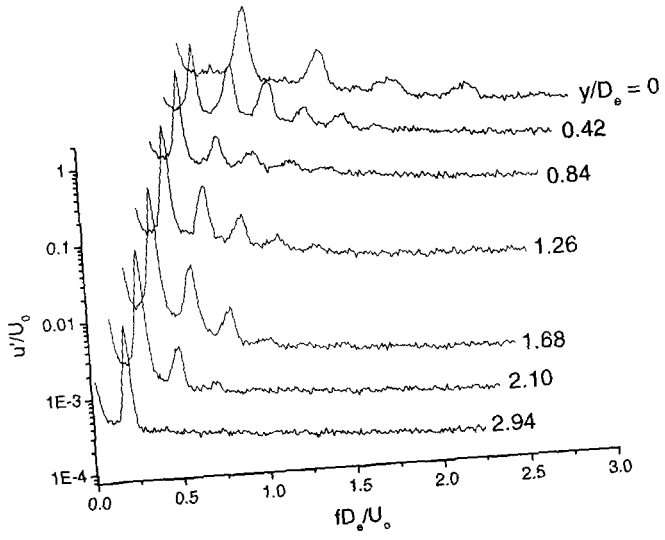

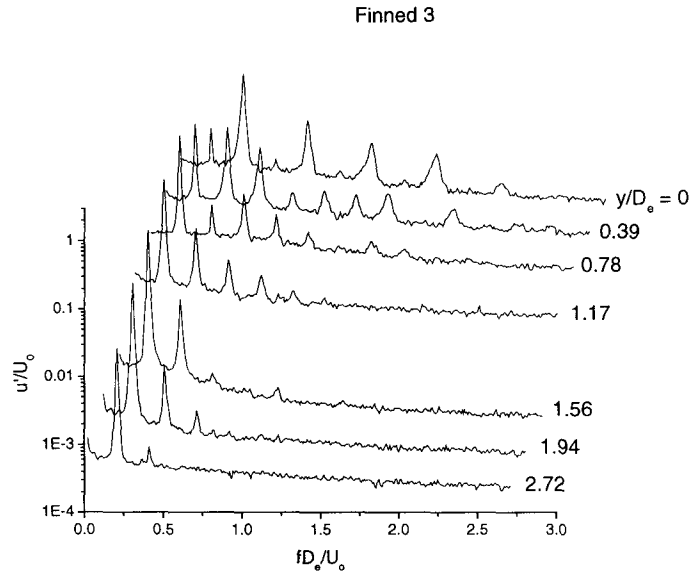

Figure 4.19: Frequency spectra at various transverse positions for all tubes at high Re and x/D = 2.5.

The most significant difference seen between the spectra of the four tubes is the existence of a larger number of higher harmonics with the increase in fin density. Far away from the wake centerline, the maximum number of harmonic peaks for any tube is one, which increases as the tube axis is approached. Close to the wake centerline, for the bare tube, three harmonic peaks are observed while for finned 3, as many as ten are seen. This is a considerable difference caused by the fins and could account for the differences observed in the turbulence intensity profiles. Also of interest is the strength of these peaks as the wake centerline was approached. As could be seen, harmonic frequencies appear as the wake centerline was approached and in general, all peaks are seen to increase in magnitude. Much closer to the wake centerline, the fundamental frequency as well as the even harmonic frequencies are observed to decrease in magnitude until the wake

centerline is reached where the peaks eventually disappear. The spectra for finned 3 are similar except that at the wake centerline, small peaks are still discernable. Simultaneously, as those frequencies decrease, the odd harmonic frequency peaks increase in magnitude. As mentioned in Chapter 2, Mair et al (1975) noticed that fins tended to increase the sharpness of the peak from frequency spectra and it was suggested that the fins increased the two-dimensionality of the flow. Consequently, similar results are expected from the present tests as well as the sharpening of the peak with increased fin density. As can be seen from *Figure 4.19*, such a trend occurs for all tubes but finned 2, for which the peaks are obviously not as sharp as for any of the other tubes. From these spectra, it can also be seen that the vortex shedding peak and its harmonics become larger in magnitude as the fin density increases at similar transverse distances which may explain why these components are more significant in the total turbulence intensity for tubes with higher fin densities.

4.2.3 Strouhal Number

Similar to the bare tube, the frequency of vortex shedding increases with velocity (*Figure 4.20*). From this figure, it is inferred that for the same flow velocity, the addition of fins has the effect of reducing the vortex shedding frequency. This is expected since the addition of fins has the effect of increasing the diameter of the tube and as known for bare tubes, larger diameters give rise to lower vortex shedding frequencies for the same flow velocity. From the slopes of these curves, the Strouhal number was calculated and it is seen that it decreases with fin density. Mair et al. (1975) also discovered that the Strouhal number decreased with fin density.

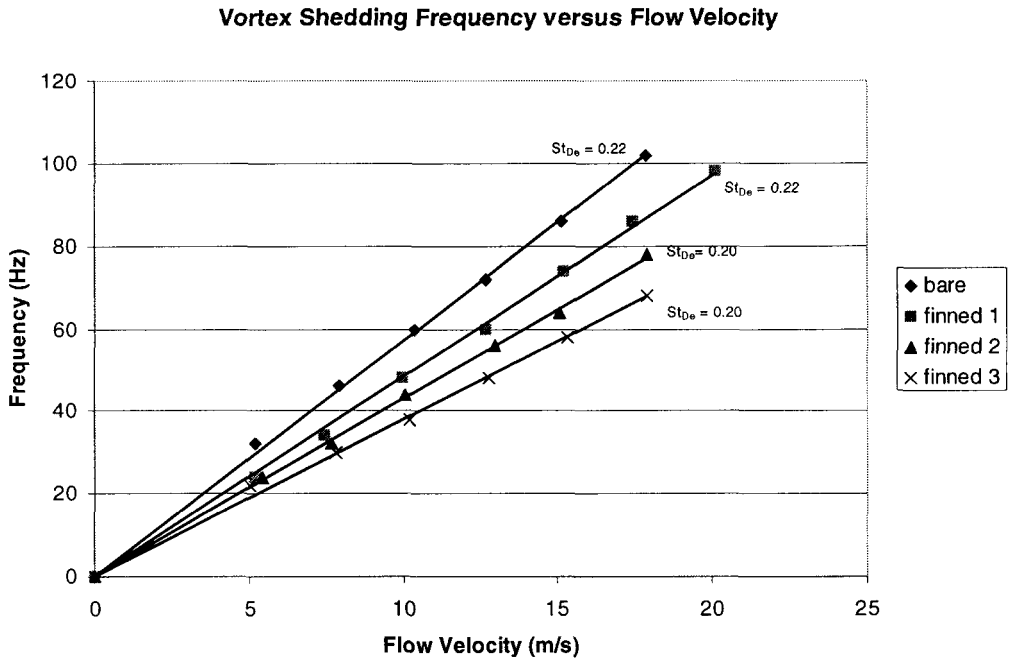

Figure 4.20: Vortex shedding frequency as a function of flow velocity for all tubes.

For the bare tube, the Strouhal number is a bit larger than what would be expected (St ≈ 0.2) at the Reynolds number of this study. It should be noted however, that this St calculation is based on measurements taken over a much larger Re range (0 – 46000) over which there is St variation (refer to *Figure 2.3*). In addition there is experimental error associated with these measurements as high as 8% for the bare tube. The non-dimensional form of *Figure 4.20* is shown in *Figure 4.21*.

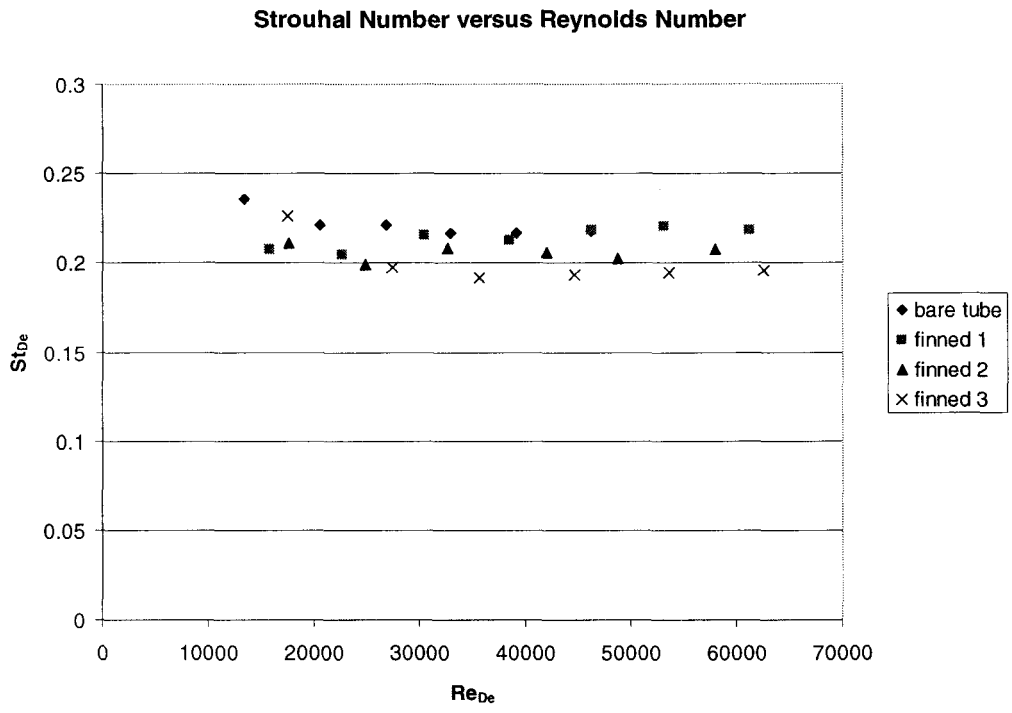

Figure 4.21: Strouhal number as a function of Reynolds number for all tubes.

However, it should be noted that in the calculation of Strouhal number, the equivalent diameter proposed by Mair et al (1975) was used. As that proposal was only an estimation of the effective diameter, there is some doubt as to whether the trend observed in *Figure 4.20* is true. If D_e properly accounted for the effective increase in the tube diameter, the Strouhal number based on D_e would be the same for all finned tubes. As this is clearly not the case, D_e as an effective diameter measure is not completely correct and seems to underestimate the effect of the fins.

During analysis of the data, the idea of using momentum thickness, θ, which is defined as a length scale for turbulent wakes, as the characteristic dimension for the tubes was explored. Although this proved unsuccessful, it did reinforce points made about the

effective diameter. Considering *Figure 4.22*, it is seen that momentum thickness increases with fin density suggesting that the assumption of an increased effective diameter with fin density is correct.

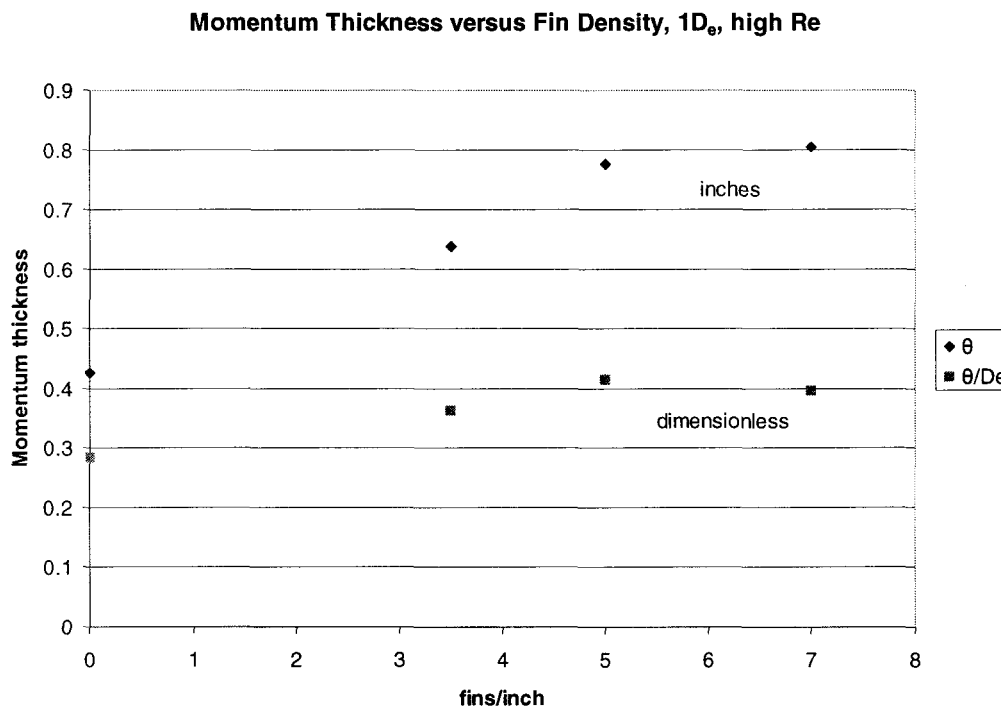

Figure 4.22: Momentum thickness measurements for all tubes taken at $1D_e$ and high Re.

In addition, it is seen that when the momentum thickness is non-dimensionalized with respect to D_e, this is somewhat effective in collapsing the data once again emphasizing that D_e is just an approximation.

4.2.4 Correlation Length Measurements

Correlation coefficient measurements were performed for all tubes. Given that only one other set of research on correlation coefficient measurements had been found for

finned tubes (Hamakawa et al 2001), it is still somewhat uncertain what kind of results would be obtained. *Figure 4.23* shows the results for one Reynolds number and downstream distance. The results for all four tests show similar trends and are given in Appendix A.

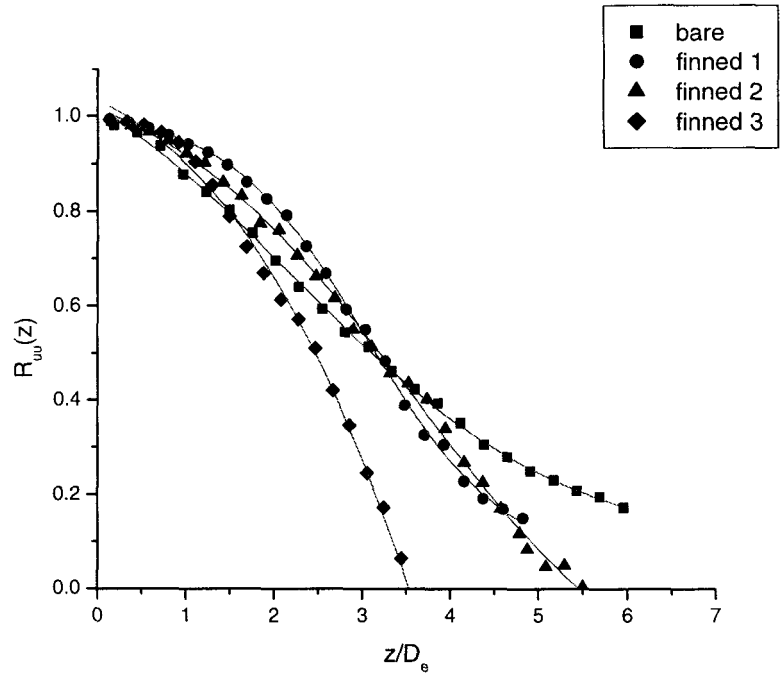

Figure 4.23: Measurements of correlation coefficient along the span of the tubes at x/D_e = 2.5 and high Re.

As can be seen, finned 1 and finned 2 exhibit similar trends when compared to the bare tube in that they start at around $R_{uu}(z) = 1$, pass through an inflection point, and tend to asymptote to $R_{uu}(z) = 0$ although they do so more quickly than the bare tube. While those three tubes tend to asymptote to $R_{uu}(z) = 0$, finned 3 shows a different trend with no inflection point and intersects the x-axis with the reduction of correlation coefficient with

separation distance being more drastic. Once again this suggests that perhaps high density fins cause significantly different flow phenomena.

During the tests to determine correlation length, one unfortunate discovery was made. After performing tests on one of the finned tubes, it was decided to repeat the test and as such, the finned tube was placed into the wind-tunnel once again and measurements were taken. It was discovered that significantly different results were obtained. After checking the equipment and measurement process for possible sources of error without success, it was decided to repeat the measurements after rotating the tube about its axis by 120°. Determining that the results changed considerably, it was then decided to take measurements for all finned tubes at three different angular locations and repeating one location to ensure repeatability of the results. All finned tubes show angular variation to some degree (*Figure 4.24*).

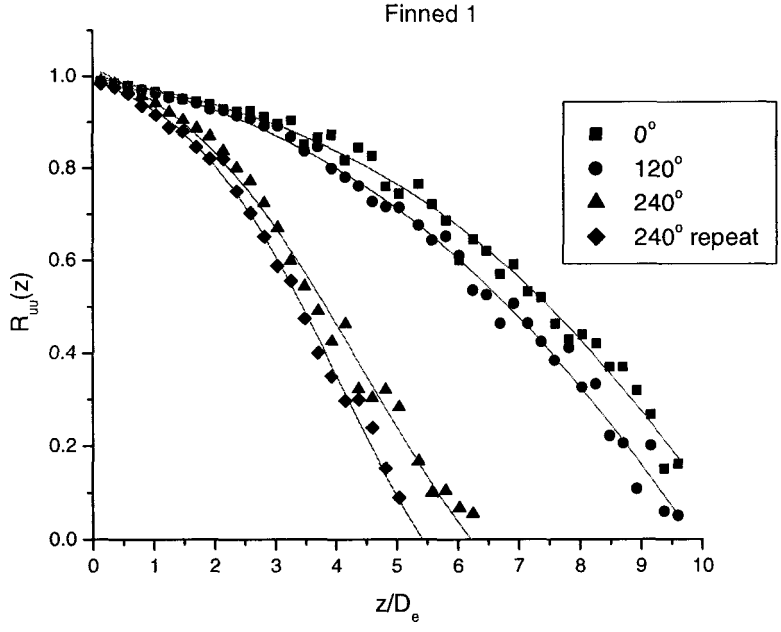

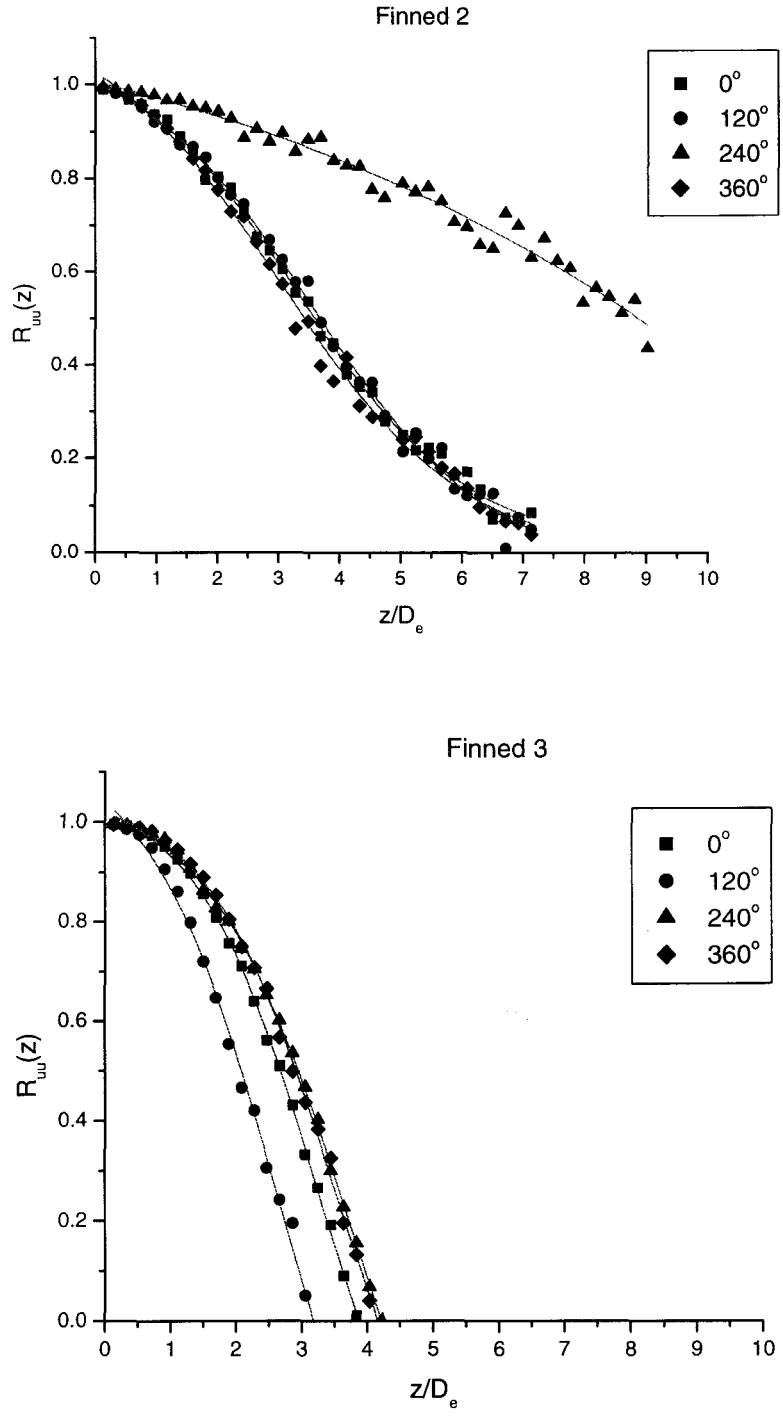

Figure 4.24: Correlation coefficient measurements along the span of the finned tubes at x/D_e = 2.5 and low Re and at different angular positions.

All of the finned tubes show relatively good agreement for the results that were repeated at the same angle.

At 240° for finned 1, the curve seems to follow the normal trend exhibited by the bare tube although it asymptotes to zero more quickly. The curves at 0° and 120° are similar to each other but differ from the normal shape exhibited by the bare tube. No inflection point is seen and it appears as if the curves would intersect the x-axis. Also, these $R_{uu}(z)$ values are noticeably larger than those at 240° with positive values extending to nearly double the separation spacing.

For finned 2, the results are almost identical for 0°, 240°, and 360° with these curves being very similar in shape to those of a bare tube. The 240° curve deviates significantly from the others showing no inflection point and appears that it would not reach $R_{uu}(z) = 0$ until well after $z/D_e = 10$.

The curves for finned 3 exhibit the least deviation when compared with each other. The curves follow the same trend of rapidly reaching and crossing $R_{uu}(z) = 0$ without displaying an inflection point.

In light of this discovery, it therefore would be unwise to compare the current results for λ_z of the finned tubes against each other or with the bare tube results until a more thorough study can be performed on this phenomenon. This is a very interesting and unexpected discovery that needs to be further explored. Currently, the only hypothesis to possibly explain the drastic changes in λ_z with rotation angle, is related to the manufacturing of the tubes. It was noticed that looking along the axis of the tube

Figure 4.25, the fins seem to line up in a wavy pattern which changed as the tube was rotated.

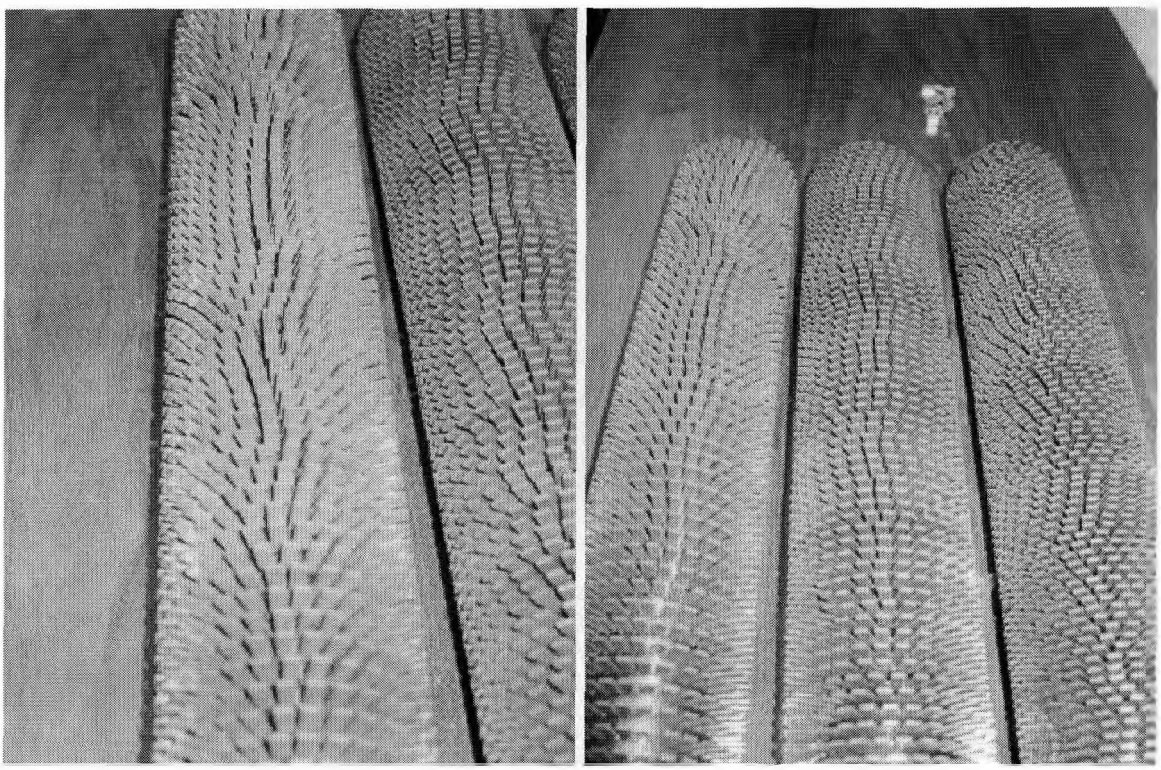

Figure 4.25: Photographs of the finned tubes showing the wavy pattern.

A summary of the correlation length measurements are shown below in *Table 4.2*. As discussed earlier, the correlation length measurements for the bare tube are in good agreement with previous research (*Table 2.1* and *Table 4.1*). In addition, it is seen that when the results were repeated for the finned tubes at the same rotation angle, they were in relative good agreement with each other.

Table 4.2: Compilation of correlation length measurements in terms of D_e recorded during this study. For the first table, the finned tube results were obtained at unknown rotation angles.

	Bare	Finned 1	Finned 2	Finned 3	Source
$2.5D_e$, low Re	3.24	3.28	3.10	2.06	Figure A.17
$2.5D_e$, high Re	3.11	2.99	2.95	2.16	Figure 4.21
$5D_e$, low Re	2.78	3.49	3.13	2.02	Figure A.18
$5D_e$, high Re	2.67	3.21	3.05	2.32	Figure A.19

Finned 1 rotated	0°	120°	240°	240° repeated	Source
$2.5D_e$, low Re	6.74	6.23	3.57	3.15	Figure 4.22

Finned 2 rotated	0°	120°	240°	360°	Source
$2.5D_e$, low Re	3.60	3.61	8.30	3.47	Figure 4.22

Finned 3 rotated	0°	120°	240°	360°	Source
$2.5D_e$, low Re	2.41	1.85	2.65	2.63	Figure 4.22

Considering the finned 1 and finned 2 rotated correlation results and the larger peaks of turbulence intensity due to the vortex shedding frequency for finned tubes, this seems to suggest that more noise would be generated from finned tubes.

4.2.5 A Further Look at Finned Tube 3

As was noted in the majority of all tests, the results from finned 3 deviated from those of the other tubes. Consequently, it was decided to map the evolution of the wake behind finned 3 (*Figure 4.26*) in an attempt to shed some light on these apparently anomalous results.

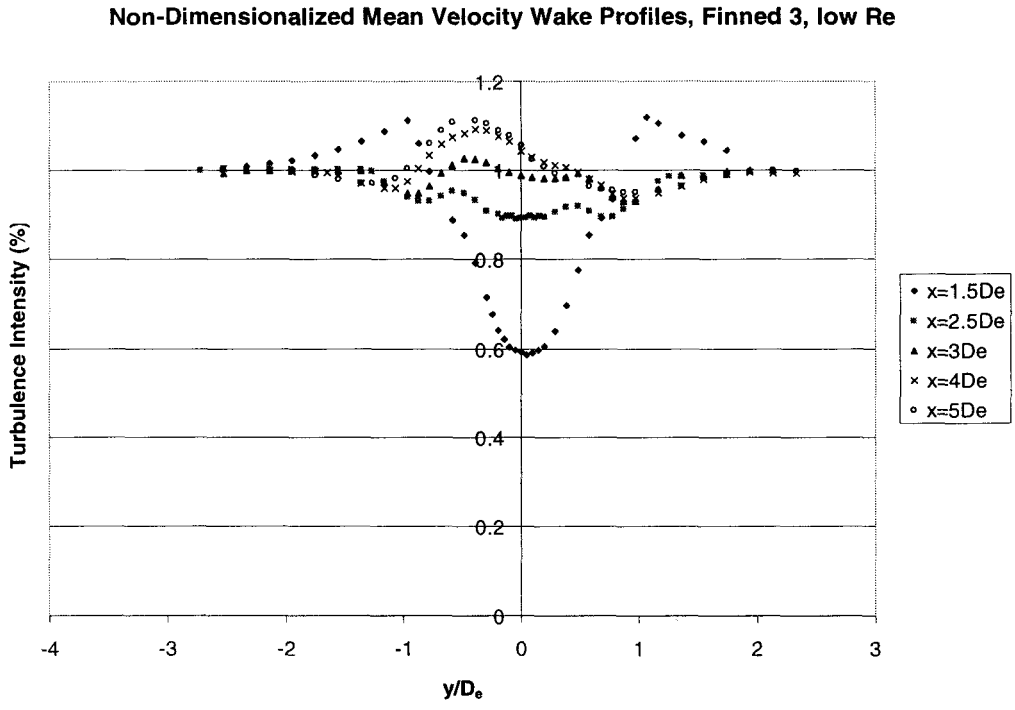

Figure 4.26: Mean velocity wake profiles at various downstream distances for finned 3.

As is seen, at x/D_e = 1.5 the profile looks similar to what would be expected with a velocity deficit in the wake centred and symmetrical about the tube axis. At x/D_e = 2.5 and larger, the deviation from the wake of the bare tube is noted with asymmetry occurring at x/D_e = 3 and larger. This seems to suggest a transition in the flow around the tube between x/D_e = 1.5 and 2.5. When looking at the total turbulence intensity wake profiles (*Figure 4.27*), asymmetry also starts to occur at x/D_e = 3. However, what is quite surprising is that in the profiles of the fundamental component of turbulence intensity (*Figure 4.28*) shows no asymmetry. This suggests that whatever phenomenon is responsible for asymmetry does not affect vortex shedding at the fundamental frequency.

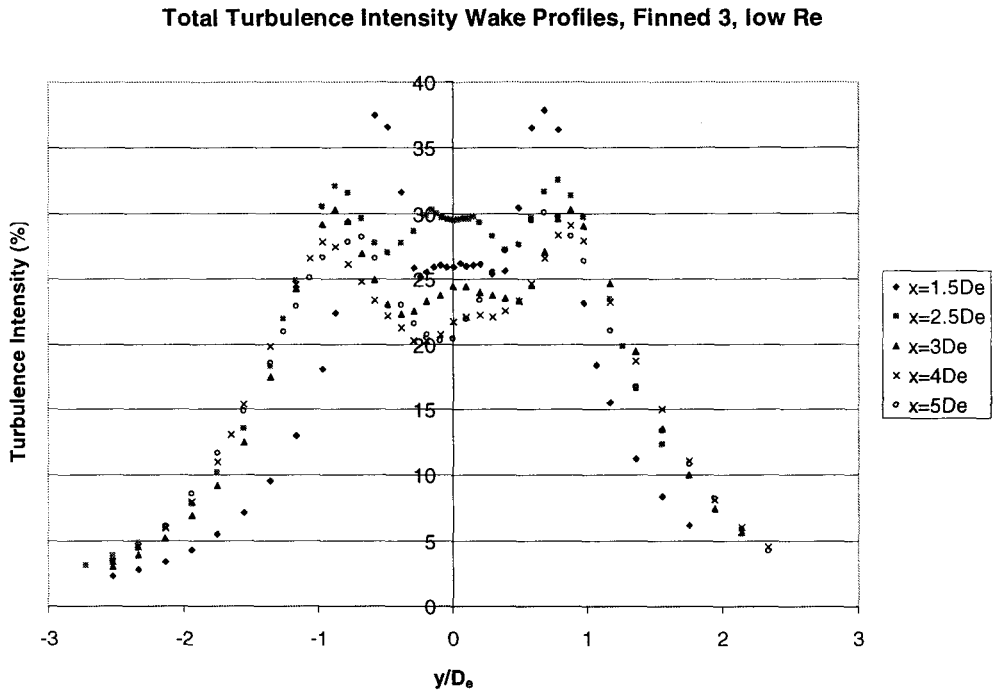

Figure 4.27: Total turbulence intensity wake profiles at various downstream distances for finned 3.

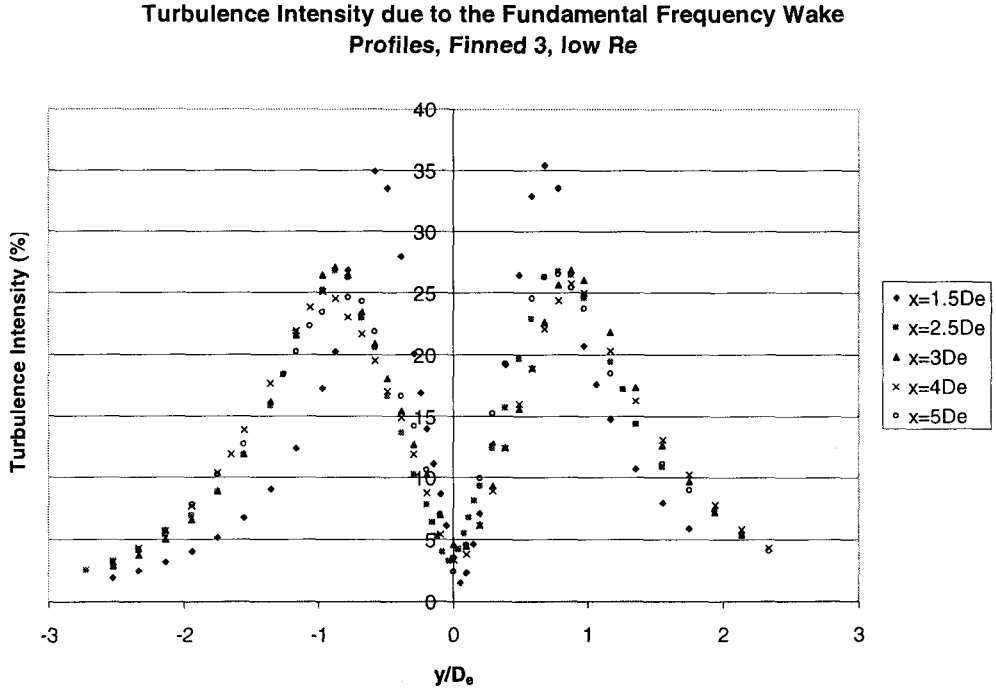

Figure 4.28: Total Fundamental frequency component of the total turbulence intensity wake profiles at various downstream distances for finned 3.

Chapter 5

5 Conclusions

Flow tests were performed on the bare tube as well as the three segmented-finned tubes. Although these tests revealed very interesting results, it is clear that there is a need for further study in this area. The conclusions derived from this study are summarized as follows:

1. The results obtained for the bare tube are in very good agreement with those in published literature. From the wake profiles, it is seen that for mean velocity, the velocity deficits increase with downstream distance. Total turbulence intensity decreases with downstream distance and the profiles become flatter. It is also seen that turbulence intensity due to the fundamental frequency of vortex shedding decreases with downstream distance and increased Reynolds number. This component of turbulence intensity also accounts for a large portion of the overall intensity. The correlation length results also compare quite well the literature as the values are similar and are seen to decrease with downstream distance and Reynolds number.
2. It is seen that the fins have a significant impact on the flow. Considering the mean velocity profiles and finned 1 and finned 2, larger velocity deficits are seen compared to the bare tube. These deficits are larger compared to the increase in effective diameter and thus downstream location of measurements suggesting an

additional influence by the fins. In addition, the wakes are seen to narrow with downstream distance which is the opposite trend to the bare tube.

3. The profiles of total turbulence intensity show the greatest difference. At $x = 2.5D_e$ and low Re, a transition in the shapes is seen indicating the influence of the fins.
4. Turbulence intensity due to the fundamental frequency shows that increasing the fin density increased the contribution to the overall turbulence levels significantly. For the $x = 2.5D_e$ and low Re case, the peak value accounts for 82% for finned 3, but only 54% for the bare tube. Although the bare tube and finned 3 have the smallest and largest values respectively (the peak value of finned 3 is 53% larger than for the bare tube at $x = 2.5D_e$ and low Re), there is not much consistency between increased fin density and increased fundamental turbulence intensity. Also, except for finned 3, the y location of the peak of these profiles increase with fin density.
5. Given the differences in the turbulence intensity profiles, it is concluded that the frequency spectra must show significant differences. It is seen from the spectra that the increase in fin density increases the number of harmonic peaks. The fundamental and even harmonic peaks increase as the wake centreline is approached and then decrease to almost zero at the axis while the odd harmonic peaks increase to a maximum at the tube axis. It is also seen that the fins increase the strength of vortex shedding as the amplitude of the fundamental frequency increases as well which is contrary to what would be expected.

6. The first harmonic turbulence intensity profiles also show a difference with the addition of fins. Another maximum peak is seen to appear on both sides of the tube which grows in strength as fin density increases.
7. The results also show that the vortex shedding frequency decreases with fin density at the same flow velocity. Even with the use of D_e in the calculation of Strouhal number, it is seen to decrease with fin density agreeing with Mair *et al.* (1975).
8. Almost all results for finned 3 show apparent anomalies. While for the other tubes symmetric profiles are observed, asymmetry is seen for finned 3 in the mean velocity, total and first harmonic turbulence intensity profiles. It is interesting to note that no asymmetry is seen for the fundamental frequency turbulence profile. From wake development profiles, it is concluded that there is a transition in the flow past $x = 2.5D_e$. In addition, considering the profiles of all tubes, it appears that maybe after a critical fin density is reached, there is a significant change in the effect of fins on the wake development.
9. From the various results presented, it is seen that the use of D_e tends to make the finned tube data collapse. The collapse is not perfect suggesting that a better estimation may be required.
10. From the correlation length measurements, it is concluded that fins complicate its estimation since the rotation of the tube changes the measured value. If as suggested, this phenomenon is related to the wavy pattern of the fins, and therefore their construction, it is proposed that tubes with more uniform finning

be obtained and these experiments repeated. If unfruitful, it maybe required to begin with taking measurements at various angles but with much smaller increments in an effort to find a pattern or trend to explain the observed irregularities.

References

Basu, R. I. (1985). "Aerodynamic Forces on Structures of Circular Cross-Section. Part 1. Model-Scale Data Obtained Under Two-Dimensional Conditions in Low-Turbulence Streams." Journal of Wind Engineering and Industrial Aerodynamics **21**: 273-294.

Blevins, R. D. (1984). "Review of Sound Induced By Vortex Shedding From Cylinders." Journal Of Sound and Vibration **92**(4): 455-470.

Blevins, R. D. (1986). Flow-Induced Vibration. Malabar, Florida, Robert E. Krieger Publishing Company.

Blevins, R. D. (1990). Flow-Induced Vibration. New York, Van Nostrand Reinhold.

Blevins, R. D. and M. M. Bressler (1987). "Acoustic Resonance in Heat Exchanger Tube Bundles - Part I: Physical Nature of the Phenomenon." Journal of Pressure Vessel Technology **109**: 275-281.

Bloor, M. S. and J. H. Gerrard (1966). "Measurements on Turbulent Vortices in a Cylinder Wake." Proceedings of the Royal Society of London. Series A, Mathematical and Physical Sciences **294**: 319-342.

Chen, S.-S. (1987). Flow-Induced Vibration of Circular Cylindrical Structures. Washington, New York, London, Hemisphere Publishing Corporation.

Eisinger, F. L. (1980). "Prevention and Cure of Flow-Induced Vibration Problems in Tubular Heat Exchangers." Journal of Pressure Vessel Technology **102**: 138-145.

el Baroudi, M. Y. (1960). "Measurement of Two-Point Correlations of Velocity Near a Circular Cylinder Shedding a Kaman Vortex Street." UTIA Technical Note No. 31.

Fan, H. (2002). Vortex Shedding and Acoustic Resonance of an Array of Tubes with Twisted Serrated Fins. Mechanical Engineering. Hamilton, McMaster University.

Goswami, I., R. H. Scanlan and N. P. Jones (1993). "Vortex-Induced Vibration of Circular Cylinders. I: Experimental Data." Journal of Engineering Mechanics **119**(11): 2270-2287.

Hamakawa, H., T. Fukano, E. Nishida and M. Aragaki (2001). "Vortex Shedding From A Circular Cylinder With Fin." AIAA.

Kacker, S. C., B. Pennington and R. S. Hill (1974). "Fluctuating Lift Coefficient For A Circular Cylinder In Cross Flow." Journal Of Mechanical Engineering Science **16**(4): 215-224.

Katinas, V., E. Perednis and V. Svedoscius (1991). "Crossflow-Induced Vibrations of Staggered Bundles of Finned Tubes." Fluid Mechanics - Soviet Research **20**(3): 80-88.

Katinas, V., E. Perednis and V. Svedoscius (1991). "Vibrations of Smooth and Finned Tubes in Crossflows of Viscous Fluids with Different Turbulence Levels." Heat Transfer - Soviet Research **23**(6): 844-851.

King, R. (1977). "A Review of Vortex Shedding Research and its Applications." Ocean Engineering **4**: 141-171.

Kouba, J. (1986). "Vortex Shedding and Acoustic Emission in Finned Tube Banks Exposed To Cross Flow." PVP **104**: 213-217.

Leehey, P. and C. E. Hanson (1971). "Aeolian Tones Associated With Resonant Vibration." Journal Of Sound and Vibration **13**(4): 465-483.

Mair, W. A., P. D. F. Jones and R. K. W. Palmer (1975). "Vortex Shedding From Finned Tubes." Journal Of Sound and Vibration **39**(3): 293-296.

Marris, A. W. (1964). "A Review on Vortex Streets, Periodic Wakes, and Induced Vibration Phenomena." Journal of Basic Engineering: 185-193.

Nemoto, A. and M. Yamada (1992). "Flow-Induced Acoustic Resonance Caused By Fin-Tube Bundles." PVP **243**: 137-151.

Nemoto, A. and M. Yamada (1994). "Flow-Induced Acoustic Resonance in Staggered Tube Banks." PVP **273**: 273-282.

Norberg, C. (2001). "Flow Around a Circular Cylinder: Aspects of Fluctuating Lift." Journal Of Fluids and Structures **15**: 459-469.

Norberg, C. and B. Sunden (1987). "Turbulence and Reynolds Number Effects on the Flow and Fluid Forces on a Single Cylinder in Cross Flow." Journal Of Fluids and Structures **1**: 337-357.

Paidoussis, M. P. (1982). "A Review of Flow-Induced Vibrations in Reactors and Reactor Components." Nuclear Engineering and Design **74**: 31-60.

Pettigrew, M. J., Y. Sylvestre and A. O. Campagna (1978). "Vibration Analysis of Heat Exchanger and Steam Generator Designs." Nuclear Engineering and Design **48**: 97-115.

Polak, R. D. (1992). Vortex Shedding in Normal Triangle Tube Arrays. Mechanical Engineering. Hamilton, McMaster University.

Predergast, V. (1958). "Measurement of Two-Point Correlations of the Surface Pressure on a Circular Cylinder." UTIA Technical Note No. 23.

Reid, D. R. and J. Taborek (1994). "Selection Criteria for Plain and Segmented Finned Tubes for Heat Recovery Systems." Transactions of the ASME **116**: 406-410.

Ribeiro, J. L. D. (1992). "Fluctuating Lift and its Spanwise Correlation on a Circular Cylinder in a Smooth and in a Turbulent Flow: A Critical Review." Journal of Wind Engineering and Industrial Aerodynamics **40**: 179-198.

Stansby, P. K. (1974). "The Effects of End Plates on the Base Pressure Coefficient of a Circular Cylinder." Aeronautical Journal: 36-37.

Sviadosch, V., V. Katinas and E. Perednis "Vibrations of Smooth and Finned Tubes in a Cross Flow of Viscous Fluid at Different Turbulence Levels." 69-74.

Szepessy, S. (1994). "On the Spanwise Correlation of Vortex Shedding From a Circular Cylinder at High Reynolds Number." Physical Fluids **6**(7): 2406-2416.

Szepessy, S. and P. W. Bearman (1992). "Aspect Ratio and End Plate Effects on Vortex Shedding from a Circular Cylinder." Journal Of Fluid Mechanics **234**: 191-217.

Tombazis, N. and P. W. Bearman (1997). "A Study of Three-Dimensional Aspects of Vortex Shedding from a Bluff Body with a Mild Geometric Disturbance." Journal Of Fluid Mechanics **330**: 85-112.

Wang, C.-C., K.-Y. Chi and C.-J. Chang (2000). "Heat Transfer and Friction Characteristics of Plain Fin-and-Tube Heat Exchangers, Part II: Correlation." International Journal of Heat and Mass Transfer **43**: 2693-2700.

Weaver, D. S. (2001). Personal Communication.

Weaver, D. S. and J. A. Fitzpatrick (1988). "A Review of Cross-Flow Induced Vibrations in Heat Exchanger Tube Arrays." Journal Of Fluids and Structures **2**: 73-93.

Zdravkovich, M. M. (1981). "Review and Classification of Various Aerodynamic and Hydrodynamic Means for Suppressing Vortex Shedding." Journal of Wind Engineering and Industrial Aerodynamics **7**: 145-189.

Zukauskas, A. and V. Katinas (1979). Flow-Induced Vibration in Heat-Exchanger Tube Banks. Proceedings of the Symposium on Practical Experiences with Flow-Induced Vibrations, IUTAM, Karlsruhe.

Appendices

Appendix A

This appendix contains other results which were not presented in the body of this report.

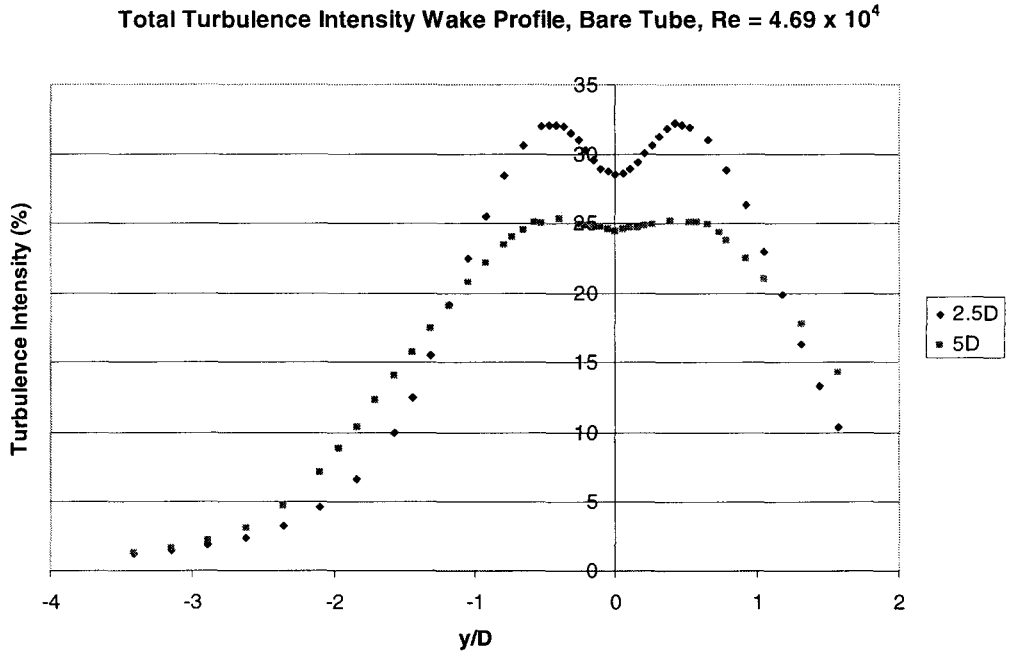

Figure A.1: Distribution of total turbulence intensity across the wake of a bare tube at high Re.

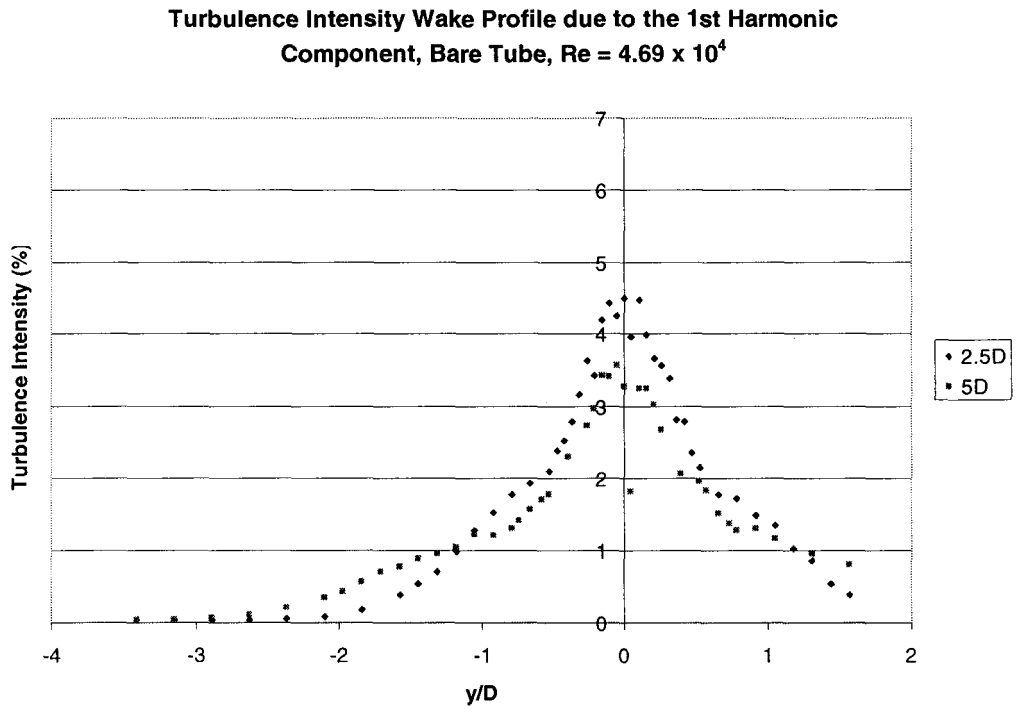

Figure A.2: Distribution of turbulence intensity due to the first harmonic component across the wake of a bare tube at high Re.

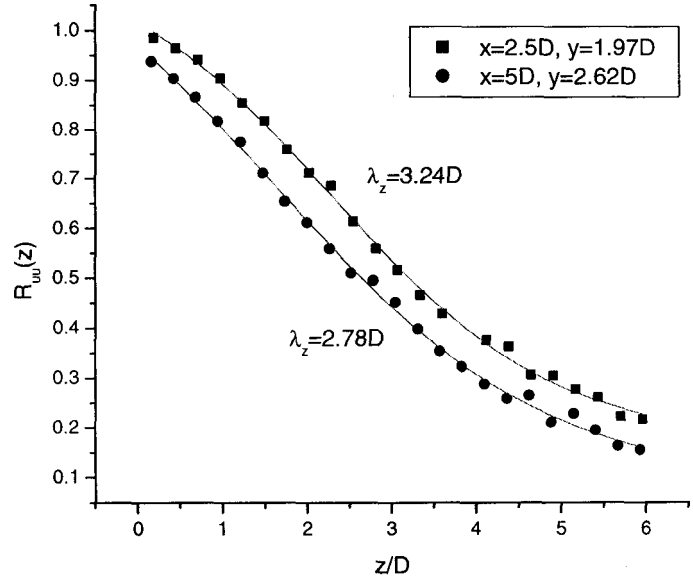

Figure A.3: Measurements of correlation coefficient along the span of the bare tube at low Re.

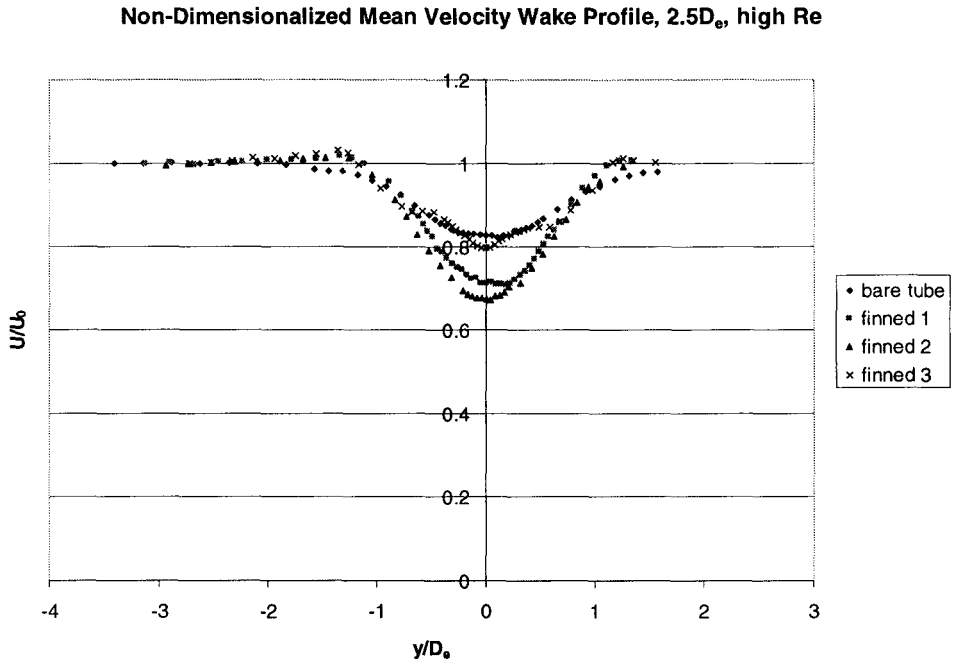

Figure A.4: Non-dimensionalized mean velocity wake profiles of all tubes at high Re and $x/D_e = 2.5$.

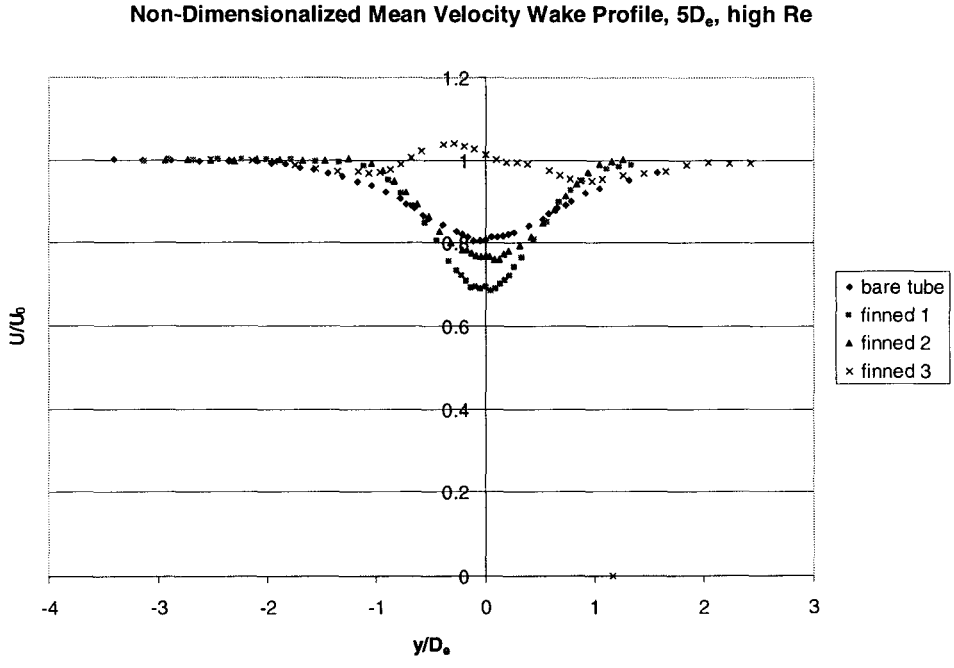

Figure A.5: Non-dimensionalized mean velocity wake profiles of all tubes at high Re and $x/D_e = 5$.

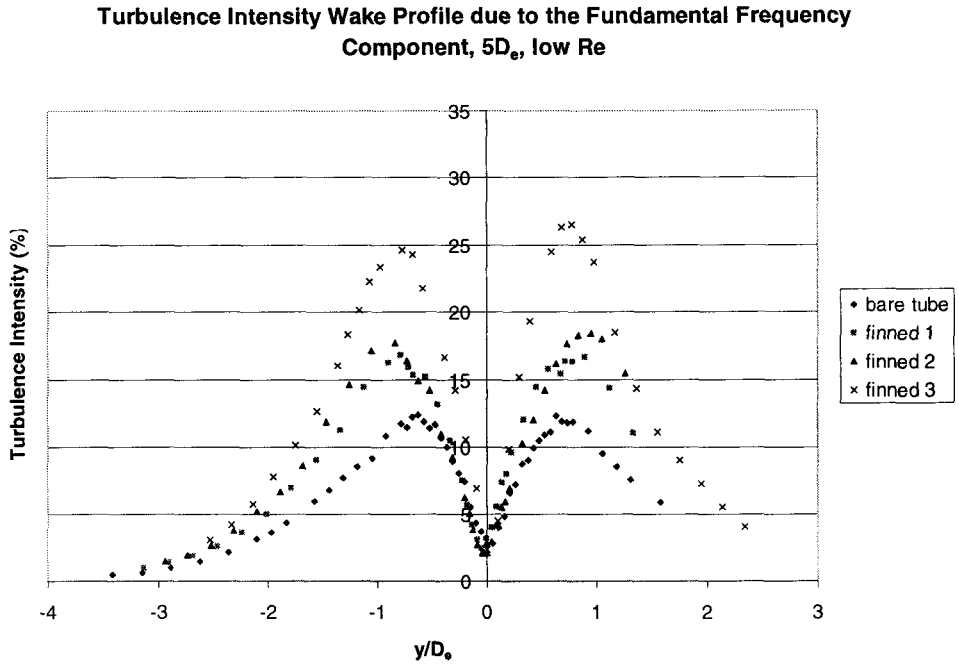

Figure A.6: Fundamental frequency component of the total turbulence intensity wake profiles of all tubes at low Re and $x/D_e = 5$.

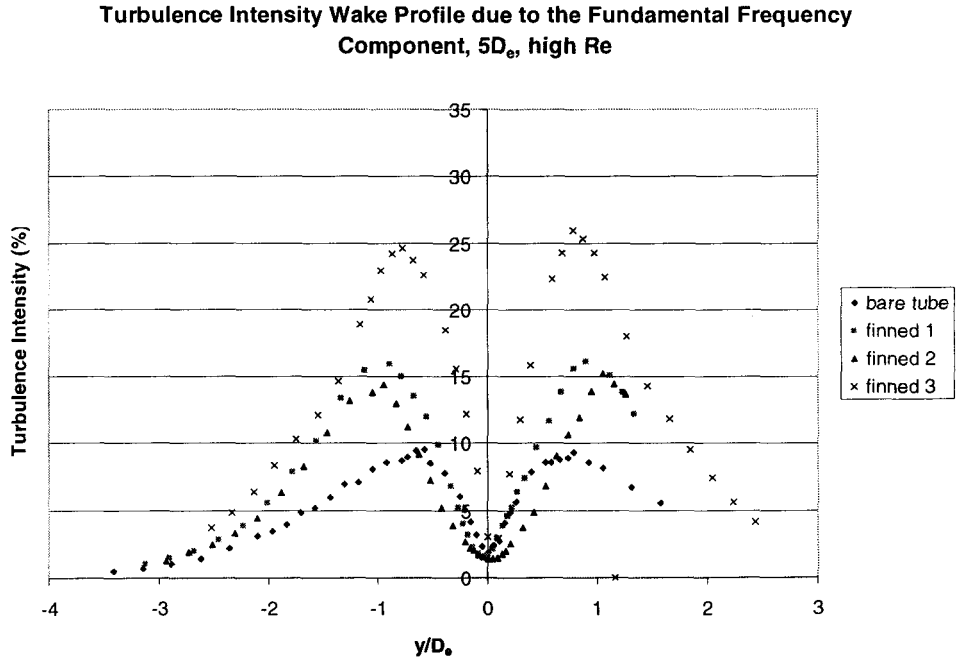

Figure A.7: Fundamental frequency component of the total turbulence intensity wake profiles of all tubes at high Re and $x/D_e = 5$.

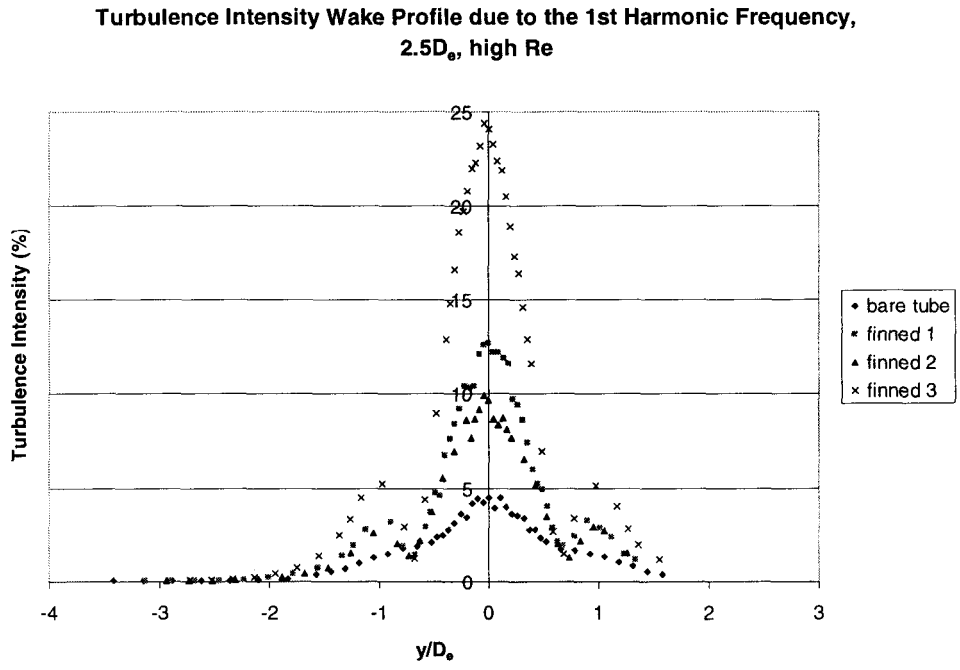

Figure A.8: First harmonic component of turbulence intensity wake profiles of all tubes at high Re and $x/D_e = 2.5$.

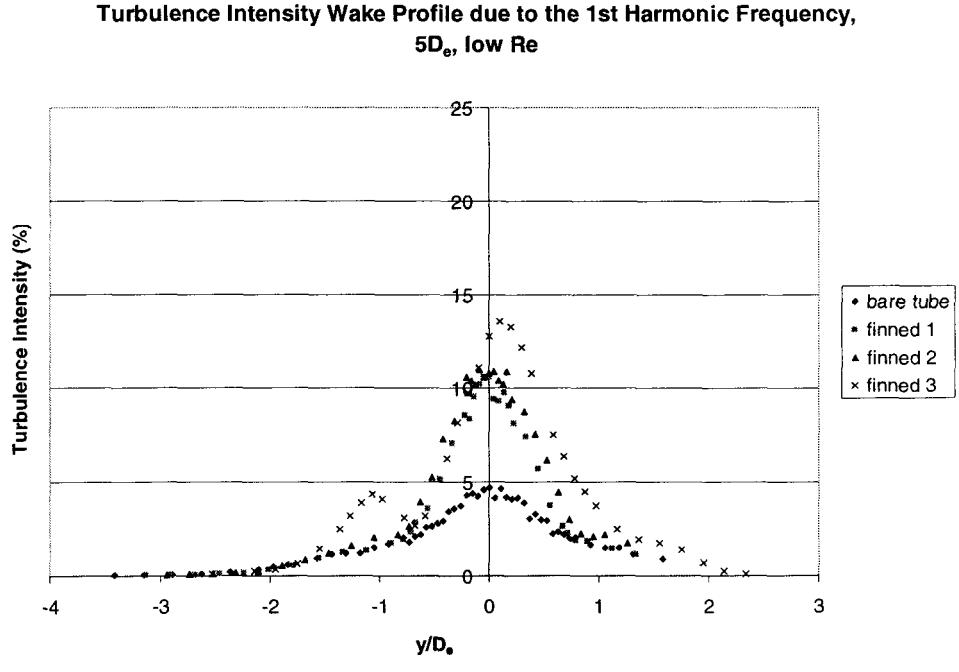

Figure A.9: First harmonic component of turbulence intensity wake profiles of all tubes at low Re and $x/D_e = 5$.

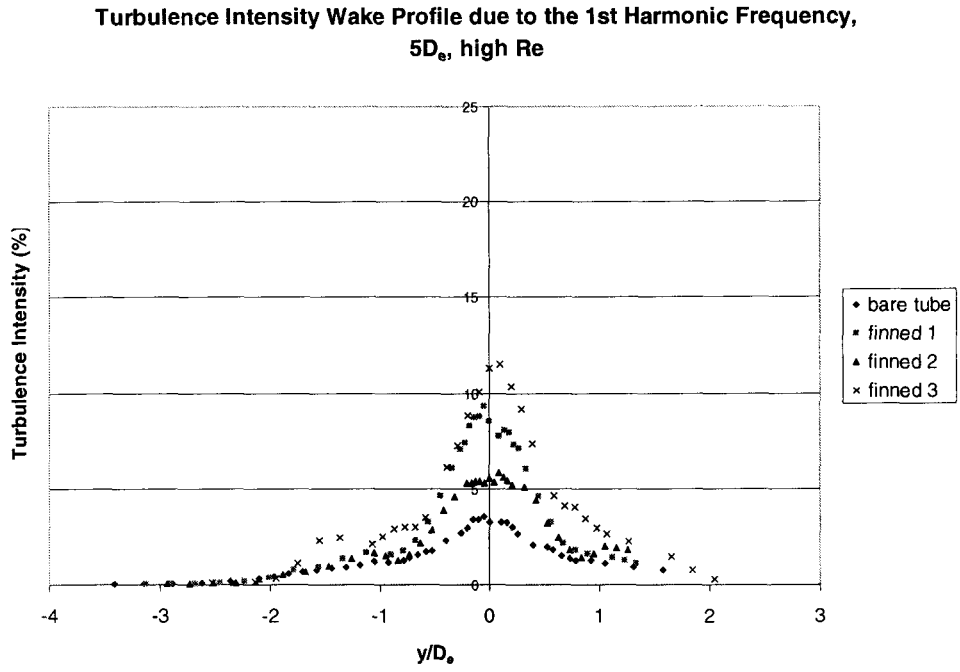

Figure A.10: First harmonic component of turbulence intensity wake profiles of all tubes at high Re and $x/D_e = 5$.

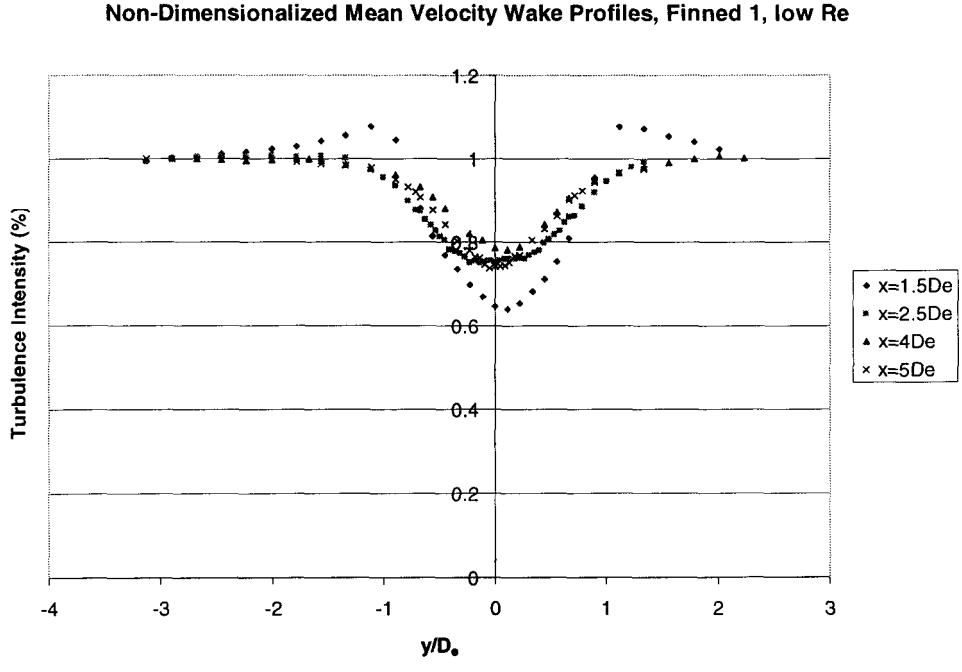

Figure A.11: Mean velocity wake profiles at various downstream distances for finned 1.

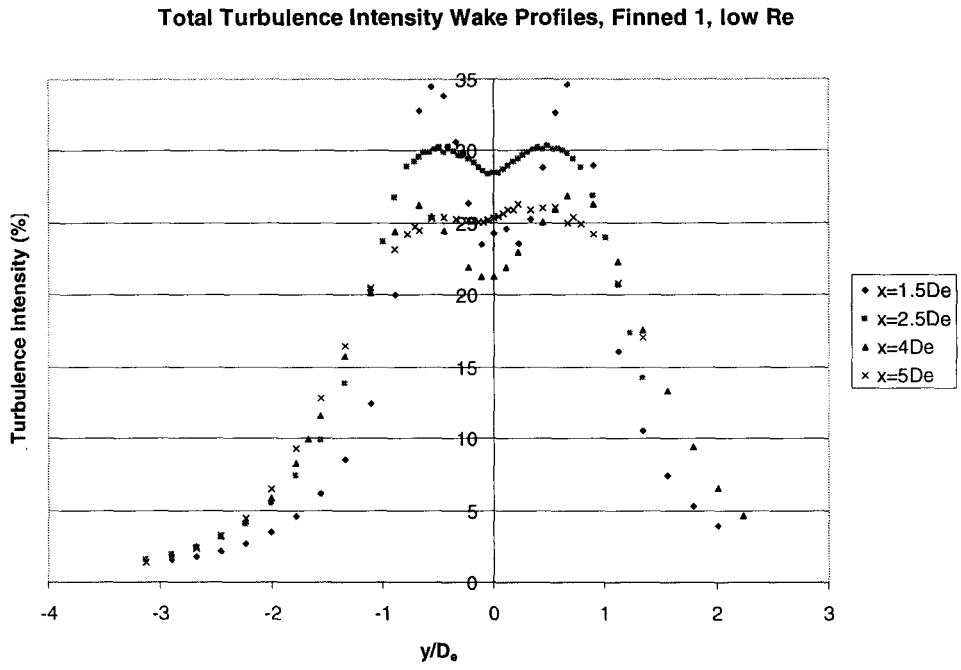

Figure A.12: Total turbulence intensity wake profiles at various downstream distances for finned 1.

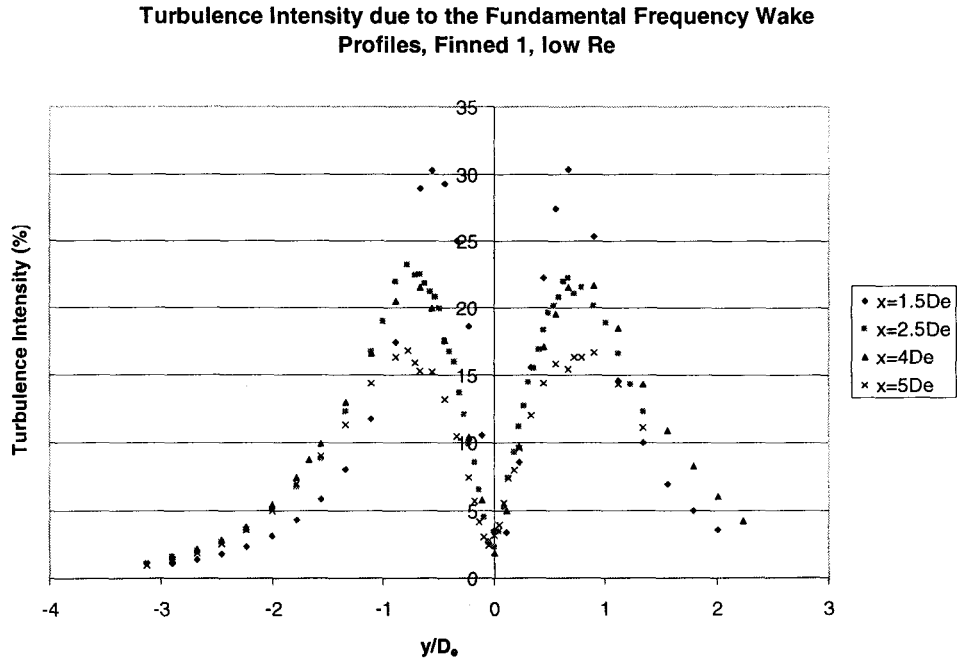

Figure A.13: Total Fundamental frequency component of the total turbulence intensity wake profiles at various downstream distances for finned 1.

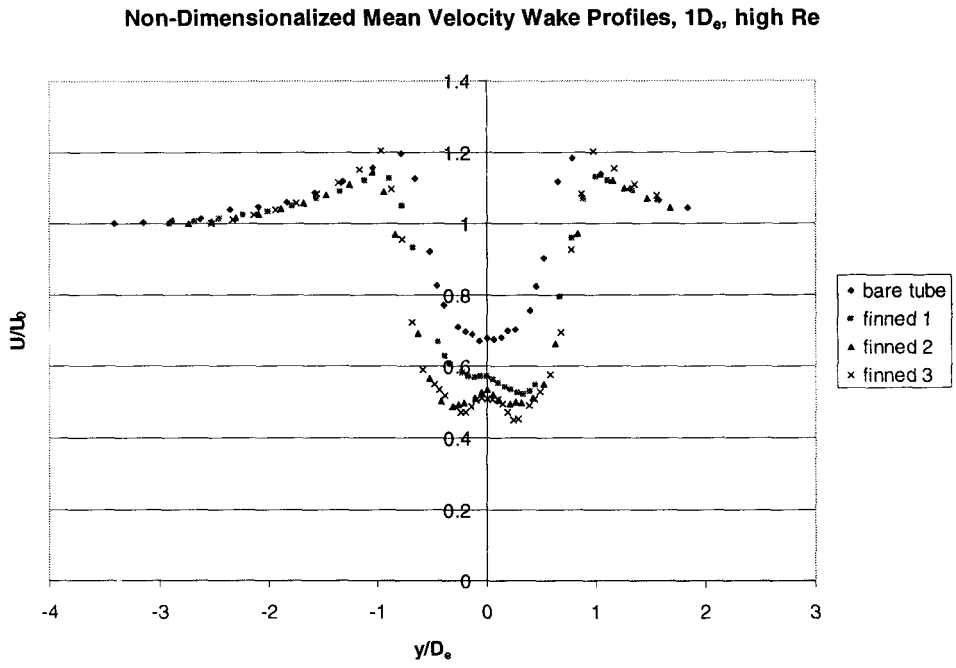

Figure A.14: Non-dimensionalized mean velocity wake profiles of all tubes at high Re and x/D_e = 1.

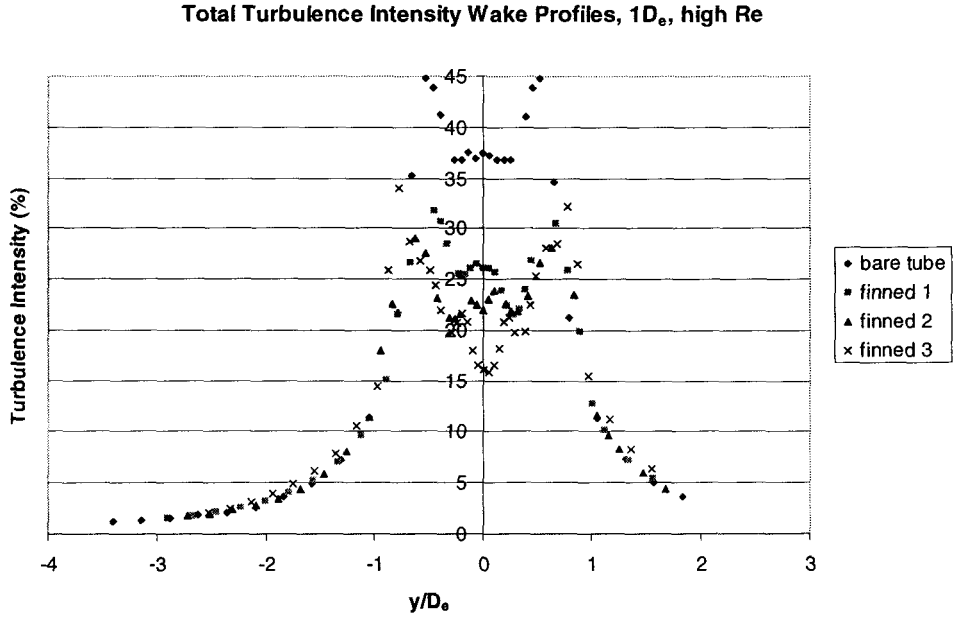

Figure A.15: Total turbulence intensity wake profiles of all tubes at high Re and x/D_e = 1.

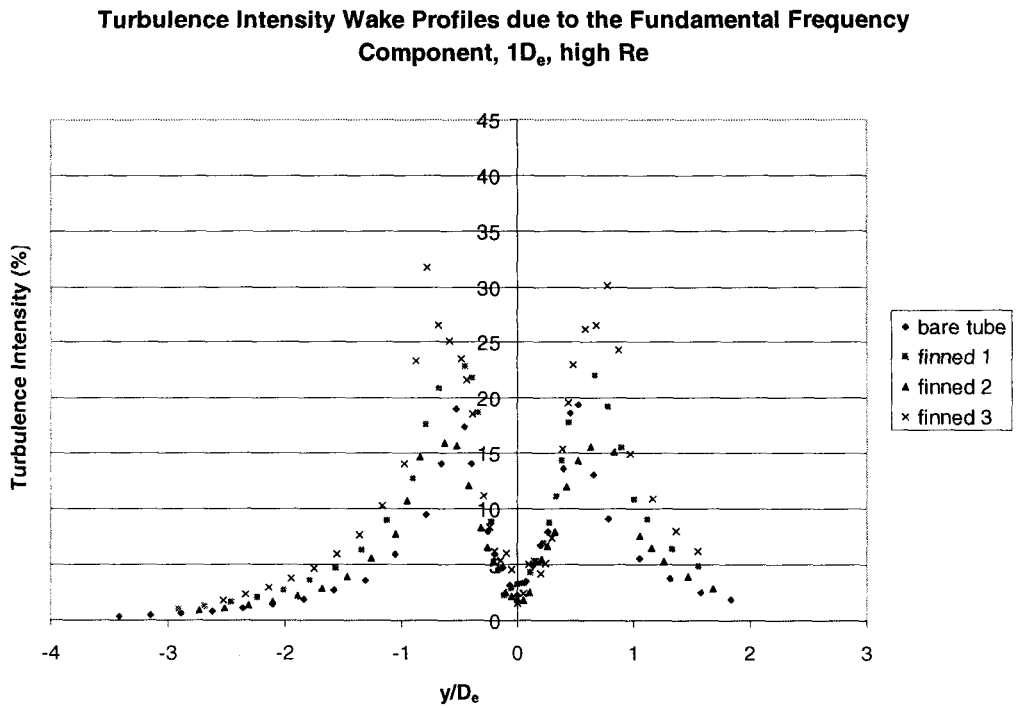

Figure A.16: First harmonic component of turbulence intensity wake profiles of all tubes at high Re and x/D_e = 1.

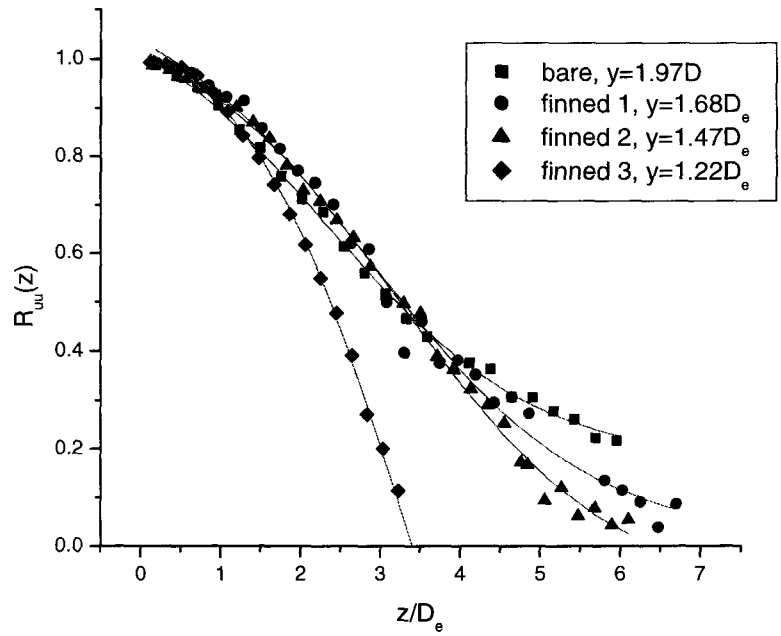

Figure A.17: Measurements of correlation coefficient along the span of the tubes at x/D_e = 2.5 and low Re.

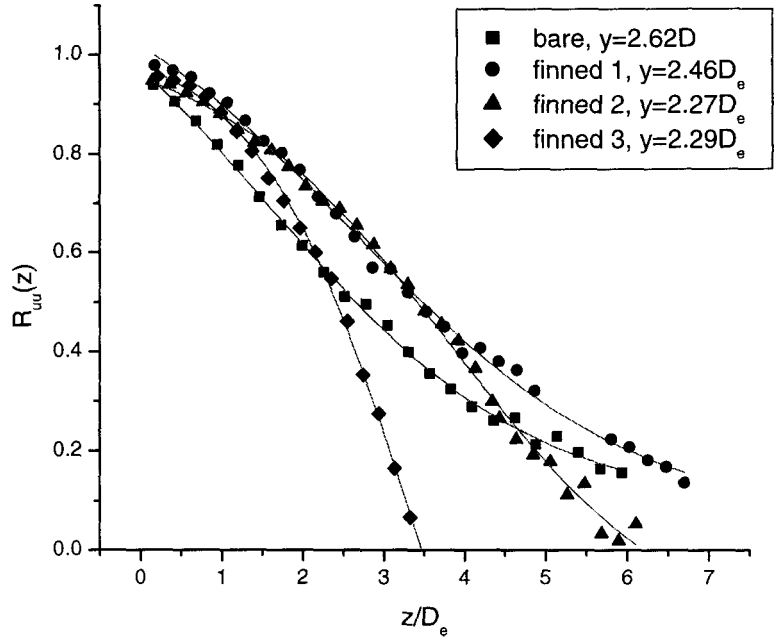

Figure A.18: Measurements of correlation coefficient along the span of the tubes at x/D_e = 5 and low Re.

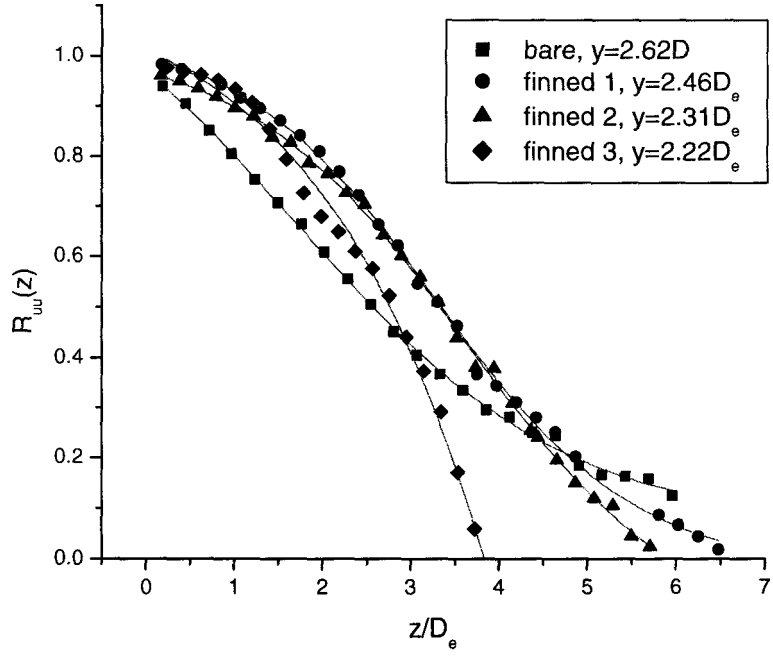

Figure A.19: Measurements of correlation coefficient along the span of the tubes at x/D_e = 5 and high Re.

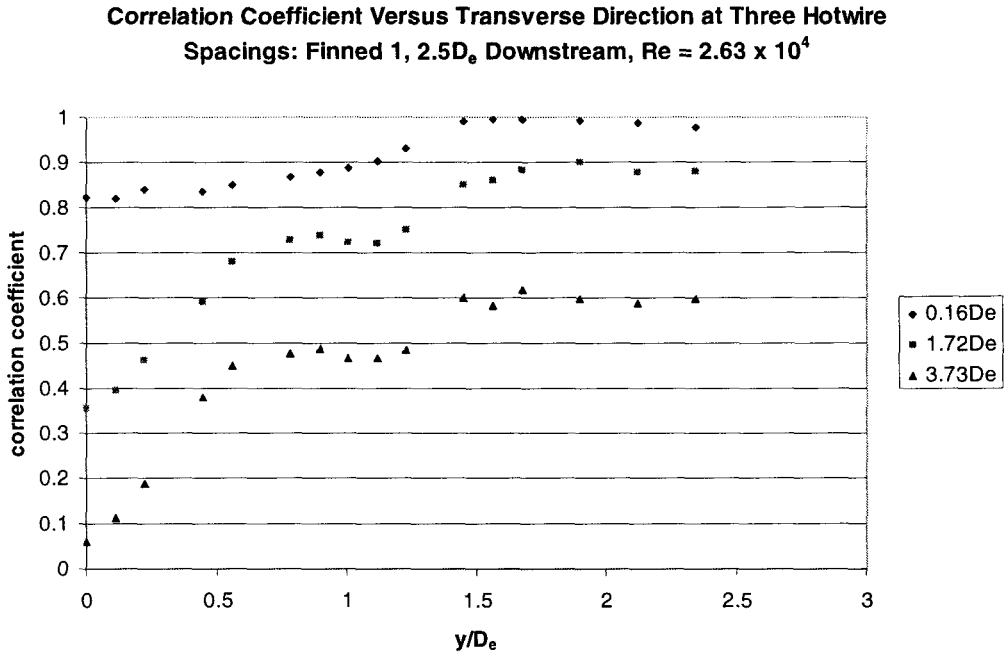

Figure A.20: How correlation coefficient varies in the transverse direction.

Appendix B

The following is the Labview program which was designed for this study.

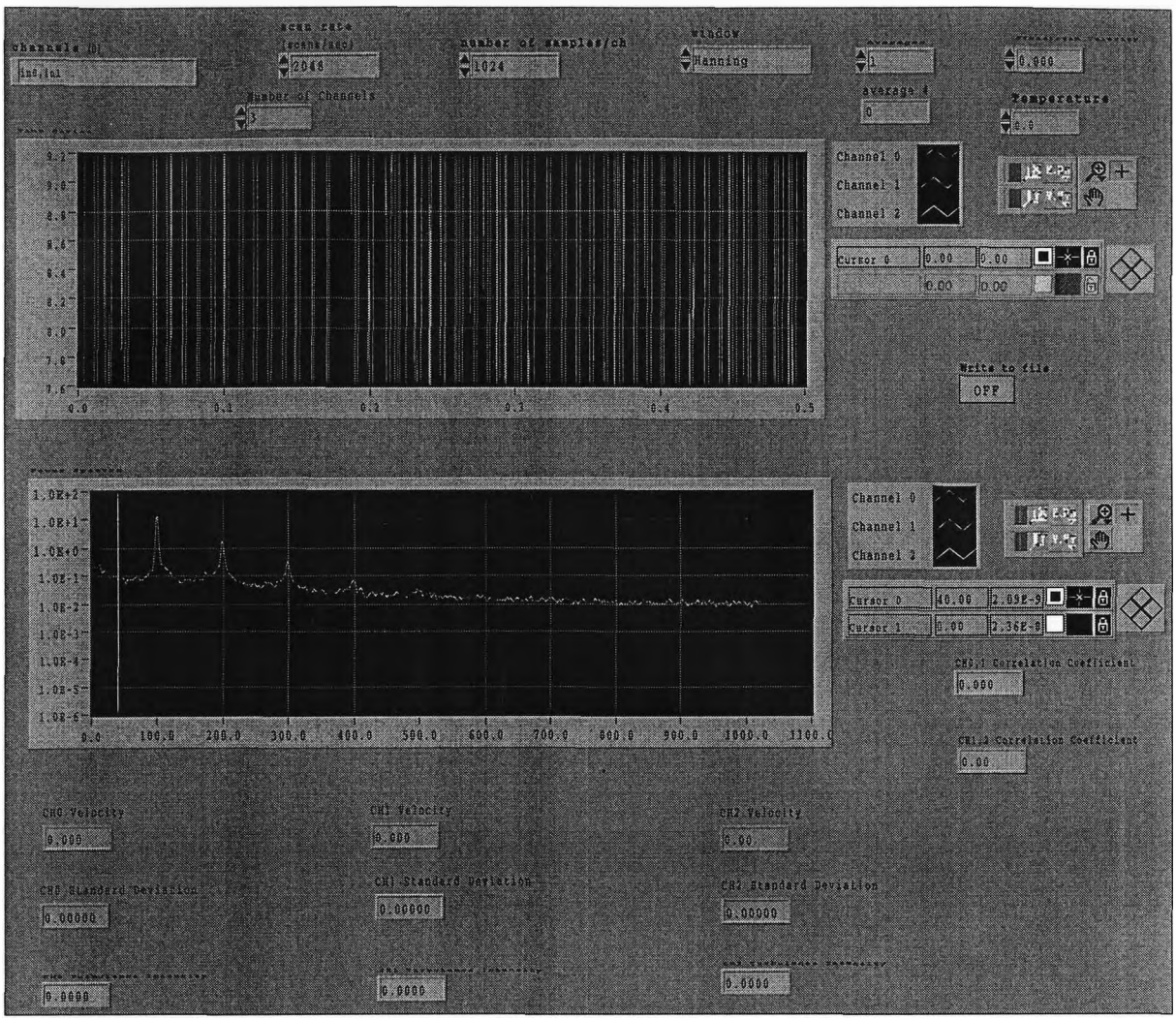
channels
Scan rate (scans/sec)
2048
Number of samples/ch
1024
Window
Hanning
Number of Channels
Temperature
Channel 0
Channel 1
Channel 2
Cursor 0
Cursor 1
Write to file
OFF
CH0,1 Correlation Coefficient
CH0,2 Correlation Coefficient
CH0 Velocity
CH1 Velocity
CH2 Velocity
CH0 Standard Deviation
CH1 Standard Deviation
CH2 Standard Deviation

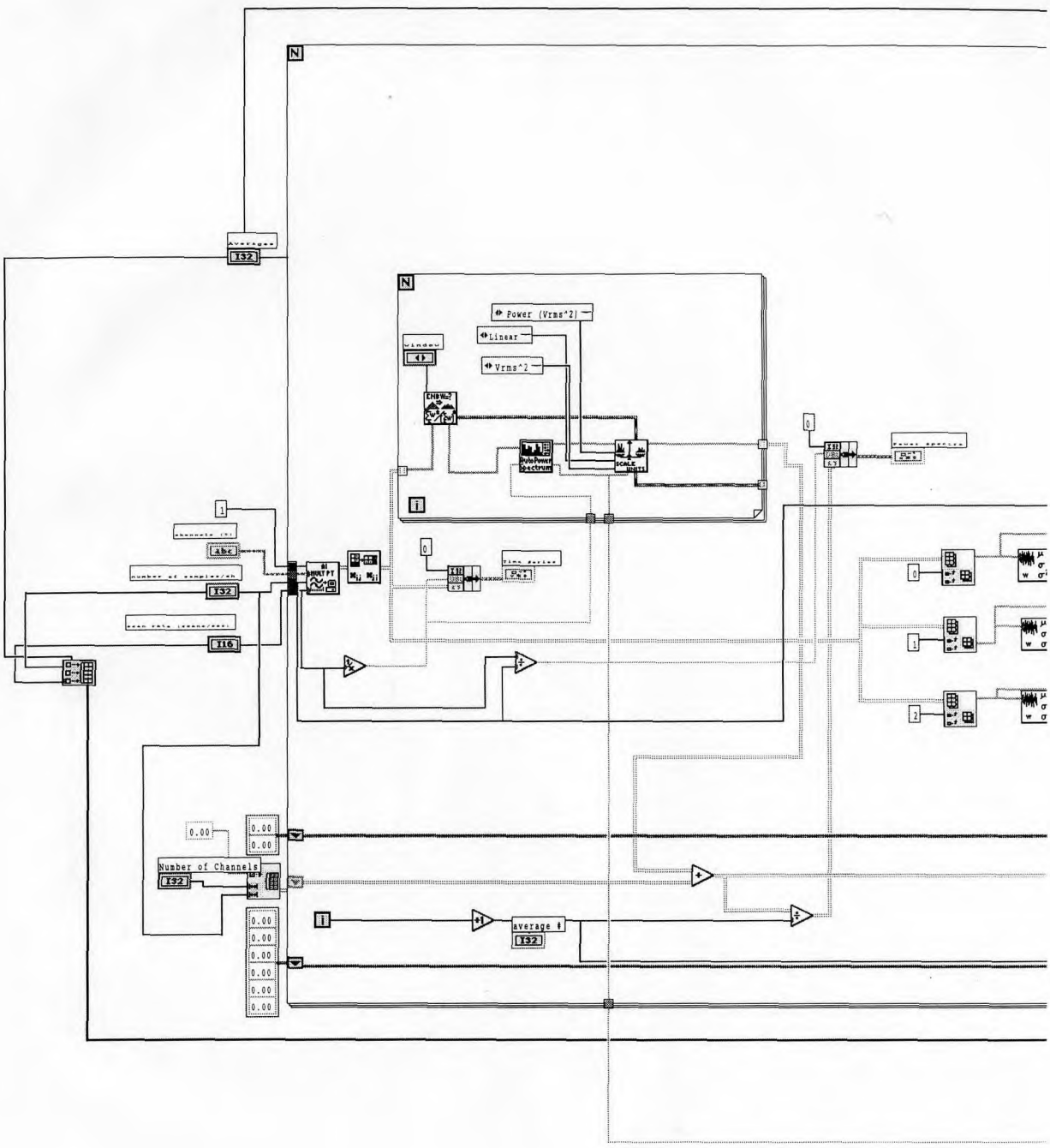
N
Average
I32
N
Power (Vrms^2)
Linear
Vrms^2
Window
ENBW-2
Auto Power Spectrum
SCALE
i
0
1
abc
number of samples/ch
I32
scan rate (samples/sec)
I16
AI 1DVOLT PT
Time Series
Number of Channels
I32
0.00
average #
I32

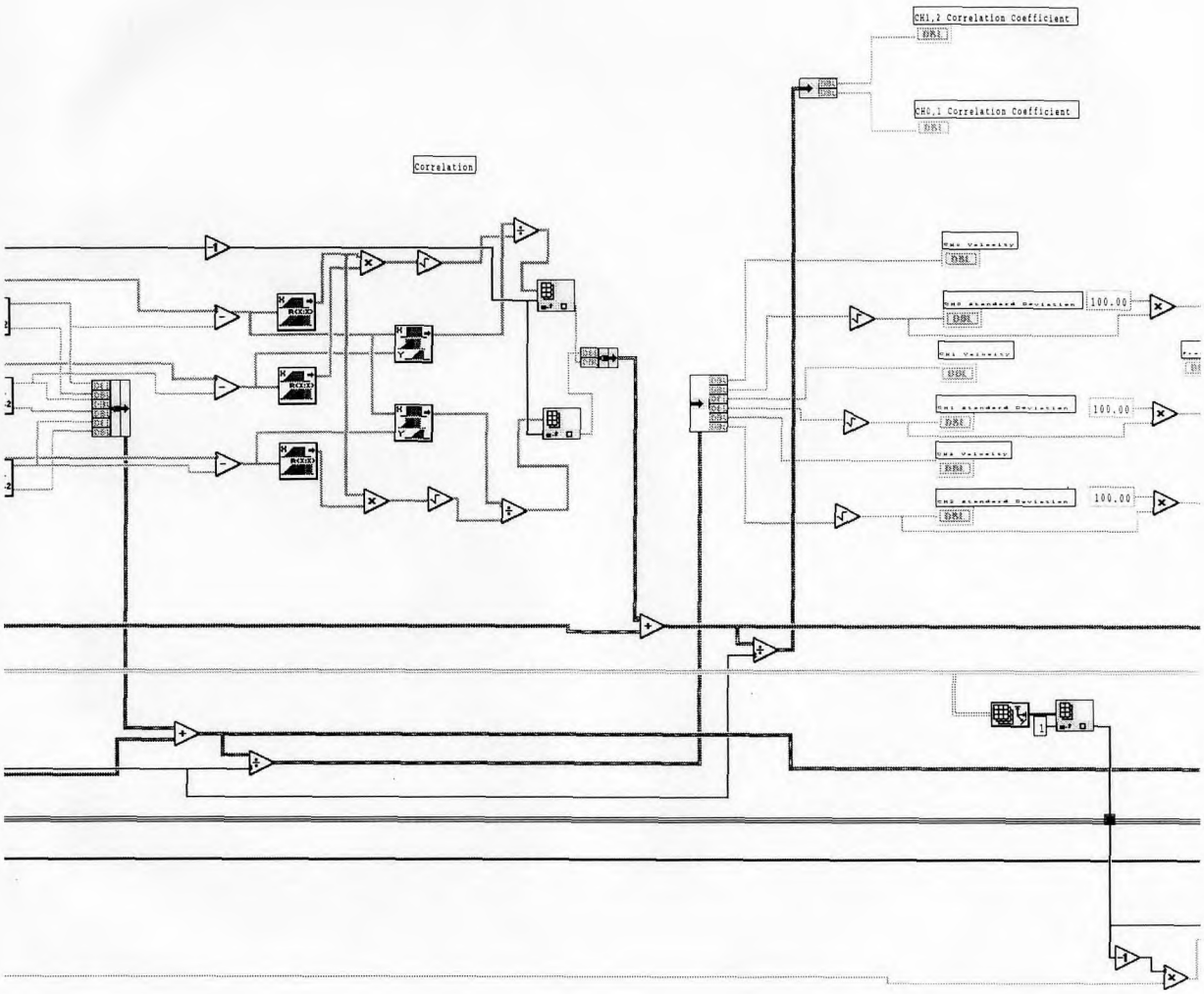
CH1,2 Correlation Coefficient
DBL
CH0,1 Correlation Coefficient
DBL
Correlation
100.00
100.00
100.00

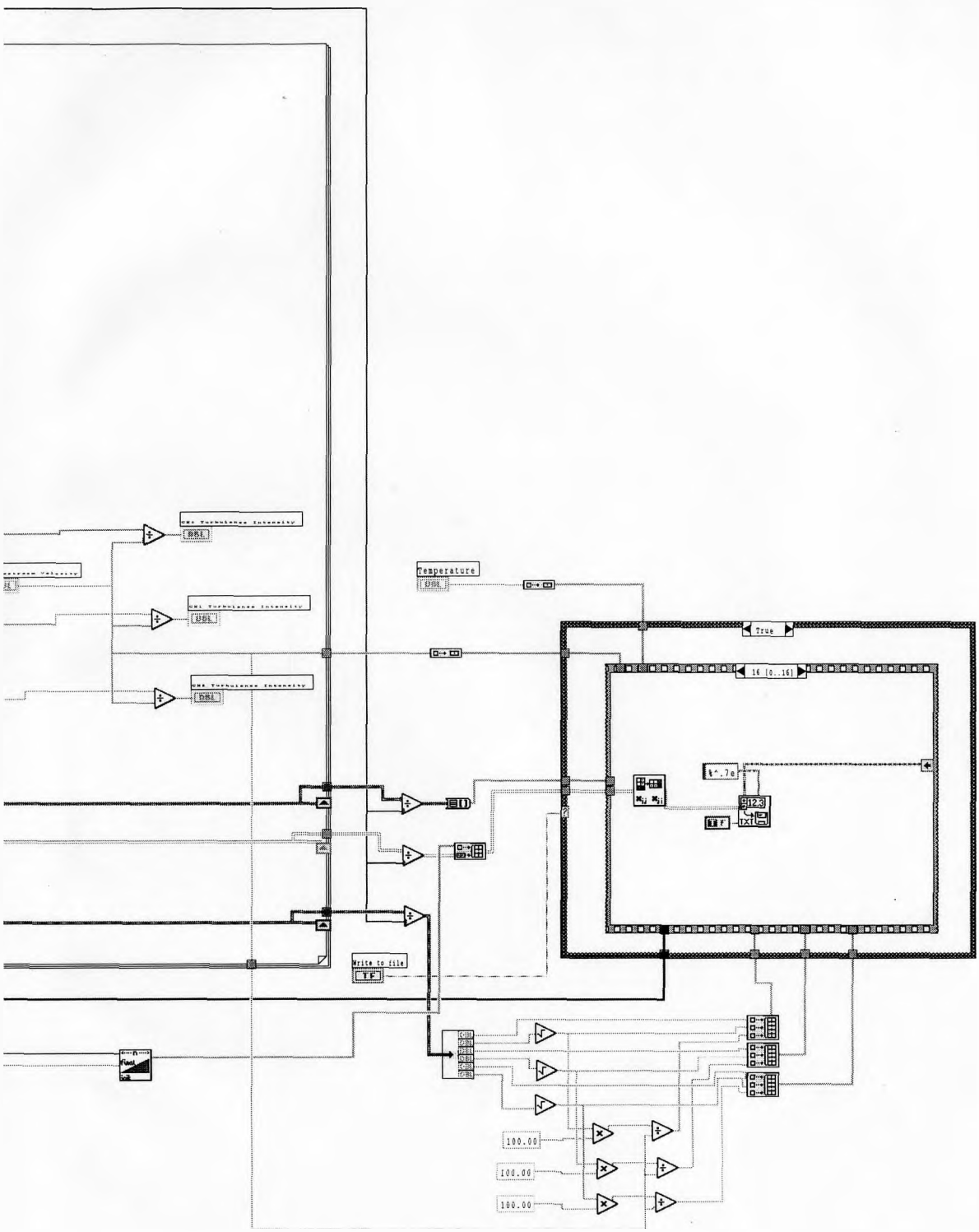
Temperature
DBL
True
16 [0..16]
%^.7e
Write to file
TF
100.00
100.00
100.00